SANDIA REPORT

SAND2013-7779
Unlimited Release
Printed September 2013

Acoustic Emission Non-Destructive Testing of Structures using Source Location Techniques

Alan G. Beattie

Prepared by
Sandia National Laboratories
Albuquerque, New Mexico 87185 and Livermore, California 94550

Sandia National Laboratories is a multi-program laboratory managed and operated by Sandia Corporation, a wholly owned subsidiary of Lockheed Martin Corporation, for the U.S. Department of Energy's National Nuclear Security Administration under contract DE-AC04-94AL85000.

Sandia National Laboratories

Issued by Sandia National Laboratories, operated for the United States Department of Energy by Sandia Corporation.

Available to DOE and DOE contractors from
U.S. Department of Energy
Office of Scientific and Technical Information
P.O. Box 62
Oak Ridge, TN 37831

Telephone: (865) 576-8401
Facsimile: (865) 576-5728
E-Mail: reports@adonis.osti.gov
Online ordering: http://www.osti.gov/bridge

Available to the public from
U.S. Department of Commerce
National Technical Information Service
5285 Port Royal Rd.
Springfield, VA 22161

Telephone: (800) 553-6847
Facsimile: (703) 605-6900
E-Mail: orders@ntis.fedworld.gov
Online order: http://www.ntis.gov/help/ordermethods.asp?loc=7-4-0#online

SAND2013-7779
Unlimited Release
Printed September 2013

Acoustic Emission Non-Destructive Testing of Structures using Source Location Techniques*

Alan G. Beattie, Retired
Sandia National Laboratories
Consultant to the Department of Wind Energy Technologies
P.O. Box 5800
Albuquerque, New Mexico 87185-1124

Sandia Contract No. 1145363

Abstract

The technology of acoustic emission (AE) testing has been advanced and used at Sandia for the past 40 years. AE has been used on structures including pressure vessels, fire bottles, wind turbines, gas wells, nuclear weapons, and solar collectors. This monograph begins with background topics in acoustics and instrumentation and then focuses on current acoustic emission technology. It covers the overall design and system setups for a test, with a wind turbine blade as the object. Test analysis is discussed with an emphasis on source location. Three test examples are presented, two on experimental wind turbine blades and one on aircraft fire extinguisher bottles. Finally, the code for a FORTRAN source location program is given as an example of a working analysis program. Throughout the document, the stress is on actual testing of real structures, not on laboratory experiments.

*The work described in this report was performed for Sandia National Laboratories under Contract No. 1145363.

ACKNOWLEDGMENTS

The author would like to acknowledge the encouragement and support of Mark Rumsey to write this monograph. The experimental work described was supported directly and indirectly by the Sandia National Laboratories Wind Energy Department. Much of the testing was conducted at the National Wind Technology Center near Boulder, Colorado where the aid and advice provided by Scott Hughes, Mike Jenks, Jeroen van Dam, and Mike Desmond was invaluable. Finally, Mike Desmond, Dale Berg, Dr. Didem Ozevin, and Alex Rinehart reviewed in detail the draft version and greatly improved the presentation.

Contents

FIGURES

TABLES

Foreword

Acoustic emission techniques in both Non-Destructive Testing (NDT), and Research and Development were first investigated by Kaiser [1] over sixty years ago. The ability to triangulate to the source of an emission by detecting the same sound wave at several different sensors was recognized early. In 1966, Green [2] reported successful use of triangulation in an actual NDT test on a hydrotest of a Saturn S-II propellant tank. Since then, the art of acoustic emission source location has rapidly expanded, pushed in part by the many technological advances in the field of personal computers with changes from simple analog systems to sophisticated digital systems. A premium has been placed not only on acquiring data, but also on using universal-type programs, included in the commercial systems, to analyze the data. Although these programs are quite versatile and significantly advanced over the first analysis programs included in the early source location systems, they cannot cover all of the possible types of analysis in the field of acoustic emission testing.

For the last forty years, the author has been using acoustic emission techniques at Sandia National Laboratories in widely varying applications, many of which required the development of specialized testing and/or analysis techniques. Obviously, as in any new field, not all the new techniques worked, but a general approach emerged. This monograph will detail the testing and analysis techniques developed in two areas: Wind Energy and Small Pressure Vessels. These applications use multiple sensors to perform acoustic emission source location and involve analysis of the digital data. Because early commercial programs were not readily adaptable for analysis, custom programs in FORTRAN were written. As the field has evolved, many of the custom techniques have been incorporated in the software furnished with the commercial systems. However, the details of the commercial software are hidden in executable files. A few of the Sandia-developed FORTRAN programs are included here to illustrate the methods and assumptions used in acoustic emission programs. (FORTRAN is one of the easier languages in which to follow the workings of a code; it is still used despite the rise, decline, and death of many other computer languages.) These working programs can be used with necessary minor adaptations to fit an acoustic emission source location test.

This treatise was written to describe some acoustic emission testing procedures which have worked well for the author. Neither a text book nor a rigorous scientific paper, this publication assumes that the reader already has some familiarity with acoustic emission (AE). References are sparse, partly because upon my retirement 15 years ago, I gave my collection of reference papers to a university library. For readers who want either more detail on particular AE applications, or just a wide survey of the field, I recommend the second edition of the *Nondestructive Testing Handbook, volume 5, Acoustic Emission Testing*, edited by Ronnie Miller. For a source of reviewed technical papers on acoustic emission, I recommend the *Journal of Acoustic Emission* published and edited by professor Kanji Ono. The *Journal* is available on the internet and the entire 28 years of publication can be purchased on 2 DVDs.

Following a general discussion of acoustic emission and acoustic emission sources, this monograph then offers a general discussion of the properties of elastic waves in materials. To understand what is occurring in an acoustic test, either Ultrasonics or Acoustic Emission, one needs this basic background. It is included both to aid readers who are new to the field of acoustics in solids, and to serve as reference material for those with some prior knowledge.

Briefly covered are elastic waves in solids including different vibration modes, reflection and refraction of waves, attenuation, superposition and dispersion of waves, resonance effects, and other phenomena which will be encountered in an acoustic emission test. Also discussed are sensors, couplants, preamplifiers and other topics involved in performing an acoustic emission test. Two brief sections cover acoustic emission source mechanisms, and parameters of acoustic emission waveforms which are used in most commercial systems. All of this material was covered in the author's early review article [3] and makes no pretense of being new or different. It is hoped that the most useful parts of this monograph will be the discussions of the design, conduction, and analysis of several types of acoustic emission tests. No two tests are ever identical but the general methodology is widely applicable.

1.0 CHAPTER 1

1.1. Introduction to Acoustic Emission

Acoustic Emission (AE) is the study and practical use of elastic waves generated by a material subjected to an external stress. The phenomenon was recognized by early miners who exited a mine when the rocks or supporting timbers started groaning. Tin cry, the sound produced when a tin bar is bent, was known soon after the production of metallic tin. More recently, C.S. Barrett [4] mapped a low temperature phase transition in Lithium-Magnesium alloys by sticking a phonograph needle into the crystal and recording the output as the temperature was changed. J. Kaiser [1] investigated the signals produced by samples undergoing tensile testing and discovered the **Kaiser effect**, i.e. that no signals were generated by a sample upon the second loading until the previous maximum load was exceeded. After Kaiser's thesis was published in 1950, several groups investigated the phenomena for possible use in testing structures. In the early 1960s, Allen Green and a group at Aerojet Corporation started using AE in the testing of Saturn Rocket propellant tanks. They used a form of triangulation based on the **arrival times** of the acoustic pulse at several acoustic emission sensors. This was the direct precursor of the work that is described in this paper.

Despite its longstanding use, the definition of "acoustic emission" has been a source of controversy for the last fifty years. Strictly, "acoustic" refers to the pressure waves detected by one's ear. However, elastic waves in solids are not limited to pressure waves, and all types of vibrational modes are generated by acoustic emission sources. Even so, the term "acoustic emission" has become almost universally used for the phenomena of elastic waves generated by an internal event in a media. In this monograph, "acoustic" will refer to any elastic wave generated by an acoustic emission source. Acoustic emission, then, is the generation of an elastic wave by the rapid change in the stress state of some region in the material. This change is usually caused by the application of an external stimulus to the material. The material can be a solid, liquid, gas or plasma and the external stress can be applied mechanically, thermally, magnetically, etc. The stress change must be rapid enough to transmit some energy to the surrounding material and dissipates as an elastic wave. On a macroscopic scale this definition includes earthquakes and thunder, while on a microscopic scale it includes the fracture of crystallites and Martensitic phase transformations. The occurrence of the burst of energy is completely determined by the local conditions, the local stress field, and the physical state of the region. As a result, neither the exact time when the energy burst occurs nor the exact details of the generated wave can be determined beforehand. In general, the event generating the emission is irreversible; neither a ruptured geologic fault nor a fractured crystallite in a metal plate will heal spontaneously.

Once the elastic wave is generated, it then travels throughout the material and can be detected at considerable distances from its point of origin. Traveling from its source to the point of detection, the wave is subjected to all the characteristics and variations of its acoustic path. Its energy is attenuated by geometric spreading and scattering by both microscopic and macroscopic variations in the material's structure. Other kinds of attenuations may also be present. The wave's frequency content is generated by the source and modified as it travels the acoustic path. The primary information carried by the wave is the time of arrival and the elastic energy detected at each sensor on the structure. The excitation of a sensor indicates that something happened in

the specimen at a specific time, while the amplitude indicates the level of the disturbance. The apparent location of the source and all other characteristics of the detected signal are modified by the characteristics of the wave's path to each sensor as well as the characteristics the sensor. As a result, in a highly controlled laboratory experiment, a reasonable estimate can be made of the characteristics of the emission source; however, in a test on an actual structure, we are limited to what are basically statistical estimates from multiple emissions to tell us what is happening in the specimen. Statistical analysis is not generally used in the study of acoustic emissions, but the state of the specimen and the location coordinates of the sources are inferred from averages of calculated values from multiple emissions.

Elastic energy is ubiquitous. It travels through all materials where there is an interaction between atoms. Only a hard vacuum does not transmit elastic energy. The distance from its source over which an acoustic signal can be detected depends on its initial amplitude and the acoustic characteristics of the material through which it is traveling. For many structural materials, acoustic emission signals can be detected from almost anywhere on the structure. This allows an AE test to cover an entire structure instead of only a small region. However, many acoustic signals which have nothing to do with the test can be present and detected. Acoustic isolation of the test object is highly desirable. Most acoustic emission testing filters out acoustic signals at frequencies below 20 KHz, thus ignoring background noise and verbal communication in the test area.

An acoustic emission test occurs in real time. The test does not find preexisting defects, but detects flaw growth as it occurs. If the stress application simulates the conditions that the test structure is designed to experience in actual operation, serious acoustic emission will indicate pathological flaws that could lead to failure of part or all of the structure. The amount of emission detected and the locations of the emission sources will depend both on the design of the structure and the materials used in its fabrication. For example, compare the bending of a strip of glass and a strip of FRP (Fiber Reinforced Plastic) with identical dimensions. The strip of glass will likely give a single high-amplitude burst of emission just at failure while the FRP will show a period of low level emissions followed by a few higher level emissions and then one or more high amplitude emissions as the strip starts to fail and then tears apart or snaps. Interpreting detected emissions is the test engineer's job. The value of the information obtained from a test is determined first by the design of the test and second, by the analysis of the detected emission. For complex structures, both the test design and interpretation are seldom simple. It is the purpose of this monograph to aid the test engineer in both areas.

1.2. Sources of Acoustic Emission

Acoustic emissions are acoustic waves generated by a rapid change in the stress state of a region in a material. Acoustic waves are one of two non-electromagnetic methods of transmitting energy through a material; the other method is thermal diffusion. A difference between the two is that thermal diffusion involves direct energy transfer between individual atoms, while an acoustic wave transfers energy by a cooperative motion of many atoms. An acoustic wave can be as simple as a pressure pulse in a gas or liquid, or as complicated as the many modes of transmission in a bounded solid. The generation of an acoustic wave invariably involves a large region of atoms.

The most common acoustic waves are sound waves in air and water. These are produced by vibration of a surface such as the vocal apparatus of an animal, a leaf in the wind, or the diaphragm of a speaker. These sources are quasi-continuous, involving a modulated vibration of an interface between the generating region and the transmitting medium. Another type of acoustic wave is generated by a sudden disturbance in or on the material itself, a transient event that produces a transient acoustic wave. Such a transient wave is what we define as acoustic emission. It may have the form of a single damped wave with complex frequency content or it may appear as many small transient events which sum into quasi-continuous noise. Its primary characteristics are that it is generated in the medium which transmits it, and it is transient in nature. Any sudden movement of a group of atoms at velocities near the sound velocity in a material can produce a transient acoustic wave. The apparent quasi-continuous signals which are often seen can be generated by the overlap of many transient events instead of a continuous vibration of a surface. Figure 1-1 shows waveforms both from a transient event and from a superposition of many transient events. The long decay of the transient event is produced by reflections of the original wave in the complex metal specimen.

The size of the region generating an emission can vary from a relatively small row or plate of atoms moving simultaneously into a new crystal position during a Martensitic phase transition to a fracture in a subduction zone between two continental plates. The energy released in an **acoustic emission event** will be roughly proportional to the volume of the source. Energy from these waves ranges from smaller than an electron volt to the energy contained in a thunder clap or that of a magnitude 9 earthquake. Wave frequencies are generally related inversely to the volume of the generating region, ranging from thousandths of a Hertz for earthquakes to several MHz in fine grain metals. An important characteristic of acoustic emission in solids is that the fracture of the region occurs when the local stress vector exceeds the strength of the region to withstand that vector. In other words, the exact time when the emission occurs strictly depends on the local conditions. In a metal, for example, the precise environment of every crystallite differs, and the fracture of one crystallite or of the boundary between two crystallites will make small changes in the local stress vectors in the other crystallites. This complete dependence on local conditions means that it is impossible to predict the exact time of any one emission or the time interval between any two emissions. Acoustic emissions occur unpredictably in time. They are a response not to the applied external stress but to the local stress fields produced at each position throughout the material. The parameters of the detected emission depend not only on the characteristics of the emission source, but also on the characteristics and geometry of the medium between the source and sensor, and on the characteristics of the sensor and of the couplant between sensor and medium.

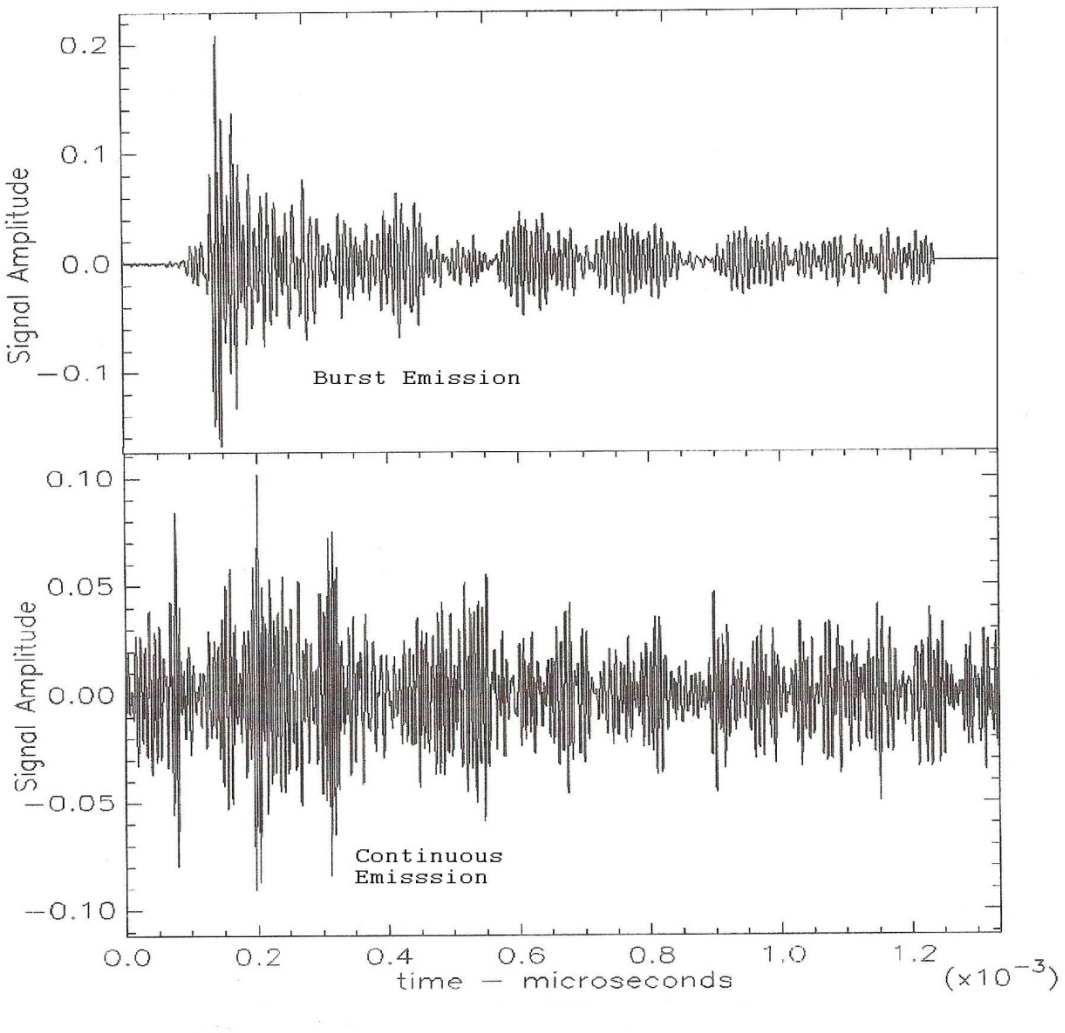

Figure 1-1. Examples of burst emission and continuous emission from a high strength aluminum alloy

The signal characteristics detected by individual identical sensors located at various positions on a specimen will often vary greatly for a single emission. The more complex the medium in which the emission is generated and transmitted, the more likely there will be large differences between detected signals from the same emission at different sensors. The unpredictable time of origination and the wide variety of waveforms in separate emissions are fundamental characteristics of acoustic emission. As such, these factors have a profound effect on the type of analysis used on the detected emissions.

In structural metals, both inter-granular and trans-granular cracking of metal crystallites can generate low level acoustic emission. Emission will also be generated at inclusions both by fracture of the inclusion and the breaking of the bonds between the inclusion and metal. Crack growth where at least several crystallites are involved can generate emission of moderate to large amplitudes. The presence of corrosion on a metal surface can be detected by the fracture of brittle corrosion byproducts while active corrosion can generate emission from bubble formation. In high stress environments, twinning (a form of crystalline distortion) can occur in some metals

and this can produce emission. Room temperature creep in metals may involve the movement of dislocations in the metal. Laboratory experiments have claimed to be able to detect very low amplitude emission from creep, but the author is not aware of its use in structural flaw detection. The creep rate in structural materials under normal usage is usually far too slow to generate acoustic emission useable for flaw detection.

Source mechanisms in FRP include matrix cracking, debonds between the matrix and fibers, fiber fracture, and crack propagation. These source mechanisms can all be activated by the application of an external stress. Based on the idea that the emission amplitude is related to the volume of the source, matrix cracking should produce the lowest amplitude emission, followed by matrix-fiber debonding. Fiber breakage would be louder still, partly due to the amount of energy released by the fracture of a high strength fiber. Finally, crack propagation, which includes all three of the previous mechanisms, would produce the highest amplitude emissions. This appears generally to be the case, but trying to quantify it as a rule has never worked very well, probably because FRP is usually laid up by hand and never comes close to the structural uniformity of a well annealed metal. The first loading of an FRP structure will generate acoustic emission at loads well below the strength of the structure. The most likely cause of this emission is the relief, by minute fractures in the FRP during the first loading, of high residual stresses which developed in local regions during the curing process. The fractures have little effect on the strength of the material, and the emission usually stops before the design loads are reached. This emission is seldom seen upon the second and subsequent loadings. Another source of emission in FRP structures is often seen during cyclic loading. This emission appears in the middle ranges of the cyclic load when the rate of change in applied stress is highest, instead of at the peak loads. It appears to be caused by friction between small regions in the structure which are not bonded. This type of emission can be present during the entire cyclic load test; however, it does not correlate with structural damage in the test object. Structural damage is associated with emission that occurs near the peak loads, especially during the rising load.

As discussed above, most acoustic emission mechanisms involve a permanent change in the micro structure of the material. Once a micro fracture occurs, it will not happen again unless there is some sort of healing mechanism. Therefore, acoustic emission appears irreversible. The Kaiser effect, where the re-stressing of a specimen will not generate acoustic emission until the previous load level has been exceeded, is caused by this irreversibility. The Kaiser effect holds very well for the immediate re-stressing of a metal specimen, but less well for composites. The problem is that the reapplication of an external stress does not necessarily take the specimen along the same micro-stress path. One often sees emission on subsequent loadings at loads lower than previously reached. The ratio of the load value, when emission starts on subsequent loadings, to the maximum load value reached on the previous loading, known as the **Felicity ratio,** indicates possible damage induced by the previous loading. Many NDT tests of FRP structures apply the test load in a series of steps, returning to zero between each step. The appearance of Felicity ratios much less than 1.0 is a good indication that significant damage occurred in previous loadings.

2.0 CHAPTER 2

2.1. Acoustic Waves in Solids

Acoustic emissions are acoustic waves generated by a material, usually in response to a change in stress. Once generated, these waves propagate under the same rules as any other acoustic wave. They are a collective motion in a collection of atoms. Acoustic wave motion is a cooperative movement of the atoms in a material extending over a huge number of atoms. This collective motion implies that the wavelength is long compared with the distance between the atoms. Wavelength is inversely proportional to the frequency of a wave; therefore, an acoustic wave is usually assumed to be of relatively low frequency. For example, a frequency as high as 10^9 Hz in Aluminum would still imply a wave extending over 1.5×10^4 lattice sites. The simplest type of acoustic wave is a pressure wave which occurs when a shell of material around a region is suddenly compressed by a disturbance in that region. This compression can be either positive or negative, such as a bubble exploding or imploding. The material in this shell experiences a change in its density. This density change is then passed to the next shell by coupling between the atoms. The density in the first shell then rebounds, usually going past the original density value to a smaller density change in the opposite direction. This variation in the density is transmitted to the next shell, and so on, throughout the material. The strength of the coupling between the material's atoms or molecules and the density of the material determines the speed with which the disturbance propagates . The resulting wave is known as a compressional wave and occurs in all materials, solids, liquids, gases, and plasmas . In a compressional wave, the average motion of the atoms parallels the wave's direction of travel. As materials become more rigid and ordered, the forces between atoms become far more complex and dependent on the geometrical positions of the atoms. More modes of wave motion are possible and the averaged atomic motions are no longer restricted to be parallel to the propagation direction . The introduction of boundaries in a material will introduce further complications As a wave passes through an intersection into another material, the difference in physical propertied between the materials will produce reflections and refractions as well as changes in the modes of propagation. A wave traveling along a surface will have far different particle motions than one propagating in the bulk.

2.2. Characteristics of Acoustic Waves

Acoustic emission signals generate complexity as the wave travels through the medium. Understanding acoustic emission signals requires knowledge of the wave characteristics, starting with the properties of the medium through which the wave travels. All materials are collections of atoms held together by attractive forces while simultaneously prevented, by short range repulsive forces, from approaching each other too closely. The superposition of these forces results in an equilibrium position for the atom at its lowest energy, the material's most stable configuration. In crystals, for example, long range forces between the atoms result in defined locations for these equilibrium positions. The result is a crystal structure. In a liquid the structure is amorphous, but an approximate distance between atoms results in a uniform density. In a liquid, only the density is defined. There are no fixed positions for the atoms as there are in a crystal lattice. The ability of the atoms to change position is measured by the viscosity of the liquid, which can range from very low to extremely high. At the two extremes are a gas and a solid. A gas is a liquid with very low viscosity, and glass is a liquid with very extremely high viscosity. The density of a gas can be defined by its total mass and the volume of its container.

The acoustic properties of a material depend on its density and the long-range coupling constants between its atoms.

The long-range correlations in an acoustic wave result in many atoms in a small region being displaced in the same direction from their equilibrium positions. This displacement is a local dynamic strain in the crystal; the strain's direction and magnitude are constantly changing as the atoms move. When the atomic motion is pseudo-oscillatory, so is the strain. An acoustic wave is an oscillating strain moving through a material. Because stress and strain are always directly related in a material, there is also an oscillating stress field. Therefore, an acoustic wave can be described as either a dynamic stress or strain field in a material.

2.3. Wave Motion

The most familiar depiction of a wave is a sinusoidal curve such as shown in Figure 2-1a. The amplitude oscillates between positive and negative limits at a fixed rate, known as the frequency, and the curve extends indefinitely. This curve can be plotted equally well as a function of space or time. In a medium, a wave has both a spatial and a time component. An equation for such a curve is

$$Y = A \sin(\omega t - kx) \qquad \textit{and} \qquad v = \lambda \upsilon \qquad (2.1a, 2.1b)$$

where A is the amplitude; ω is 2π times the frequency, υ; and k, the wave number, is 2π over the wave length, λ. The frequency, wave length, and wave velocity, v are related by equation 2.1*b*. The wave described in equation 2.1*a* propagates in one direction only. In three dimensions, the wave front, which is a surface of constant phase for the wave, is a plane perpendicular to the X axis. Such a wave is known as a plane wave. Most waves originating at a point in an extended medium initially have a spherical wave front. However, at some distance from the point of origin, the spherical surface will approximate a plane over a small area. For simplicity, we will assume plane waves for the rest of this discussion.

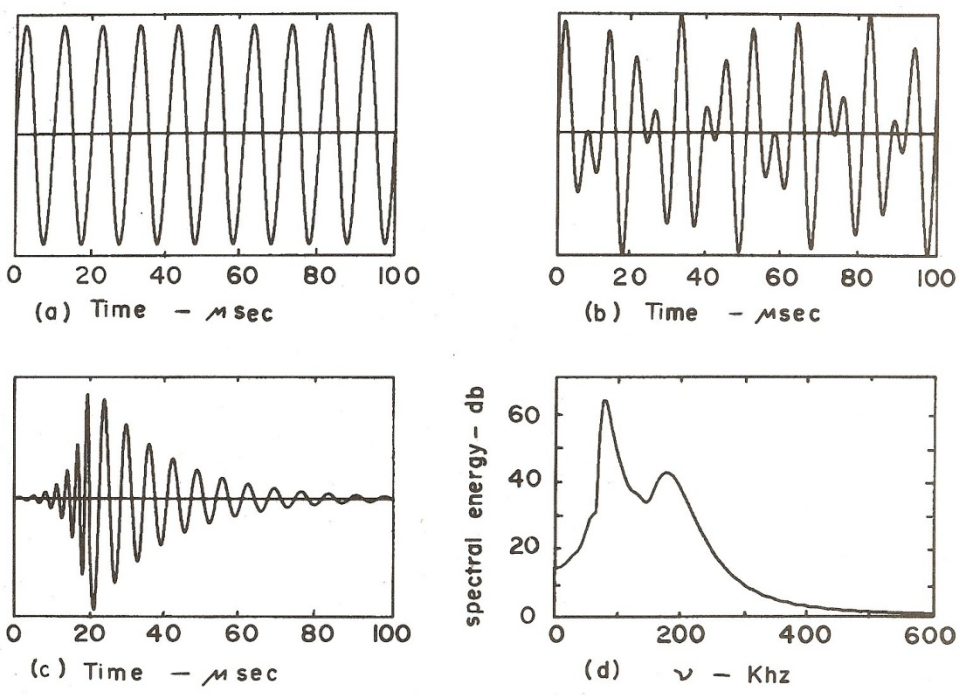

Figure 2-1. (*a*) simple sine wave, (*b*) sum of two sine waves, (*c*) transient wave, (*d*) spectrum of transient wave

If two waves exist in a medium simultaneously, their amplitudes will add algebraically. Fig.2-2 shows the sum of two waves

$$Y = A_1 \sin \omega_1 t + A_2 \sin \omega_2 t \qquad (2.2)$$

where only the time component is plotted for clarity. Thus the sum of simple waves can represent a complex wave form. It has been long known that any arbitrary transient function which does not contain a discontinuity can be represented by an infinite sum of sinusoidal curves known as a Fourier series. One form of such a series can be written as

$$f(t) = A_o/2 + \Sigma A_n \sin (n\omega_n t + \alpha_n) \qquad (2.3)$$

where A_o and A_n are the amplitudes of the sine curves, the ω_n are the frequencies, and the α_n are the phases. The Fourier series does not dictate that the curve or wave form be continuous. A transient wave such as that shown in Fig. 2-1(*c*) can be described by a Fourier series. A useful method of analyzing a wave is to look at its frequency components. A plot of the square of the amplitudes of the frequency components, A_n in equation 2.3, against the frequency, υ, is known as the frequency spectrum of the wave. Fig. 2-1(*d*) shows the spectrum for the wave shown in Fig. 2-1(*c*).

2.4. Acoustic Media

An acoustic wave exists only in a material, whether a solid, liquid, gas or plasma. The material's characteristics determine the wave's velocity. The stronger the force between neighboring atoms, the more closely coupled will be their motion. On the other hand, the larger the mass of the

atoms, the more force must be applied for the same acceleration. Because a wave is a synchronized movement of a large number of atoms, it is actually the density of the material, ρ, rather than the mass of the individual atoms which governs wave motion. Thus the wave velocity should be directly proportional to the atomic restoring force between the atoms or molecules, and inversely proportional to the density. The actual relationship is

$$V_i = \sqrt{C_i/\rho} \tag{2.4}$$

where V_i is the velocity for the particular type of wave and C_i is known as the elastic constant for that type of wave. The elastic constant is a measure of the strength of the coupling between atoms for that particular kind of motion. Different relative motions of the atoms will have different values of the elastic constant. Another property of the material is the characteristic impedance, defined by equation 2.5, as follows:

$$Z_i = \rho v_i = \sqrt{\rho C_i} \tag{2.5}$$

The reflection and transmission of acoustic waves at an interface between two materials depend on the characteristic acoustic impedances of the two materials. This dependence is given in equation 2.10. Acoustic velocities, acoustic impedances, and densities for some materials often seen in acoustic emission tests are given in Table 1.

2.5. Types of Acoustic Waves

The path traced out by a particle under the influence of an acoustic wave can generally be represented by an ellipse with one of its axes oriented along the direction of the wave's travel. The type of wave in bulk materials is determined by the relationship between the average particle motion and the direction of travel of the wave. For materials with boundaries, the exact details of the wave and particle motion will be determined by the materials properties, the physical geometry of the sample, and the frequency of the wave.

Table 1. Acoustic velocities and impedances for longitudinal, shear, and Raleigh waves for several materials

Material	V_l	V_s	V_r	ρ	Z_l	Z_s	Z_r
Units	mm/μsec	mm/μsec	mm/μsec	mg/mm3	mg/mm2μsec	mg/mm2μsec	mg/mm2μsec
Aluminum	6.42	3.04	2.87	2.70	17.30	8.20	7.70
Brass	4.70	2.11	1.99	8.60	40.60	18.30	17.10
Steel	5.94	3.25	3.03	7.80	46.50	25.40	23.60
Nylon	2.62	1.07	1.01	1.11	2.86	1.18	1.12
Lucite	2.68	1.10	1.04	1.18	3.16	1.30	1.23
Water	1.50	-	-	1.00	1.50	-	-
Air	0.33	-	-	0.00123	0.0004	-	-

Waves traveling through an extended medium (one whose dimensions are much larger than the acoustic wave length) are called bulk waves. The two types of pure bulk waves are longitudinal (compressional) and shear (transverse) waves. In both these waves, the minor axis of the elliptical atomic paths collapses toward zero, resulting in an approximate linear oscillatory

motion. For longitudinal waves, the average motion of the atomic paths in a region of the material is parallel to the direction of the wave propagation; shear waves have the average of this motion perpendicular to the direction of propagation. (The motion of atoms around their equilibrium position is very complicated with much higher frequency components than acoustic waves. The acoustic waves are averages over a very large number of atoms in the lattice. The average acoustic motion will be ellipses around the lattice position, but there is no requirement that the axes of the ellipse correspond to symmetry directions in the lattice). Particle motion in longitudinal and shear waves are illustrated in Figures 2-2(*a*) and 2-2(*b*). Since the relative motions of the particles in these two waves are different, the elastic constants and the wave velocities, therefore, also differ. Generally, the shear velocity is slightly greater than one half of the longitudinal velocity. Waves often have both shear and longitudinal components with each component traveling at its own velocity. In a non-attenuating, non-dispersive medium, a transient wave—sampled at some distance from its point of origin—may appear to be two separate waves, one longitudinal and one shear, as illustrated in Fig. 2-3.

The anisotropy of the coupling forces between atoms at the surface of a bounded solid will produce additional types of waves. A surface wave has its maximum amplitude at the surface of the solid; its amplitude decreases with distance from the surface. The plane of the particle motion ellipse can be either parallel (Love waves) or perpendicular (Rayleigh waves) to the surface. However, because most acoustic emission sensors detect

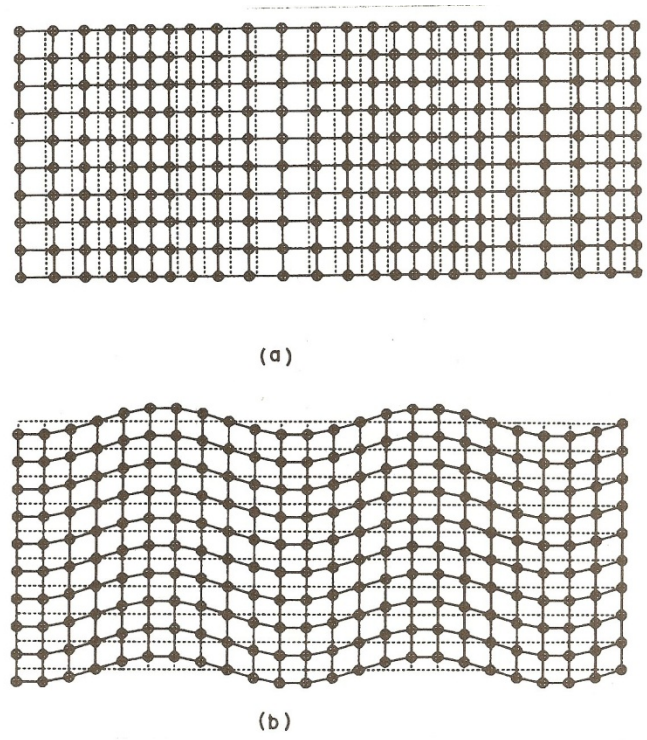

Figure 2-2. Particle displacement for Bulk acoustic waves, (*a*) compressional wave, (*b*) shear wave

motion perpendicular to the surface, the parallel component is seldom seen. The velocity of Rayleigh waves is slightly lower than the shear velocity. If the solid is bounded by two surfaces so that it is a plate, and the thickness of the plate is on the order of a few acoustic wave lengths

or less, plate waves (Lamb waves) can occur. A plate wave is essentially two surface waves synchronized either symmetrically or antisymmetrically. Particle motions in Rayleigh waves and plate waves are illustrated in Fig. 2-4.

Bulk waves, surface waves, and plate waves are the most important types of waves seen in the field of acoustic emission. However, these are not the only types of waves found in solids. In general, bounded solids of moderately symmetrical geometry can support unique types of waves.

2.6. Dispersion and Group Velocity

The velocity defined in 2-4 is the phase velocity. For unbounded media and surface waves on a single surface, this wave velocity is independent of frequency. By contrast, all waves traveling in bounded media (where the physical dimensions are within an order of magnitude of the acoustic wave length) are dispersive, that is, the phase velocity is a

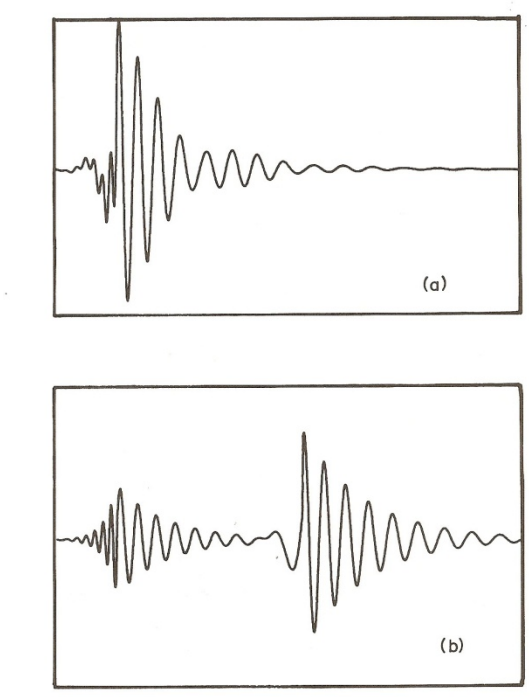

Figure 2-3. Waveform with compression and shear wave (*a*) at origin, (*b*) some distance from origin

function of frequency. Fig. 2-5 illustrates this principle, showing the frequency dependences of the velocities for symmetric and anti-symmetric plate waves Dispersion would have little effect on continuous waves. However, acoustic emissions are packets of waves which can be thought of as a superposition of continuous waves, as shown in equation 2.3. If each wave train, making up the packet, travels at a different velocity, the wave packet will change shape as it travels through the medium. As a result, the same acoustic emission may look quite different when detected by the same sensor at different positions. Energy in a wave packet travels not at the phase velocity, but at the group velocity. The phase velocity can be defined by rewriting equation 2.4 as

$$V_p = \omega/k \qquad (2.6)$$

while the group velocity is defined as

$$V_g = d\omega/dk. \tag{2.7}$$

In the absence of dispersion, these are the same velocity, but in most bounded solids the group velocity will be less than the phase velocity. A frequency dependent velocity can have real effects in acoustic emission when one is attempting source location by measuring the differences of arrival times at two or more sensors.

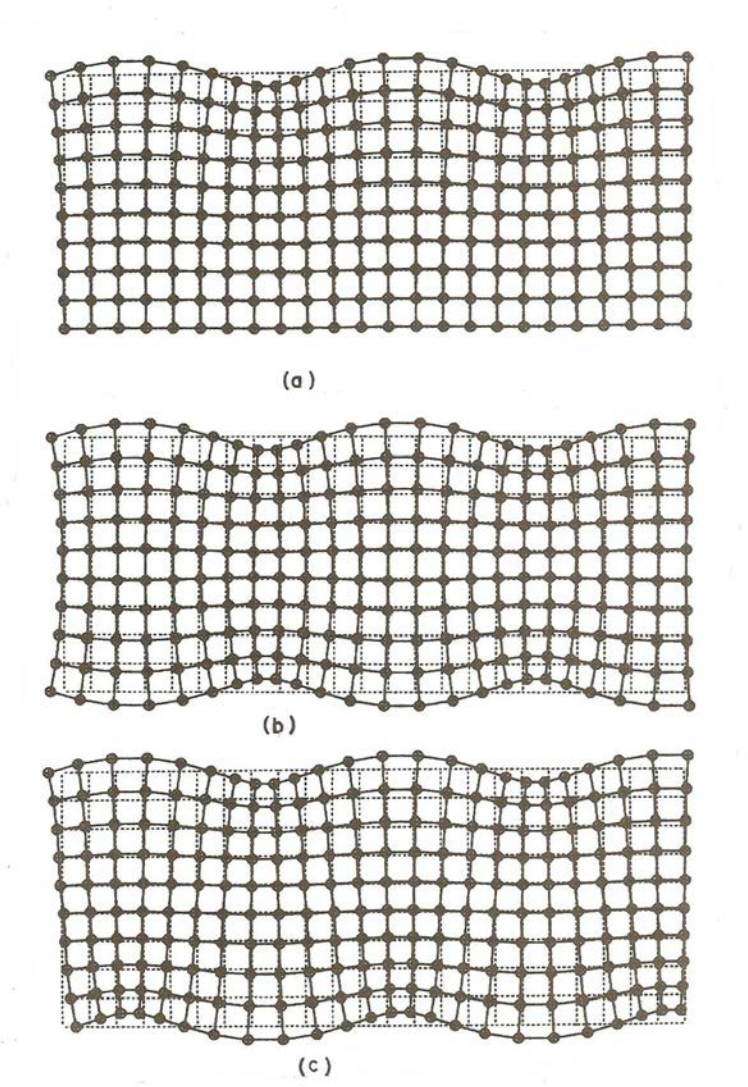

Figure 2-4. Particle displacements for acoustic waves: (*a*) Rayleigh Wave, (*b*) Plate wave, first symmetric mode (*c*) Plate wave, first antisymmetric mode

2.7. Attenuation

A wave packet is generated with a well-defined energy. As the packet propagates away from its source, the energy content will remain constant in the absence of any dissipative mechanisms.

However, if the wave front of the packet is expanding, the energy per unit area on the wave front must decrease to conserve the total energy on the wave front. The rate of this decrease will depend on the geometry of the medium. In three dimensions, the energy per unit area will decrease as the square of the distance from the source, while in two dimensions the energy per unit area will decrease linearly with this distance. If the packet is confined to one dimension, as in propagation down a rod, the energy per unit area will be independent of the distance from the source. Normally, in the context of acoustic waves, one assumes a plane wave traveling in only one dimension. Therefore this geometrical effect on the wave packets' energy is ignored. However, in an acoustic

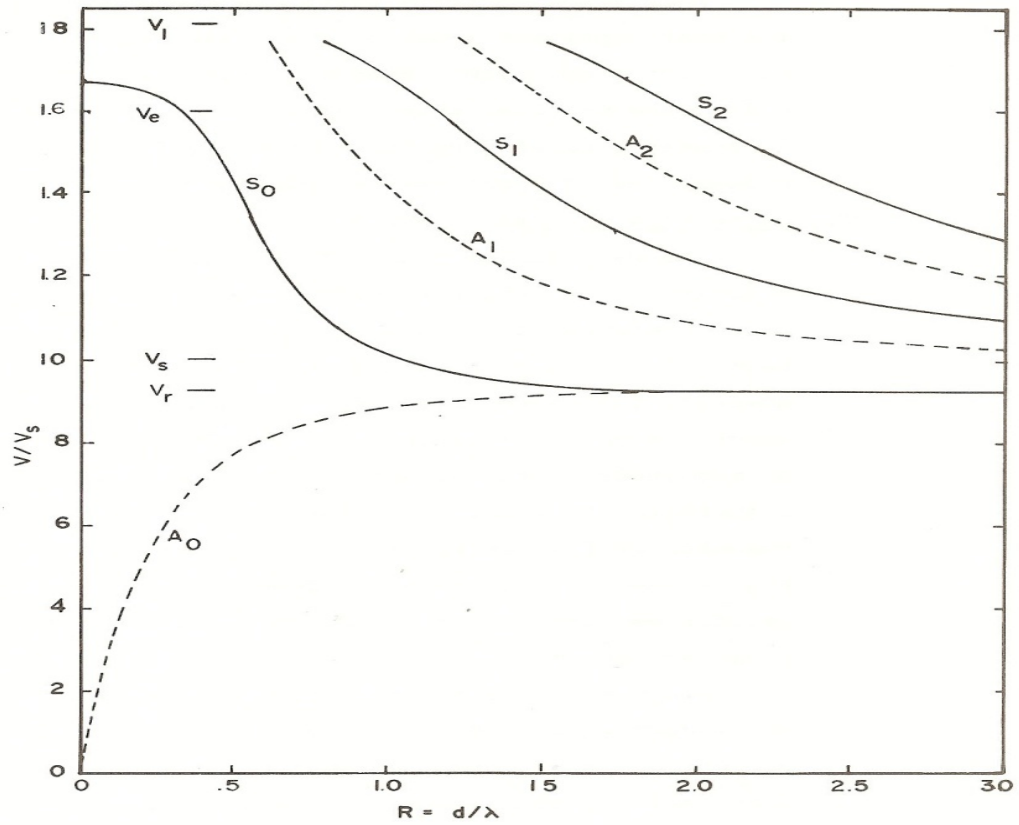

Figure 2-5. Phase velocities for different plate wave modes plotted against the ratio of plate thickness to acoustic wavelength. Plotted for steel with a Poisson's ratio of 0.28. The longitudinal, extensional, shear, and Raleigh wave velocities are shown.

emission test, where neither the location of the source nor the geometry of the sample are under the investigator's control, this geometrical effect should be considered in any attempt to measure the energy of the generated wave packet. The attenuation of a plane wave arises from dissipative mechanisms or scattering as the wave propagates. In a homogeneous medium, these losses usually occur as a fixed percentage of the wave packet energy per unit length of travel. Mathematically, this is an exponential decrease in the wave amplitude with distance that can be expressed as

$$A = A_o e^{-\alpha x} \qquad \text{or} \qquad A = A_o e^{-\beta t} \tag{2.8}$$

where α is an attenuation constant per unit length, and β is an attenuation constant per unit time. The two constants are related by the acoustic velocity as shown by

$$\beta = \alpha V \tag{2.9}$$

Both forms of the attenuation constant are seen in the literature.

Most of the many types of acoustic attenuation mechanisms have some form of frequency dependence. Fortunately, in the normal acoustic emission frequency range of 50 kHz to 1.0 MHz, both the frequency dependence and the magnitude of many of these attenuation mechanisms are small in metallic structural materials. However, in composites, geological materials, and concrete the attenuation can be a severely limiting factor in acoustic emission tests, often restricting the useable frequency range to 100 KHz and below.

2.8. Interfaces, Reflection, Transmission, and Mode Conversion

If a plane wave strikes a surface between two materials with different acoustic impedances, part of the wave will be reflected and part transmitted. The intensities of the reflected and transmitted components are given by:

$$A_t = 4Z_1Z_2/(Z_1 + Z_2)^2$$

$$A_r = [(Z_1 - Z_2)/(Z_1 + Z_2)]^2 \tag{2.10}$$

where the Z_i are the acoustic impedances of the materials. These equations are symmetrical, i.e. it does not matter in which medium the wave is traveling when it hits the interface. The differences in acoustic impedances can result in large differences in the acoustic intensities transmitted through interfaces. For example, the transmitted intensity of longitudinal waves is 78% for a steel-aluminum, 12% for a steel-water, and 0.004% for a steel-air interface.

When a plane wave strikes the interface, the angles of the reflected and transmitted waves are governed by Snell's law

$$\sin \theta_1/V_1 = \sin \theta_2/V_2 \tag{2.11}$$

where θ1 is the angle of incidence, θ2 is the angle of reflection or refraction, and the Vi are the velocities in the materials. In equation 2.11, a transmitted velocity is positive and a reflected one, negative. The particle motion anywhere on a wave front of a plane wave is the same. It wants to remain the same even when the wave passes an interface. However, at an interface, the direction of propagation will change even though the particle motion does not. For a wave perpendicular to the surface (θ1 = 0o), this results in a phase change of l80° in the relative motion of the particle to the wave direction without changing the character of the wave. For non-perpendicular angles of incidence, the reflected and transmitted waves will have both longitudinal and shear components (unless the particle motion is parallel to the interface) because of the change in the angle between the particle motion and the propagation direction. This is illustrated in Fig. 2-6. The process of generating both modes of bulk waves upon

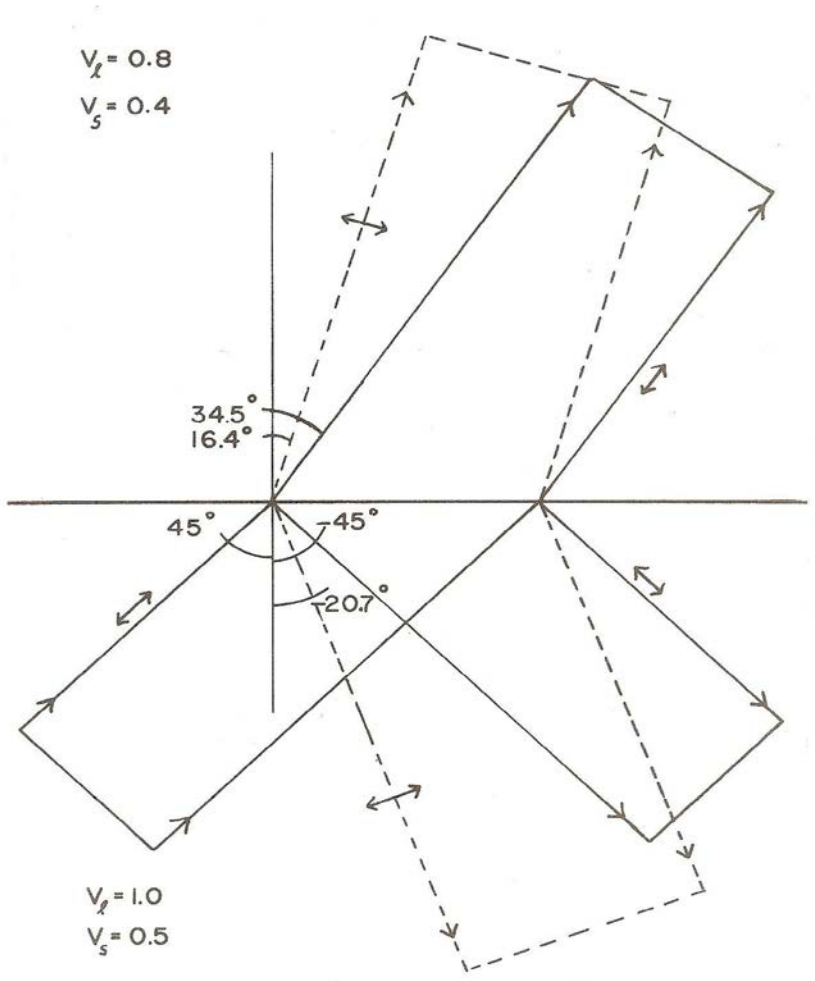

Figure 2-6. Reflected and transmitted waves across an interface. The incident wave is a longitudinal wave with an angle of incidence of 45°. The double arrows show the direction of particle motion associated with each wave.

reflection or refraction is known as **mode conversion**. In acoustic emission, where there is no control of the wave path, almost inevitably the wave reaching the sensor is composed of both longitudinal and shear components, no matter what its original polarization was. In most situations, surface waves are also present. Since mode conversion occurs at almost every reflection, it is an almost continuous process as the wave propagates in a bounded medium. Because of this continuous transformation between modes traveling at different wave velocities, the transient wave form will lengthen in time as it travels instead of dividing into separate longitudinal and shear components as shown in Fig. 2-3.

2.9. Resonance

The phenomenon of resonance occurs with reflected waves and regular geometries. Consider placing a plate of one material into another material, such as a steel plate submerged in water. When an acoustic wave is directed at it, there will be transmitted and reflected waves at each interface. Figure 2-7*a* shows how the waves will bounce back and forth in the plate. The number of reflections will depend both on the acoustic impedances of the steel and water, and the

attenuation in the steel. If the plate is one half of a wavelength thick, as shown in Fig. 2-7*b*, each reflected wave will be in phase and the strains will algebraically add.

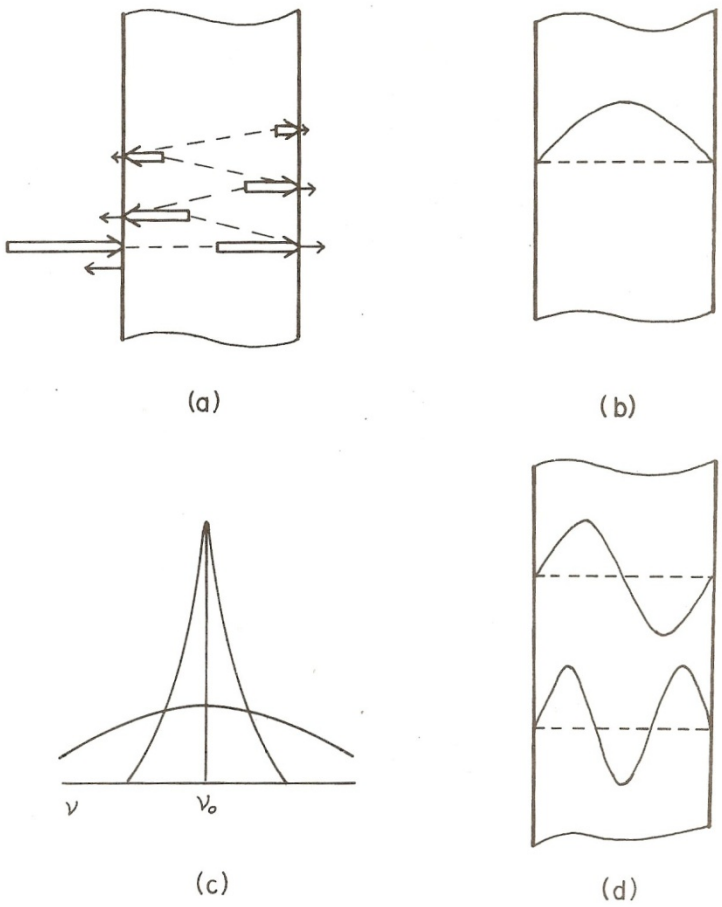

Figure 2-7. Reflected and transmitted waves inside a plate immersed in water. (*a*) Successive reflections have been displaced for clarity. (*b*) Strain in a plate one half wavelength thick. (*c*) Amplitude as a function of frequency in the plate for high and low Q materials. (*d*) Strain in a plate one wavelength and one and one half wavelength thick.

If there are a great many reflections, the peak strain can reach a very high level. If there are only a few reflections, the amplitude of the peak will be much less, and the peak will spread over a wider frequency range. The frequency of this wave need not be exactly that of a half wave length to get some re-enforcement; however, the greater the number of reflections, the narrower will be the allowed frequency range at maximum strain, and the larger this maximum strain will be. This is illustrated in Fig. 2-7*c*. The sharp high amplitude peak is said to have a high Q, where Q is the per-cycle ratio of energy stored to energy dissipated. This increase of the stress or strain level in a material at a half-wave thickness is known as a resonance; υ_o is the resonant frequency. From Fig. 2-7*b*, we see that at resonance, the average strain throughout the plate is a maximum. Resonances can occur wherever a regular geometry allows acoustic waves to reflect in such a way that the strains from several reflections of the wave are superimposed. In piezoelectric crystals, very high Q resonances allow precise generation of single frequency waves.

3.0 CHAPTER 3

3.1. Detection of Acoustic Emission

3.1.1. Sensors

A sensor is a device which generates an electrical signal when it is stimulated by an acoustic wave. Acoustic emission (AE) sensors can be based on several physical principles. The signals can be generated by electromagnetic devices such as phonograph pickups, capacitive microphones, magnetostrictive devices, piezoelectric devices, and by the use of laser interferometers to detect the surface displacement of the sample. The exact relationship between the characteristics of the wave and those of the signal will depend on both the sensor and the wave. An ideal sensor would produce a voltage-time curve identical to the amplitude-time curve of the wave at the point where the sensor is located. Although no sensor approaches this ideal, for certain types of acoustic waves, laser interferometry will come close. Many available sensors operate quite well for specified types of waves over limited ranges of parameters. Because of the wide range of frequencies and different acoustic modes contained in most acoustic emission signals, almost any sensor can detect some AE. However, an optimal sensor will always improve the data and is often the difference between a successful or unsuccessful test or experiment, especially where low amplitude emissions are involved. For use in NDT, most AE sensors are piezoelectric; the rest of this discussion will be limited to such devices.

3.1.2. Piezoelectricity

Piezoelectricity [5] is the name given to the coupling between strain and electric polarization which occurs in many crystals. This geometrical effect occurs only in materials that lack a center of crystal symmetry. This is not a severe restriction as 2l of the 32 classes of crystal structure lack a center of symmetry. In such crystals, a strain will shift the centers of positive and negative charge distribution so that they no longer coincide. This shift produces an electric dipole moment throughout the crystal. The polarization of a crystal is defined as the dipole moment per unit volume. When a polarization exists in a non-conducting crystal, electric charges will appear on certain surfaces. Conducting electrodes on these surfaces allow the measurement of the charge which is directly proportional to the strain. The effect is symmetrical because application of charges to the electrodes changes the strain. Since the stress and strain fields in a material are directly related, the piezoelectric effect can be defined equally as the coupling between the stress and the polarization in a crystal. The exact stress or strain which is measured (or generated) can be chosen based on careful selection of the crystal surfaces to be electroded. In any physical measurement, a linear output is highly desirable. That is, the output signal must differ from the input signal only by the same multiplicative constant over a wide range of amplitudes. The piezoelectric can fulfill this requirement over nine orders of magnitude.

Initially, all piezoelectric devices were made from single crystals. The most useful of these were quartz, Rochelle salt, and ammonium dihydrogen phosphate. Later, a class of materials known as ferroelectrics (piezoelectric materials which have a polarization even in the absence of a strain) were investigated and found useful. Ceramics made of ferroelectrics could be given a uniform direction of polarization similar to that found in a piezoelectric crystal. It became possible to produce ferroelectric ceramics with many properties superior to piezoelectric single crystals with

the result that almost all acoustic emission sensors today are made from a variety of ferroelectric ceramics.

3.1.3. Size Effects

An infinitesimal piece of piezoelectric material with many different sets of electrodes totally embedded in a sample would come close to the ideal sensor. However, when we scale up the piezoelectric to a manageable size, placing one set of electrodes on the outside surface of the sample, we rapidly depart from that ideal. The physical size of the sensor results in two main effects, resonance and strain averaging. Both can become important when the physical dimensions of the sensor approach or exceed the wavelength of the acoustic wave. Since the output of a piezoelectric crystal is proportional to the strain (and proportional to the average strain for a crystal of finite dimensions), the maximum output of a sensor occurs at its resonant frequencies. The fundamental resonant frequency of a plate occurs when the plate thickness is one-half wave length as shown in Fig.2-7b. The reflected wave is in phase with the incident wave at the surface and the strains add. If the frequency is increased until there is one full wavelength in the crystal, there will again be strain re-enforcement due to the reflected waves. However, we can see in Fig. 2-7d that while the strain level may be very great at this frequency, $2\upsilon_o$, the average strain over the crystal exactly cancels so that the output of the sensor is zero. Increasing the frequency to $3\upsilon_o$, we see 1.5 wavelengths in the crystal and re-enforcement again occurring. The average strain over two-thirds of the crystal now cancels out, but the average strain over the last third reaches a maximum. The result is that a piezoelectric sensor will have a maximum output whenever the thickness, d, is

$$d = (2n - l)\lambda/2 \qquad (3.1)$$

and no output when

$$d = n\lambda \qquad (3.2)$$

Thus a sensor can be operated either at its fundamental frequency, υ_o, or its harmonic frequencies $n\upsilon_o$ where n is odd. The Q of the transducer depends only on the number of reflections in the sensor; therefore, the Q is independent of the harmonic at which the sensor is operating, as long as the material of the sensor does not show a frequency dependent attenuation. Also, the sensor will always have an output at frequencies below the fundamental frequency, υ_o. At frequencies less than about $3\upsilon_o/4$, the resonance will have no effect and the output will be essentially independent of frequency. In reality, a material cannot be strained in one dimension without producing strains in other directions, as shown in Fig. 3-1a. Many acoustic emission sensors use this to get a maximum response, using a piezoelectric element in the shape of a squat cylinder. A wave with a vertical displacement on the cylinder face will excite the radial resonance. This resonance will then give a large output signal. This type of sensor is a very sensitive detector of acoustic emission. However, it should not be used to measure the frequency spectrum nor the actual wave form of the acoustic wave since this cross coupling of vibration modes can give a distorted representation of the wave

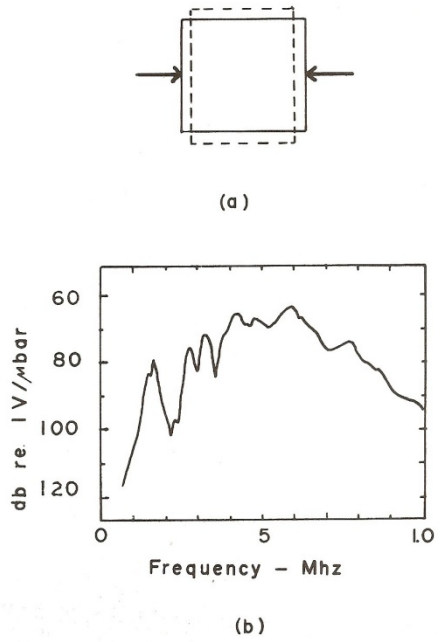

Figure 3-1. (*a*) Deformation of a material showing multiaxial strain resulting from uniaxial force. (*b*) spectral response of an acoustic emission sensor

Piezoelectricity is quite complex. A large part of its history in acoustics has been a search for particular crystal orientations where only certain strains will generate charge on a pair of electrodes. Modern acoustic emission sensors, made of polarized ferroelectric ceramics, also suffer from multiple resonances. However, because the ceramics have an intrinsically low Q, neither the peaks nor valleys are especially sharp. Thus, most sensors have a broad but highly "colored" spectral response curve as shown in Fig.3-1*b*.

In addition to resonance effects, there is another important aspect of strain averaging by a sensor. Fig.3-2a shows a block with a sensor mounted on it. If the sensor is excited with a compressional wave moving perpendicular to its surface, the entire sensor face will move in phase. Excluding resonances, the average strain in the sensor will be independent of frequency. Next, consider a Rayleigh wave which is traveling parallel to the sensor face and has the particle motion perpendicular to the sensor face. In this case, the strain distribution in the transducer will vary as a function of distance along the wave. Fig.3-2b shows the strain variation where the diameter of the sensor is less than $\lambda/2$. Here the output is still proportional to the amplitude of the wave. In Fig. 3-2c, the diameter of the sensor is larger than the wavelength. In this case, for every complete wave-length under the sensor, the strain averages to zero. Only the extra fraction of the wavelength under the sensor contributes to its output. This averaging essentially reduces the effective area of the sensor, and the higher the frequency, the greater the reduction. Additionally, at certain frequencies, depending on the shape of the sensor and the acoustic velocity of the sample, the total strain averages to zero. These effects are illustrated in Fig. 3-2d where the response for this type of surface wave is plotted for a sensor with a flat frequency response to compressional waves perpendicular to its face. The high frequency response of such a sensor is going

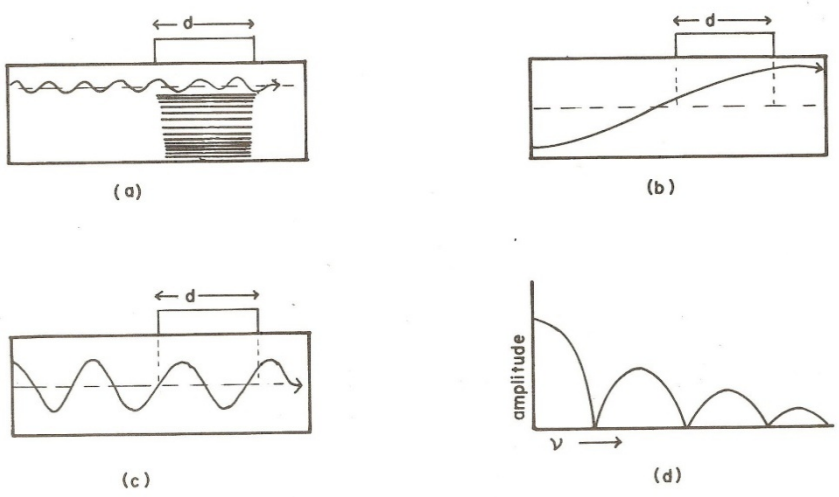

Figure 3-2. (*a*) Sample block with a sensor mounted on one side, a compressional wave is shown traveling perpendicular to the sensor face and a Rayleigh wave travelling parallel to the face. (*b*) Instantaneous strain on the block's surface from Rayleigh wave with wavelength much greater than sensor diameter. (*c*) Strain on surface from Rayleigh wave with wavelength shorter than sensor diameter. (*d*) Sensor output as a function of frequency for Rayleigh waves with equal amplitudes.

to depend drastically on the angle of incidence with which the wave strikes the sensor. This averaging effect depends on the acoustic wave-length in the material. Therefore, the sensor response not only is going to vary with frequency and angle of incidence, but also it is going to vary when used with different materials. The best answer to this problem of averaging several wavelengths of sound over the surface of the sensor is to make the sensor physically small. For steel, a 3mm diameter sensor should work reasonably well below 500 kHz. The inevitable tradeoff is that the smaller sensor has a lower capacitance and thus, as will be discussed later, a reduced effective sensitivity.

3.1.4. Couplants

We have assumed to this point that the sensor has simply been placed on the surface of the material containing the acoustic wave. When this is tried, it is found that the sensor produces a very weak signal. If a thin layer of a fluid is placed between the sensor and the surface, a much larger signal is obtained. This fluid acts a couplant that ensures good contact between two surfaces on a microscopic level. The use of some type of couplant is almost essential for the detection of low level acoustic signals. Physically, this can be explained by looking at the acoustic wave as a pressure wave transmitted across two surfaces in contact. On a microscopic scale, the surfaces of the sensor and the material are quite rough; they actually touch in only a few spots when they are in contact. Stress is force per unit area and the actual area transmitting a force is very small. If the microscopic gaps are filled with a fluid, the pressure will be uniformly transferred between the surfaces. For a shear wave with a variable strain component parallel to the surfaces, very little strain will be transferred between the surfaces because of the few points of actual contact. In this case, filling the gaps with a low viscosity liquid will not help much since such a liquid will not support a shear stress. However, a high viscosity liquid or a solid will help transmit the parallel strain between surfaces.

Although the terms *bond* and *couplant* have been used interchangeably in many AE reports (including the author's), their meanings significantly differ. Strictly, a couplant is any material which aids the transmittal of acoustic waves between two surfaces, while a bond is a couplant which physically holds the sensor to the surface. For example, water is a couplant, but cured epoxy resin is a bond. Many problems have come about from using a bond in an inapplicable way. If a rigid bond is used to attach a sensor to a sample which elastically deforms during the test, the normal result is a broken bond and poor or no sensitivity to the acoustic wave. Similarly, in an experiment where the temperature is changed appreciably, the use of a rigid bonding material can lead to broken bonds due to differential thermal expansion between the sensor and the sample. Bonding agents, then, must be chosen carefully, considering the compatibility of the materials under the test conditions. Usually, if the bond will hold the sensor on, it will be an adequate couplant. For a compressional wave, any fluid will act as a couplant. A highly viscous fluid will transfer some shear stress across the boundary which may or may not be an advantage. In one study [6, 7], the author tested a large number of couplants with compressional waves. Almost all couplants showed an increase in the signal strength over no couplant of 30$\pm$2 dB. The variation was little more than the uncertainty of the measurement. Practically, a couplant can be a thin layer of any viscous fluid that wets both surfaces. The sensor should be held against the surface with some pressure furnished by magnets, springs, tape, rubber bands, etc. The secret is to use as thin a layer as possible. If a rigid bond is used, there must be minimal differential expansion between the two surfaces.

A flexible bond can also be used. Over the years, the author has had excellent results with GE Silicone II sealant. It is available as a clear household glue which will set up within about 12 hours when used between a one inch diameter sensor and a metal or plastic surface. In one test using this glue, a perpendicular sinusoidal force of about 100 G produced no bond failures. It is quite flexible, allowing for sensor removal from a surface with a knife blade or wood chisel slid between the sensor and the surface. In Table 2, a few commonly used couplants are listed along with the temperature range in which they can be used [6, 7].

Table 2. Some Common Acoustic Emission Couplants and their Approximate Temperature Ranges

Couplant	Approximate Temperature Range
Dow Corning V-9 Resin	~ -40^{o} C to 100^{o} C
High Vacuum Stop Cock Grease	~ -40^{o} C to 200^{o} C
Ultrasonic Couplants	Room Temperature
Petroleum Grease	Room Temperature
Dow Corning 200 Fluid	-273^{o} C to -70^{o} C and -30^{o} C to 200^{o} C
Dental Cement	~ 0^{o} C to ~50^{o} C
50 % Indium – 50 % Gallium mixture	~20^{o} C to 700^{o} C
GE Silicone II	5^{o} C to 200^{o} C

3.1.5. Temperature Effects

The temperature dependence of piezoelectricity is complicated and a detailed discussion of its effect on sensors is beyond the scope of this chapter [5]. However, certain effects can lead to problems when a sensor is used at different temperatures. First, ferroelectric materials [8], such as the PZT ceramics, have a Curie temperature above which the material transforms to another, and usually non-ferroelectric, phase. Taking a ferroelectric sensor through the Curie temperature will remove the polarization, destroying the piezoelectric properties of the sensor, and may shatter the ceramic as well. Ferroelectric sensors will usually work well up to temperatures within 50°C of the Curie temperature, if the other materials in the sensor can stand that temperature. The Curie temperatures of PZT ceramics lie between 300 and 400°C.

Ferroelectric ceramics are poly-crystalline. Each crystallite may contain one or more ferroelectric domains, i.e. regions where the spontaneous polarization is all in one direction. This polarization exists only along certain directions in the crystal structure. When the ceramic is polled, these domains are aligned, as closely as the crystal orientation allows, to the direction of polarization. Because of the random orientation of the crystallites, a fair number will have several possible orientations approximating the direction of polarization in the ceramic. Small strains may be enough to cause the domain to change orientation. Such a flip of a domain may cause a very small change in the polarization of the sensor. However, this change is the same order of magnitude as the change caused by a small acoustic wave. In general, it is impossible to distinguish an electric signal caused by a flipped domain from one caused by acoustic emission. The strain necessary to produce a domain flip can come from changing the temperature of a sensor. Thus, changing the temperature of a ceramic sensor can produce signals, indistinguishable from acoustic emission, which arise in the sensor and not the sample. Empirically, the temperature change necessary to produce appreciable amounts of these domain flip signals is around 100°C in PZT. This effect does not prevent ferroelectric ceramic sensors from being used at different temperatures, but thermal equilibrium should be achieved before data is taken. If one wishes to measure AE while changing temperature, it is recommended that ferroelectric ceramics be used only for temperature deviations of less than 100 degrees C. To measure acoustic emission over large temperature deviations, a sensor made of a single crystal, such as quartz or lithium niobate, should be used.

3.1.6. Sensor Sensitivity - Effects of Cables

The sensitivity of a sensor is governed by the intrinsic sensitivity of the piezoelectric material, the dimensions of the piezoelectric element, and the design and materials used in its case. Practically, one receives from a manufacturer a measured response curve to a standard signal and the capacitance of the sensor. This curve is often presented as if it were independent of the measurement technique. However, the sensitivity of a sensor will always depend, in part, on the equipment with which it is used. The open circuit voltage produced by a sensor is a property of the piezoelectric element and is

$$V_o(S) = Q(S)/C_o \tag{3.3}$$

where Q is the charge produced by a strain S, and C_o is the capacitance of the sensor. When connected to a preamplifier, the actual voltage across the input resistor of the preamplifier (given large input resistance) is

$$V(S) = Q(S)/(C_o + C_c + C_I) \quad (3.4)$$

where C_c is the cable capacitance and C_I is the input capacitance of the preamplifier. Acoustic emission sensors usually have a capacitance that falls between l00 and 1500 pf. Preamplifier input capacitances range between 20 and 40 pf. The capacitance per unit length of coaxial cables depends on the cables' impedance with approximate values of 30 picofarad (pf)/ft for 50 ohm cable, 20 pf/ft for 75 ohm cable and l5 pf/ft for 95 ohm cable. To see the range of this reduction in sensor sensitivity assume an input capacitance of 30 pf and 5 ft of 50 ohm cable. For a sensor with a capacitance of 100 pf, the output voltage would be $V = 0.36V_{o,}$ or a decrease in sensitivity of 9 dB. A sensor of l600 pf capacitance would have $V = 0.9\ V_{o\ ,}$ a decrease in sensitivity of l dB. Thus, the loss in sensitivity can be appreciable for low capacitance sensors. Since most of the extra capacitance comes from the cable, it is a good practice to keep the length of the cable between the sensor and preamplifier as short as possible. This is also a problem for small sensors, as the capacitance is directly proportional to the area of the disk.

3.1.7. Sensor Sensitivity - Effect of Preamplifier Noise

The spectral response curve of a sensor cable-preamplifier combination to an acoustic signal is shown in Fig. 3-3 Also shown are three response curves of the preamplifier without an acoustic signal. The exact shape of the spectral response of a sensor to an acoustic signal will

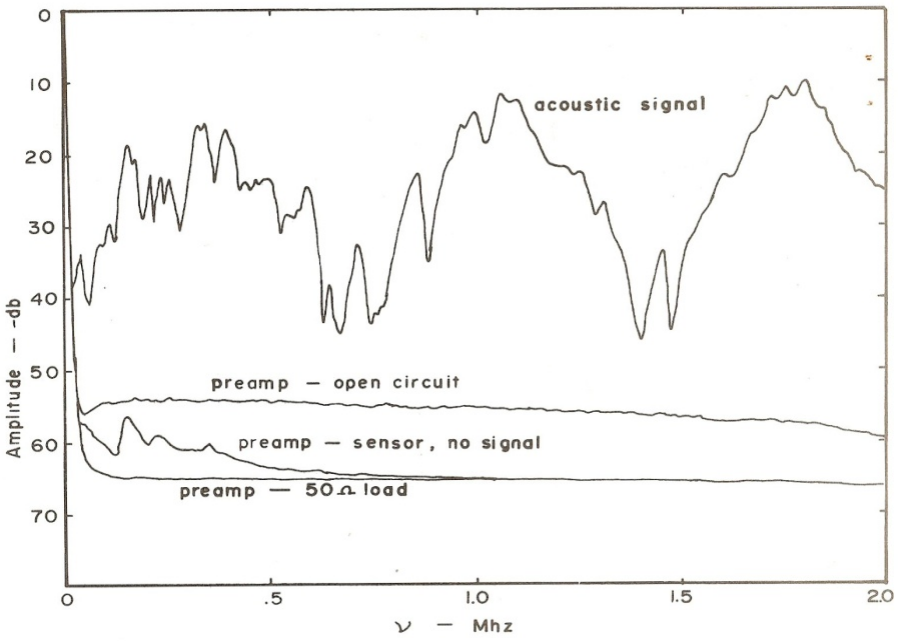

Figure 3-3. Frequency response of sensor-preamplifier combination. The top is the signal response and the rest are no signal responses with the preamp input circuit open, sensor only, or 50-ohm load only.

depend to some extent on the preamplifier input characteristics and on the cable capacitance. Too much cable capacitance will tend to short out the high frequencies relative to the low frequencies. Different preamplifiers will give different response curves even with the same cable—sensor combination, although the difference is small between most commercial acoustic emission preamplifiers. The use of preamplifiers not designed for acoustic emission can have an appreciable effect on a sensor's spectral response characteristic.

The three preamplifier spectral response curves in Fig**.** 3-3 are, from the top down, the open circuit response, the response with cable and sensor in the absence of an acoustic signal, and the response of the preamplifier with the input shorted with a 50-ohm load. The noise in a shorted preamplifier is generated by current fluctuations in the first amplification device. If the input is not shorted, the noise can be regarded as being generated by current fluctuations in the input resistor. The RMS noise voltage [9] for such a resistor is given by

$$V_n^2 = 4KTR\Delta\upsilon \tag{3.5}$$

where K is Boltzmann's constant, T is the temperature, R is the resistance and $\Delta\upsilon$ is the bandwidth of the preamplifier. If the input stage of the preamplifier is open, R is the input resistance of that stage but if there is a sensor connected, R is some equivalent resistance. The capacitance of the sensor and cable will tend to short out the higher noise frequencies. The peaks in the sensor curve in Fig. 3-3 are caused by the mechanical resonances of the sensor raising the impedance of the sensor-cable combination at the resonant frequencies. The noise level of a preamplifier is commonly specified by the manufacturers as the output RMS voltage divided by the gain when the input is shorted.

$$V_s = V_o/G \tag{3.6}$$

The noise contributed by the sensor-cable combination can be estimated from equation 3.5. A value of 295 K should be used as the temperature and the output impedance of the sensor-cable combination used as the equivalent resistance, R. This output impedance can easily be measured by a simple circuit. A variable resistance in parallel with the preamplifier input is reduced until the preamplifier output is one-half the level seen without the parallel resistor. The output impedance of the sensor cable combination is then equal to the input impedance of the preamplifier (essentially the value of the parallel resistor network formed by the preamplifier input resistance and the value of the variable resistor). For most acoustic emission sensors, this impedance will be between 50 and 1000Ω (see equation 3.5), and can be rewritten

$$V_n^2 = .004\sqrt{Z_o}\Delta\upsilon \tag{3.7}$$

where Z_o, the sensor impedance, is in Kohms and $\Delta\upsilon$ is in Hertz. The approximate noise voltage of the preamplifier–sensor–cable combination will be

$$V_{noise} = \sqrt{(V_s^2 + V_n^2)} \tag{3.8}$$

This noise voltage is measured by an RMS voltmeter that measures heating power. It assumes that the noise voltage is flat over the bandwidth, Δv. In Fig. 3-3 we saw that this is not strictly the case; the noise level at certain frequencies may be six to eight dB higher than the rest of the bandwidth. As long as the acoustic emission signals contain a large range of frequencies, these

small noise peaks should not matter, but if they are confined to one narrow frequency band and are at relatively low level, the noise peaks may present problems.

3.1.8. Sensor Calibration

All manufacturers furnish calibration curves with their sensors. The currently accepted units are dB referenced to l volt per meter per second. Many manufacturers will also furnish a calibration with dB units referenced to l volt per μbar. The acoustic signal used to calibrate the sensors may be either a surface wave or a compression wave. A typical calibration curve is shown in Fig. 3-1b. Calibration curves for the same transducer will not be the same for calibrations in velocity (meters/sec) or in pressure (μbar). Pressure is proportional to strain which is related to the surface displacement, while velocity is related to the time derivative of surface displacement. For a constant frequency the relationships are

$$V_{displacement} \approx D \sin \omega t$$
$$V_{velocity} \approx d/dt\,(D \sin \omega t) = D\,\omega \cos \omega t \qquad (3.9)$$

where D is the surface displacement and V is the surface velocity. That the velocity calibration curve is approximately the pressure calibration curve multiplied by the frequency tends to make the velocity curve seem flatter, since it does not fall off as fast at higher frequencies. In selecting a sensor, one should have some idea of both the frequency range and the type of waves to be expected. Calibration curves can then be compared, provided that they represent the same type of source and the same units.

The National Bureau of Standards [10] has developed a sensor calibration for Rayleigh waves which involves a point displacement in the center of a large steel block to produce the wave. The sensor is placed close enough to the source to allow a differentiation between the direct wave and reflected waves from the edge or the bottom of the block. The output of the sensor is digitized and the spectrum of the received wave is calculated. This spectrum is compared to that of a reference capacitive sensor placed at a comparable position on the block. (A capacitive sensor is sensitive only to the average displacement of the block surface produced by the Rayleigh wave). This calibration is valid only for waves traveling on the block's surface with a displacement perpendicular to the surface, but these are the most common waves seen in acoustic emission testing. Furthermore, the calibration is strictly valid only for steel or other materials with acoustic impedances similar to steel. However, the NBS calibrations offer a valid comparison of sensor characteristics. For the testing of most structures, the frequency and sensitivity characteristics of the sensors given by the NBS calibrations are more than adequate. However, any attempt to determine AE source characteristics from waveforms detected by routine AE sensors should include a far deeper study into the relationship between acoustic waves and piezoelectric sensors than is given here. Current studies [11, 12] indicate that the shape of the wave front, the angle of incidence of the displacement to the surface of the sensor, and even the construction details of the sensor can affect the output waveforms of the sensor.

4.0 CHAPTER 4

4.1. Instrumentation

4.1.1. Acoustic Emission Systems

Although acoustic emission instrumentation has changed drastically in the last forty years, the basic detector of acoustic waves is still a piezoelectric sensor. Analysis instrumentation was initially amplifiers, an oscilloscope, and an electronic counter. Computerized systems were then developed where signal parameters such as signal arrival time, rise time, peak amplitude, and duration were measured with analog circuits. These allowed the calculation of the locations of acoustic emission sources as well as more sophisticated displays and methods of analysis. However, they were limited by both the relatively slow processing speeds and small memories of the early computers, and the need for separate analog circuits for the detection of each desired acoustic emission parameter. Current computer systems are much faster and have far greater memory capacity. Instead of analog circuits for the acoustic emission signal parameters, they directly digitize the signals from the preamplifiers. This allows the use of any possible signal parameters in the analysis for which one can write a code. A commercial system may list twenty or more possible signal characteristics. In practice, however, the analysis of acoustic emission signals is often confined to digitized versions of the old analog parameters.

Besides speed and versatility, the new computer technology has resulted in much smaller acoustic emission systems. Twenty-four channel systems, which started out requiring at least a full instrumentation rack, now consist of three 8-channel PCI cards and a notebook computer. Eight channels on a single card is currently a reasonable limit. This limit is determined partly by the number of co-axial connectors that one can fit on the input of a card and partly by the amount of circuitry still required for each channel. At present, coaxial cables are still required between the circuit boards and the sensor-preamplifier combinations in large multi-channel systems. The use of RF broadcast connections between the sensors and the computer are limited to systems with only a few channels (part of this limitation is the need to use the same clock signal for every channel). Therefore, the rest of this paper assumes a notebook computer with a separate box containing multi-channel digital cards and coaxial cables to the sensors. Eight-channel cards are not quite as versatile as four- or two-channel cards – limitations include a slower maximum digitization rate and shorter maximum lengths for digitized signals. However, the increased versatility of the smaller cards' digitizing capability is more important in laboratory experiments than in field tests.

A large number of commercial acoustic emission systems have been manufactured. Systems that digitize the emission signals have been available since the mid-1990s. Three of the major manufacturers selling in the United States have been Physical Acoustics Corporation, Vallen Corporation, and Digital Wave Corporation. Other systems have been produced in many countries--Japan, China, Russia, England and Israel, to name a few. All of these systems perform the same basic functions although they may use different nomenclature and methods of analysis. This paper will be based on the operation of Physical Acoustic Corporation systems [19], with which the author is most familiar. It is hoped that the ideas expressed here will be fairly easy to apply to other systems.

4.1.2. System Operation

The basic measurement in a multi-channel acoustic emission system is the system time. This starts when the test starts and stops when it ends. The PAC systems use a 4.0 MHz clock giving a time resolution of 0.25 microseconds. Every time a sensor detects a signal, the exact time of arrival in test time is recorded. Every channel of the system is independent, thus if a strong electromagnetic noise signal were to hit the system, every channel could record the same arrival time. Each channel also has its own clock which starts when the trigger threshold of that channel is first crossed. This channel clock runs until the signal drops below the threshold for a predetermined time or exceeds the programmed maximum signal length. This clock is used to determine the **signal rise time** and the signal length. Each channel has a set **PDT** (peak definition time). When the signal amplitude reaches a maximum and starts to decline, the card notes the time and maximum amplitude, and then waits an additional PDT to see if the previous signal amplitude is exceeded. If it is, the measurement continues. If there is no higher amplitude signal within the PDT, the previous amplitude is the peak amplitude and the time from the signal start is defined as the **signal rise time**. As the signal continues, the card always records the time of the last threshold crossing. If there is no further crossing within the **HDT** (hit definition time), the last recorded time defines the signal length. After the HDT has been reached, the card waits until the **HLT** (hit lockout time) expires. At this point, the card is reset and ready to acquire the next signal. The HLT time prevents the channel from treating a reflection of the first signal as a new emission. However, an excessively long HLT time can prevent the capture of rapidly occurring emissions. In most AE tests, the exact values of these three times are not critical, but the values of the settings should be considered, especially if a high average repetition rate with short emissions is expected. Simultaneously with these time measurements, the card is also digitizing the signal and storing it, in case waveforms are desired.

Both the time measurements and the digitization of the emission waveform start when a preset threshold is exceeded. The digitization runs until a preset number of samples is exceeded. The digitizer is actually running continuously with the samples sweeping through the memory. When the card is triggered, the card stores the number of words set for the record length, but it starts the record some set time (say 50 to 200 microseconds) before the trigger occurred. As a result, one has a record of the waveform including 50+ microseconds before the original trigger time. Thus the actual start of the waveform can be examined, if necessary, to determine how accurately the first threshold crossing defines the leading edge of the signal. The signal length is defined by the last time that the signal crosses the threshold. However signals are often longer than the set digitized word length. Therefore the signal length is usually measured from the system clock, not from the digital record. The rise time and peak amplitude can just as well be measured from the digitized signal as from the system clock.

The shift from analog to digital acoustic emission systems was made possible by advances in signal digitizers. When the first computerized acoustic emission systems were designed, the available signal digitizers ran at speeds up to one MHz and had 8-bit words. With a sign bit, an 8-bit word gives a precision of one part in 128. This gives a dynamic range of 42 dB, a little over two orders of magnitude. Modern systems have signal digitizers which run up to 40 MHz and have 16-bit words which, at one part in 32,768, gives them a dynamic range of 90 dB or $4^{1}/_{3}$ orders of magnitude. This performance is more than adequate for the usual AE test. Most engineering materials have relatively high acoustic attenuations at frequencies above one MHz.

The acoustic attenuation of plastics and composites restricts useable emissions to below 500 kHz. The dynamic range of acoustic emissions from structural tests is usually somewhat less than 80 dB between the background noise level and the largest signal detected. The current digitizers thus have a satisfactory performance for most AE testing. One limiting factor, however, is the number of words in a digital signal record. The record length, chosen when designing the test, is subject to a hardware limit, usually between 4,096 and 16,384 words. For high digitization rates and large signals, the record length is often reached and the digital signal is truncated before it drops into the background noise. This is not typically a major problem as most of the energy in the transient signals occurs at the beginning of the record with the latter part of the transient consisting of a low amplitude exponential decay into the background noise.

The limitation on the digitation rate is set by the frequency of the acoustic emission signals emitted by the specimen. This content in turn is usually determined by the materials used in the specimen. The upper frequency of an acoustic emission event will be governed by the size of the region involved and the speed with which the movement occurs. On a microscopic scale, this can lead to quite high frequencies. However in tests involving structural materials, the detected frequencies will depend on the attenuation characteristics of the materials involved. For metals such as aluminum, steel, and titanium, frequencies up to one MHz are often detected. For lead and copper, maximum detected frequencies will be no more than 500 kHz; for plastics and composites, the maximum detected frequencies will be about 200 kHz. This maximum does not mean that higher frequencies will not be present, only that they will be minor components of the larger amplitude signals. This combined with the **Nyquist criteria** (the digital record must have at least two samples per wavelength of the highest frequency recorded to avoid inherent distortion) suggests that sampling rates of 2.0 MHz for plastics and composites and 10 MHz for metals are as high as is needed. The disadvantages of signals containing frequencies higher than half the Nyquist frequency is that these higher frequency components are aliased, or folded back, into the lower frequency range. In the worst cases, this can result in gross distortions of the original signal. If a lower sampling frequency is used, the low pass filters in the system should be set for considerably less than the Nyquist frequency.

It has been mentioned here that several acoustic emission parameters were described and used from the early days of acoustic emission, when signal shapes were confined to the face of an oscilloscope. To facilitate the discussions of acoustic emission testing in this paper, several of the terms and parameters (highlighted in **bold**) are defined and discussed, below.

A **hit** is defined as a transient signal from a sensor which rises above the **detection threshold**. Its **arrival time** is the time when the hit signal first exceeds the detection threshold. The detection threshold is set during the hardware set up. It is the value (in dB above 1.0 microvolt) at which that channel will detect a signal and trigger the signal digitizer. Normally all channels in the test have the same detection threshold, but if a channel develops a noise problem during a test, the detection threshold for that channel can be raised so that the channel sees only larger signals. The detection threshold is limited by the background noise in the system. If there is no acoustic noise in the specimen, the limit will be, at best, the noise level in the preamplifier. Equation 3-5 (in section 3.1.7) indicates that the noise signal in the input of the preamplifier is proportional to the square root of the input impedance, the absolute temperature, and the band width. For acoustic emission preamplifiers and sensors, this noise voltage will vary between, very roughly, 5 and 15 microvolts. This would suggest that for a quiet specimen, a detection threshold of 30 dB (32 μV)

would be reasonable. (The acoustic emission Halon Bottle tester uses a 25 dB threshold with a narrow bandwidth. The bottle is enclosed in a metal oven which helps reduce external RF noise.)

An **event group** is defined as a number of hits from different sensors that occur within a preset time window. This window is determined by the test engineer from the acoustic attenuation of the specimen, its geometry and the geometry of the sensor layout. Every hit is checked to see if it is in an event group or starts one. For example, to prevent several hits from the same channel during a multi-channel test of a sphere, the time window is set at the time an acoustic signal with the shear velocity (the slowest wave) takes to travel half way around the sphere. Any signal that occurs after this time, measured from the first hit in the group, will not be included in the group. An acoustic emission **located event** is defined as an event group for which the system program can calculate a location on the specimen from the arrival times in the event group. A **cluster** is a group of located events which occur in a defined region in the specimen. The area or volume of the cluster can be defined either in the post-test analysis or defined in the system program, which allows the system to identify the cluster in real time. The AEwin software can be set to identify clusters of different sizes and monitor them as to size or count content, but not **absolute energy** content.

Figure (4-1), below, shows a typical acoustic emission signal with several defined signal parameters: the **signal duration** (the time between the first and last threshold crossing), the **signal rise time** (the time between the first crossing and the time of the **signal peak amplitude**, the largest amplitude of the signal, usually given in decibels. For long signals, such as a large impact on a piece of aluminum, the time it takes for the signal to damp down to below the

detection threshold is far longer than the longest digital record available can hold. A very short

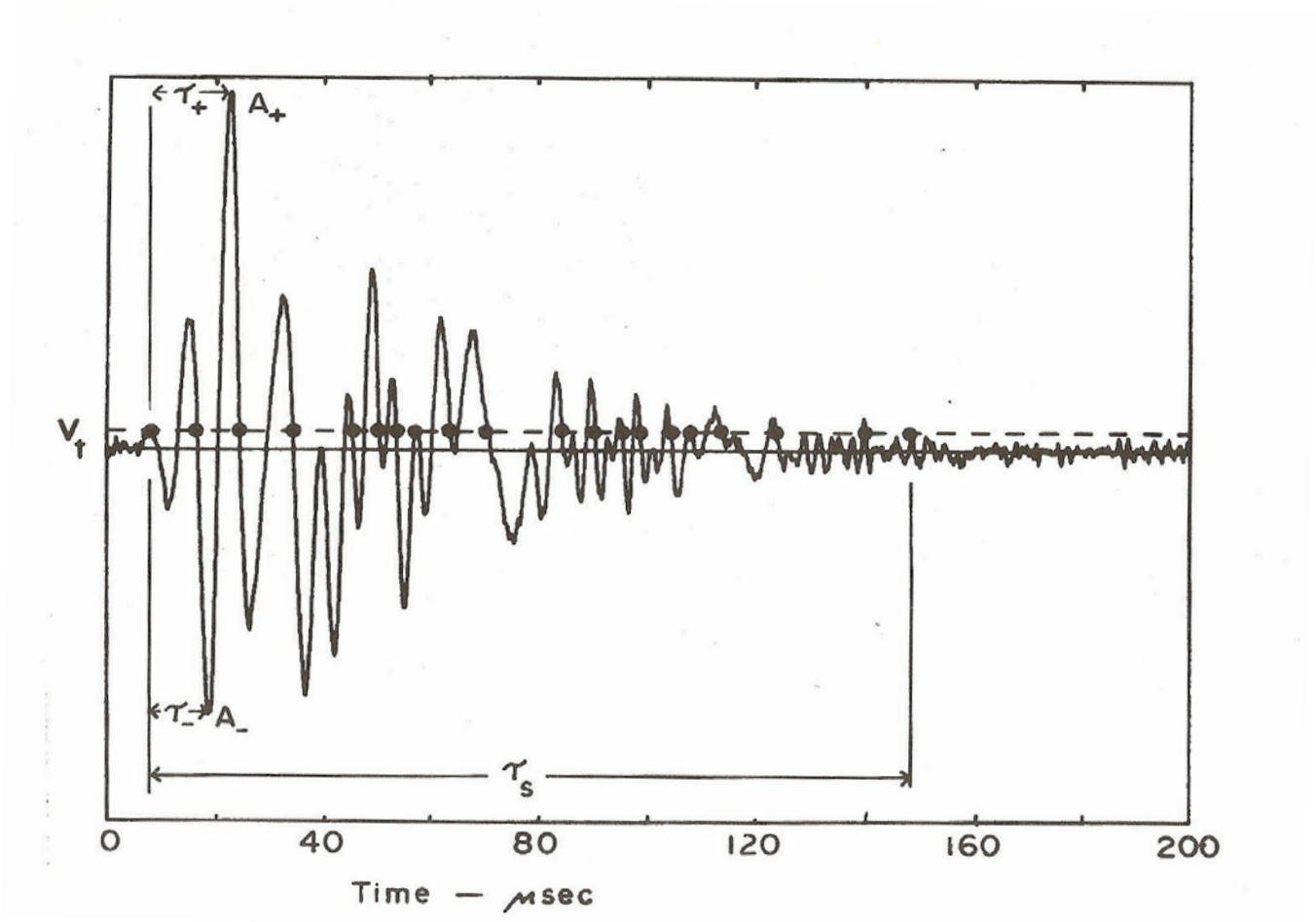

Figure 4-1. Acoustic emission signal showing the count (the number of crossings of the trigger threshold, n=20), the rise-time τ_+ , the peak amplitude A_+ and the signal duration τ_s

signal length, less than ≈ 50 μsec, indicates that the signal is probably an electrical noise spike and not an acoustic signal while a signal length greater than 10 milliseconds suggests either a frictional origin or a very low attenuation for the acoustic signal. As Figure 4-1 shows, the signal duration is very much a function of the trigger threshold as is the count. For this reason, both the count and the signal length are good qualitative measures of the amount of AE occurring, but neither should be used for quantitative calculations.

The peak amplitudes are a good indicator of how strong the emissions are. The most important property of the peak amplitude is that it is measured on a logarithmic scale. A factor of 10 in the output voltage of the sensor is equal to 20 dB in the peak amplitude. The critical factor is the difference between the channel noise level and that of the AE signals. For good location of the AE source, the peak amplitudes of the larger AE signals should be 30 dB above the channel noise level. For most tests, peak amplitudes more than 40 dB above the background noise are indications of some damage in the specimen. A reasonable place to start the trigger threshold for the system is 3 to 5 dB above the average background noise level. A good trigger level should occasionally trigger on a noise peak.

From Fig. 2-3b (above, section 2-6) which shows the time difference between peaks of an ideal signal containing both compressional and shear waves, it would appear possible to determine how far a signal had travelled from the time between the two peaks. Unfortunately, real AE signals are seldom that simple. The rise time parameter does have a use, however. If a channel is re-armed slightly after a signal has reached it, the resulting waveform is usually a decaying wave. In such cases, the rise time it often registers is the time from when the threshold is crossed to the first oscillatory peak. For normal signals the rise time will be several wavelengths long. Therefore, if the rise time is short, less than 10 to 15 microseconds, the channel likely triggered in the middle of a signal and the registered arrival time for that channel is probably wrong. All the data from that signal can be ignored unless it is a very large amplitude signal. If a signal has a very long rise time, especially greater than half the signal length, it is almost certainly not a transient; such an AE signal can also be ignored. The signal rise time can indicate whether the received signal is actually from a transient event in the sample, or if it is distorted or extraneous.

The **acoustic emission count** was one of the first parameters used in the field of Acoustic Emission. It is simply the output of an electronic counter applied to an AE signal. Every time the signal crosses a preset threshold in one direction (decreasing or increasing), a count is registered. If this count is plotted continuously, it gives a history of the emission from the specimen. If a count per unit time is plotted, one has a history of the rate of emission. One of the simplest and most useful measures of AE, it is also almost impossible to directly relate it to any physical parameter. The count depends on the detection threshold, characteristics of the sensor, the gain and bandwidth of the preamplifier, the quality of the acoustic coupling and the characteristics, and the geometry of the specimen. The one thing which can be said for the count from an AE signal is that if the signal has only a single count, it is probably electronic noise. An acoustic emission signal almost always contains several oscillations.

The **signal energy** is easy to define but hard to measure with an analog circuit. It can be defined as the integral of the voltage squared vs. time curve over the signal length. The problem with an analog measurement is the dynamic range of the signals. If an AE test has a dynamic range of 80 dB, which is relatively common, then the energy range of those signals will cover at least eight orders of magnitude. Analog circuits with that dynamic range are not common. If AE signals all had the same signal characteristics then it might be possible to design analog circuitry to measure the energy. But AE signals come in a wide variety of shapes and sizes in the same test. For a digitized signal the signal energy is defined as

$$E = (\Delta t/R)\, \Sigma_i\, V_i^2(t) = A(\Delta t/R) \qquad (4.1)$$

where Δt is the sample width in seconds, R is the resistance in ohms, $V_i(t)$ is the sample amplitude in volts, and the summation is over T, the total signal length in seconds. For a Physical Acoustics Corp. system, this is called the **absolute energy**. In the calibration of the absolute energy for a PAC system, the sum of the squares of the sample voltages, A, is multiplied by 9.31×10^{-4} to give the energy in units of 10^{-21} Joules. If A is multiplied by 6.7041×10^{-6} the energy is given in units of Mev (million electron volts), a unit the author finds more useful. The one problem with this measurement, however, is that it covers only the digitized signal length. If the transient signal is longer, the calculated energy will be somewhat less than the actual signal energy. However, most of the signal energy in a transient is near the beginning of the digital

record. The small percentage of the signal energy lost by truncating the signal is insignificant compared with the other uncertainties in the measurement of the signal energy.

It must be stressed that while the signal energy is given in physical units, it is not the actual energy of the emission, only the energy emitted by the piezoelectric sensor. The actual emission energy was radiated throughout the specimen, and only that energy actually hitting the face of the sensor is measured. The energy detected by the sensor is strongly affected by the distance between the source and the sensor. In our analyses, the absolute energies from the three sensors nearest to the emission source are summed to estimate better the actual strength of the source. This sum is graphed as energy in the analysis chapters.

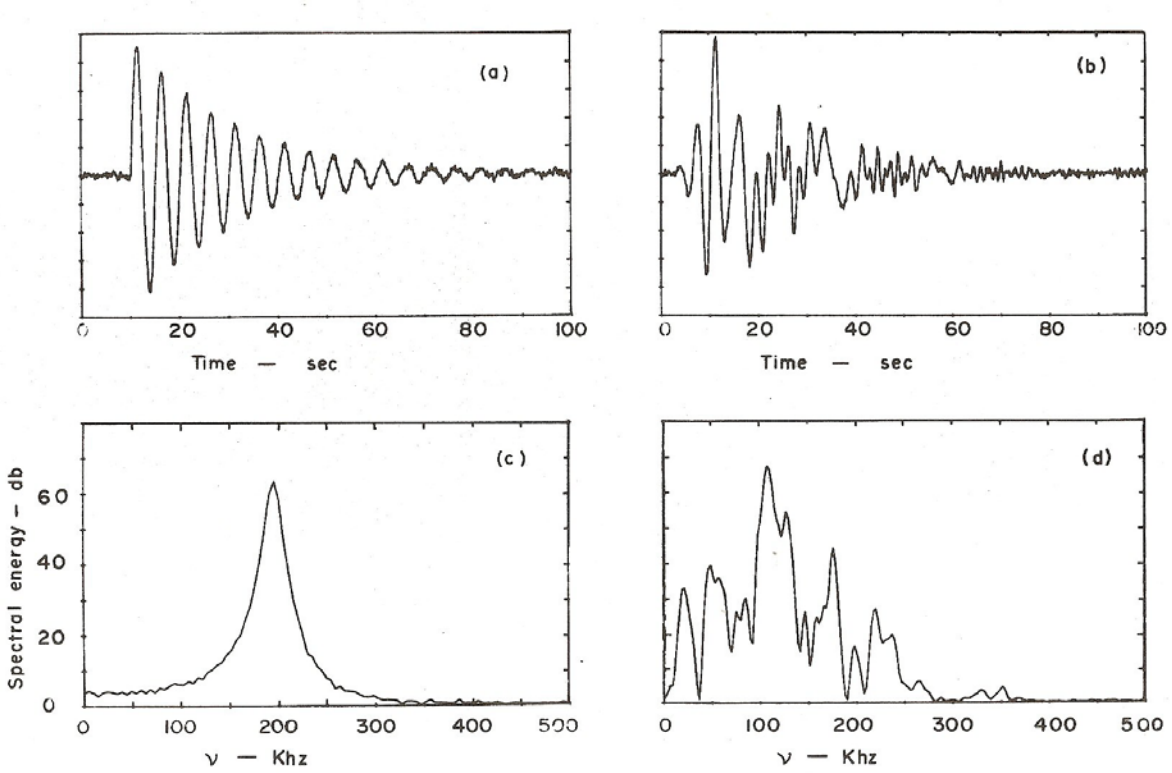

Figure 4-2. The spectra (*c*) of a damped sine wave (*a*) and (*d*) of an acoustic emission signal (*b*)

The last signal "parameter" which is useful to calculate from the digitized wave form is the **signal spectrum.** This is a Fourier Transform of the digitized signal. The signal is shown in Figure 4-2b; its spectrum is shown in Fig.4-2d. In theory, one should be able to learn a lot about the characteristics of the source from the spectrum. In practice, a back calculation to the actual characteristics of the source is almost impossible because one needs to know the response function of the sensor for the exact combination of acoustic waves which excites it. Also necessary for the calculation is the response function of the specimen for all the acoustic paths of the generated acoustic waves that reach the sensor. There have been attempts to back calculate the sensor response function in the laboratory, but these are very far from an actual test. The topic of the detailed interaction of acoustic waves and sensors has been explored in recent papers by Ono, et al. [11, 12]. Their work has shown that the subject is far more complicated than was

originally thought. The author was a far stronger advocate of spectral analysis in acoustic emission thirty years ago than he is now.

4.1.3. Noise Suppression

The defining electrical characteristics of acoustic emission signals are random occurrence in time, random frequencies, amplitudes, durations and waveforms whose sole common characteristic is that they are transients. One of the major problems in acoustic emission testing is unwanted noise**. Noise** can be defined as any signal detected by the AE system which is not a desired response to the applied stimulus. This includes all types of electronic interference and acoustic signals not produced by the stimulus as well as undesired responses to the applied stimulus. In the past, electronic noise has been a major problem. Even transient signals, if they occur fast enough, can be superimposed and appear as a continuous signal. The response to such electrical noise has been improved shielding on sensors and preamplifiers, using double-shielded coaxial cable when needed and much improved filtering in system power supplies. This has eliminated much interference from radio and television stations, ignition systems on internal combustion engines, and extraneous signals on input power lines. However, problems such as ground loops in the AE cables and multiple and poorly connected power grounds in the work facility are often encountered. Almost any industrial area can have unexpected sources of electrical noise, which would not be a problem if one were not looking for wide band signals down to the ten microvolt level.

Acoustic emission signals occur randomly and have no definite characteristics except their transient origin, so many traditional electronic methods of noise reduction are not possible. Narrow bandwidth electronics, any type of frequency locks, and predetermined time windows either do not work or eliminate real emission signals. Frequencies below 20 kHz are avoided for good reason. Most AE signals, with the exception of earthquakes, contain adequate energy above 20 kHz. It is desirable to be able to converse during a test and one does not want the local noise to be detected by the instrumentation. Radio and TV stations were once a problem, but using good coaxial cables and shielding on both preamplifiers and sensors has almost eliminated their interference. Modern AE systems have very good filters on their power supplies, but there are still situations in industrial locations where noise on the input power lines is suspect. When suspected radio frequency noise is still detected even when the sensors are in a sealed can filled with foam or, better yet, a vacuum, a good practice is to ground everything even remotely connected to the system. Still, it is possible to spend years chasing that randomly occurring signal with little success.

Electromagnetic signals are usually detected as very short, often with a single spike with a length of a few microseconds or less. In contrast, most acoustic signals have several oscillations at a minimum. Filtering out all signals with only one count usually does not remove any important acoustic signals. Another useful filter is the signal duration. Assuming that an acoustic signal has over three cycles of the dominant frequency, one could filter out any signals shorter than 10 μsec for a frequency of 300 kHz, or 50 μsec for a frequency of 60 kHz. These two filter times have worked well for the Halon Bottle tester and FRP tests discussed in later chapters.

Another problem is unwanted acoustical noise. Any two surfaces which are in contact and have the slight movement between them can generate relatively large acoustic signals that can travel

long distances in metals. Impacts on surfaces can generate large detectable signals, e.g. a rain storm hitting a railroad track a quarter of a mile from the sensor. Any test involving motion, such as rotation of a bearing or cycling of a wind turbine blade, is going to generate some continuous-type acoustic signals. In a good bearing, the normal signals will be below the 20 kHz low pass filter in the signal channel. Any bearing signals that pass this filter may indicate problems with the bearing. In fatigue cycling of FRP materials such as a wind turbine blade, large noise signals are often seen. If they are plotted against where they appear in the loading cycle, many appear in the middle of the cycle where the load is changing the fastest. This suggests that there may be some small regions of the blade which are rubbing together during the loading. On the other hand, signals from defects in the part usually appear during the rising load at or near the peak. This is where flaw growth signals should be found. Current AE systems contain provisions for an electronically controlled **voltage time gate**. This gate can be set so that the system accepts data only during the desired portion of the load cycle. In wind turbine blade fatigue tests, this gate is open only for the top ten percent of the load. This procedure has worked well to filter unwanted signals. Almost no valid AE signals are observed as the load decreases from 100% to 90%.

A final comment about noise signals: no detected signal should be removed from a data set until one has a good idea of its origin. Every acoustic signal is produced by some mechanism. In any real test, an attempt should be made to identify and understand that mechanism before signal data are discarded. Often signals can be attributed to noise only after their locations have been graphed.

5.0 CHAPTER 5

5.1. Setting up the Test and Emission System

Acoustic emission tests are performed for a variety of reasons. In this monograph, only tests of structures are considered. There are three basic types of structural tests:

1. Proof tests where the objective of the test is to prove that the structure is sound up to a proof load.

2. Failure tests where the objective is to find at what load the structure starts to fail.

3. Fatigue tests where a cyclic load is applied to the structure to obtain some idea as to what the working lifetime of the structure is.

Acoustic emission monitoring of a proof test will indicate whether the proof load itself is producing any damage in the structure. In tests to failure, whether static or cyclic, acoustic emission monitoring can indicate whether it is a sudden or a prolonged failure, and if there are several other regions which are starting to fail when the main failure takes place. Such monitoring can also provide some information on the mechanisms of the failure.

The design of an acoustic emission test involves tradeoffs in both the physical set up of the test and in the type of analysis that is used. Most of the time, the geometry and construction of the specimen and the method of applying the test stress will simplify the choices. Other limitations include the characteristics of the acoustic emission system, the number of channels in the system, and the sensors available. For clarity, various AE test topics will be discussed separately, below, although they all interact to some degree in a real test.

5.1.1. Test Assessment

The first step in setting up an acoustic emission test is to study a structure's design and function. What is its function? How well does it appear designed for that function? What is the test designed to determine? Does the proposed loading duplicate the stresses seen in actual usage? An acoustic emission test can only detect growing flaws if they are activated the same way in the test as in normal operation. If the mechanism for the test load does not correspond to the normal operation of the structure, the value of the test is questionable. The loading rate must also be considered. If the rate is too fast, the emission can swamp the instrumentation, while if it is too slow, the test can take forever. Finally what are the structural materials? Is the AE test operator familiar with them or not? If not, does any available literature provide information, such as previous AE tests on the material? Or, are there samples that could be tested? Of all these questions, the most important are the method of load application and the determination of material properties. Only then should the choice of sensors and sensor location be determined.

5.1.2. Acoustic Properties of Materials

Structural materials can be divided into five categories: metals, ceramics, glasses, composites, and wood. Composites include both metal-metal and fiber reinforced plastic materials (FRP). Wood can be treated as a complicated and non-uniform composite. Metals are generally quasi-

crystalline, composed of many small crystallites of random orientations and different compositions. On a macroscopic scale, metals are relatively homogeneous, and the acoustic wavelengths for the frequencies normally used in AE testing are much larger than the crystallites. Thus the acoustic properties of metals are averages over large number of crystallites, and will be independent of frequency and direction of propagation. These bulk properties, both acoustic velocities and impedances, are homogeneous with a single compressional and a single shear velocity. Acoustic attenuations, however, arise from a large number of mechanisms and cannot be so easily characterized. On a microscopic scale, ceramics are similar to metals as they are composed of randomly oriented crystallites. Glasses have an amorphous structure with an average density and coupling coefficient between atoms. Although both glasses and ceramics have bulk acoustic properties similar to metals, they differ from metals in that both are quite brittle and tend to fracture suddenly when their elastic limit is reached. Metals are ductile to some degree and undergo inelastic deformation before fracture appears. Plastics are seldom used by themselves as critical structural materials. They could be classified as very ductile glasses and are usually one component of composites. Composites differ from metals in being composed of several materials which are segregated into distinct substructures. In general, these substructures are larger than metallic crystallites which results in acoustic properties that are not homogenous. Each component material (fiber, resin filler, etc.) has different mechanical and acoustic properties and this results in bulk velocities which are anisotropic and can show definite frequency effects. One difference often seen in composites is that the elastic limit is not as abrupt as in ceramics or metals. Composites can experience a very long period between the load where the elastic limit is reached and the load where failure occurs. In some fatigue tests on wind turbine blades, the composite matrix in the blade skin started to turn to powder before there was a structural failure.

5.1.3. Acoustic Emission Frequencies

The acoustic frequencies generated by acoustic emissions cover a wide spectral range, from much less than one Hz in earthquakes to well over a MHz in metals and ceramics. Typically AE testing restricts itself to a low frequency cutoff around 20 kHz and a high frequency cut off dependent on the material being examined. The low frequency cutoff is set to exclude much of the extraneous noise produced in a test area, such as voices, machinery noise, and other environmentally produced acoustic noises. The upper limit is usually determined by the material and the test objective. Typical frequency ranges of 100 to 500 kHz are used with ceramics and metals, and 20 to 100 kHz with composites. The choice is often determined by what sensors are available. If locational accuracy is desired, higher frequency sensors are suggested.

5.1.4. Simple Attenuation and Velocity Measurements

Because acoustic properties vary with both material and geometry, it is advisable to measure the acoustic velocities and attenuations in the actual test specimen. The following procedure can give a reasonably accurate measurement. Mount two of the test sensors to be used on the specimen in an area free of welds, variations in specimen thickness, and other features which could interfere with the acoustic transmission path. The distance between the sensors should be about 200 mm for composites and 1000 mm for metals. Make five pencil lead breaks about 5 to 10 cm behind each of the sensors and approximately on the line joining the sensors. This procedure is designed to create at least similar acoustic waveforms exciting the two sensors. The trigger threshold used

for the measurements should be about the same as is to be used in the test. Record the arrival times and absolute energies for each lead break. The velocity is the distance between sensors divided by the transit time between the two sensors and the attenuation is ten times the log of ($energy_2$/$energy_1$) divided by the distance between sensors. The averages of the two number sets should give reasonable values for the velocity and attenuation for that path. The velocity value will probably have a smaller variation than attenuation value. For composites, the velocity and attenuation should be measured in at least three directions: along the main fiber axis, perpendicular to that axis, and 45 degrees between the two. A variation in the velocity between the two perpendicular axes of ten percent or less may not make much difference in source location accuracy, so an average of the three velocities can be used. However, a difference of thirty percent or more can make a large difference and an anisotropic velocity calculation should be considered. If this is necessary, velocity measurements should be made every ten degrees between the perpendicular axes. A FORTRAN program using an anisotropic velocity is included in the appendix. Programs that can use an anisotropic velocity in locations may also be included in some AE system software.

5.1.5. Sensor Layout

The objective of most AE structural tests is to monitor emissions from all significant regions where failures could occur. It is important to cover the areas of interest so that all parts of the area are within acoustic range of at least three sensors. Where the areas are separated, multiple location programs can be used. Where it is desirable to display adjoining areas separately, such as the upper and lower surfaces of a wing or turbine blade, common sensors can be used in separate programs (check in the system instruction manual for the correct settings to enable use of common sensors in separate location calculations). To lay out sensors, start with an overall sensor pattern such as interlocking triangles or interlocking rectangles. The triangular pattern covers somewhat more area per sensor while the rectangular pattern has a somewhat greater probability of at least four sensors hits by an emission, desirable for an over-determined data set. Once the overall pattern is set, the actual locations can be determined from the surface features. Not only is it not necessary to adhere rigorously to the starting geometric layout, it is helpful for the actual locations of the sensors to differ somewhat from the geometric points. When using a nonlinear least-squares program to locate the sources, having several sensors lying on a straight line encourages location artifacts.

An important parameter for setting up a test is the acoustic attenuation of the specimen surface. This will suggest the maximum sensor separation. The attenuation should be measured, if the value is not already known. For accurate location with an approximation calculation, an over-determined data set would have at least four **hits per event** for 2D location, or five hits per event for 3D location. Therefore, the sensor spacing must be small enough to allow sensors outside of the immediate triangle around an intense source to be excited. Generally, the maximum distance between two sensors should have an acoustic attenuation between 30 and 40 dB. Thus a surface attenuation of 0.1 dB/mm would suggest a maximum separation of 400 mm while an attenuation of 0.01 dB/mm could have a separation of 4 meters on average between sensors. This maximum distance is a goal, not an absolute requirement. Any attenuation measurement on a composite should not be considered accurate to better than one order of magnitude because of differences in acoustic scattering with different construction layups of the components.

5.1.6. AE System Setup

The setup of the AE system consists of two parts, the emission acquisition parameters and the real time graphs. The acquisition parameters include the trigger threshold, the timing parameters, possibly the gain and the channel bandwidth and waveform settings. The trigger threshold is set in dB above 1.0 microvolt out of the sensor. It can be either a fixed value, or a fixed value above the background noise level, a so called floating threshold. A floating threshold is not recommended for multichannel tests. It is hard enough to get hit data sets from multiple sensors which all trigger at approximately the same point on the waveforms without having the threshold of each sensor bouncing up and down. The fixed threshold should be set a few dB above the trigger level of the specimen's noise level. All sensors should have the same trigger level. Occasionally during a test, the noise level of one channel will increase to the point of continually triggering that channel. When this happens, the trigger level of the channel can be raised. However events located using that channel will have a greater location error. For a very high energy event, the absolute energy value of an event detected with a higher trigger level on one channel will probably still be valid even though the location is less certain.

The timing parameters PDT, HDT and HLT in PAC systems, are not critical for most tests. PDT, the peak definition parameter, is often set at 200 μsec. This parameter helps measure the rise times which typically range between 50 and 1000 μsec for emission in an FRP test. One use of the rise time is to help filter out hits which have started just before the channel was armed. Hits with rise times of less than a few cycles of the waveform are suspect. HDT, the hit definition time, helps determine when the hit has ended. The standard value of 800 μsec seems reasonable. When the last threshold crossing of a hit occurs, the system keeps the duration clock running for another HDT seconds. If another threshold crossing does not occur in that time, the clock is stopped and HDT seconds are subtracted from the hit duration. HLT, the hit lockout time, determines how soon the channel can re-arm after a hit has ended. Most tests with relatively slow load increase rates show repeated events on a channel with spacings of at least several milliseconds. A re-arm gap of one or two milliseconds has seldom produced a recognized problem. However, a gap of twenty milliseconds could start to miss data. The **Max duration** setting should be set higher than the longest duration expected in the test. For FRP, a setting of 10 milliseconds should be long enough. For metals such as aluminum and steel, a value of 50 milliseconds or longer may be needed to include the full signal length of high amplitude hits. If a test has any special signal analysis requirements, a preliminary run recording and an examination of waveforms will help in setting timing parameters.

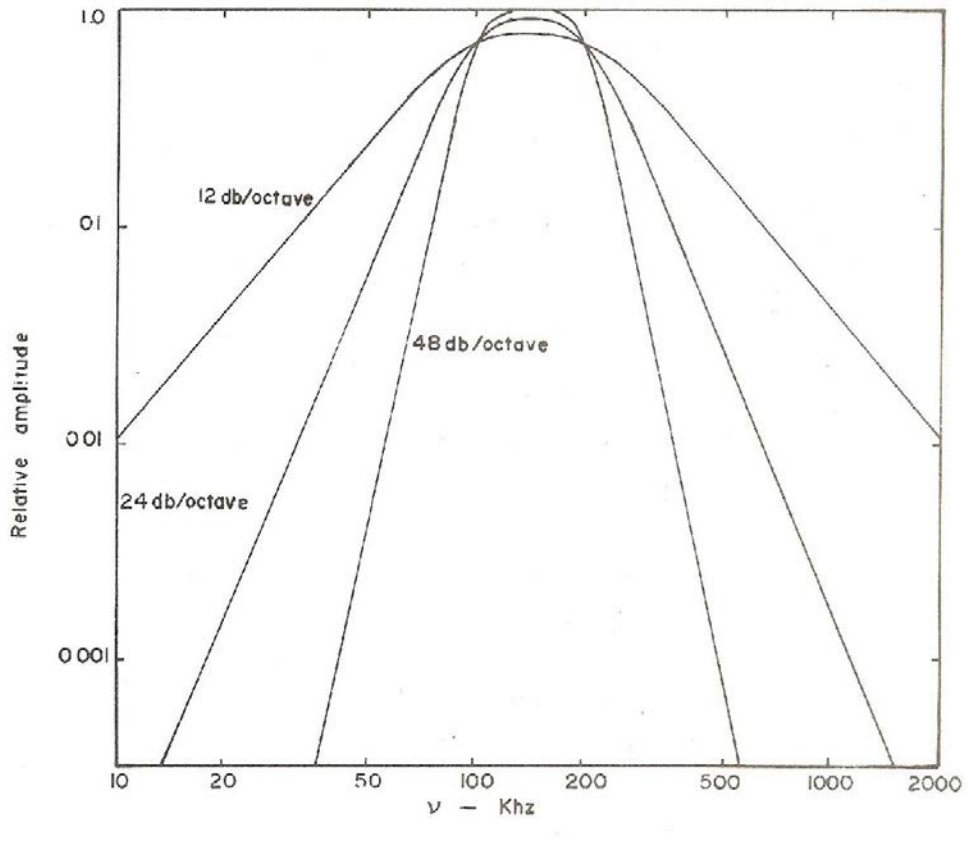

Figure 5-1. Electronic bandpass characteristics of different filters as a function of frequency.

Most of the sensor signal gain is in the preamplifier which is often fixed at 40 dB when the preamplifier is integral with the sensor. With 90 dB of dynamic range in the system, a preamplifier gain of 40 dB is usually adequate. Additional gain on the computer board seems redundant. The chosen band width should eliminate most room noise and any truly high frequency noise (1 MHz +). It must be remembered that the upper and lower band width figures are for the knees of the curve as shown in Figure 5-1. A large amplitude signal with energy outside of that bandwidth will still pass appreciable energy through the filter.

Required waveform acquisition settings are the digitization rate and the number of words in a sample. The digitization rate should be 1 to 2 MHz for composites and 4 to 6 MHz for metals. The problem with high digitization rates is that more words are needed for the same length sample. Current PAC eight-channel boards are limited to 4000 word samples which yields a 4 millisecond waveform at 1 MHz but only a 1.33 millisecond waveform at the boards maximum sampling rate of 3 MHz. Another problem is that a hit on an AE system has a record length of only about 30 bytes of while a 4000 word waveform has a record length of over 8000 bytes. If much low amplitude emission is detected, data files that include waveforms can rapidly become unmanageably long. For example, a 5 megabyte file will contain about 500 hits with 4000 word waveforms, or up to 200,000 hits without waveforms. A fatigue test of a composite structure near the failure point can produce those 200,000 hits in little more than one minute.

A useful feature of a typical AE system is front-end filters. These can be invaluable in a noisy environment, automatically excluding hits that fall outside of preset windows for signal parameters. The most useful filter parameters that I have found are the acoustic emission count, the signal duration, and for source location, the rise time. A count of one for a hit is usually meaningless – a simple excursion of a background noise spike above the threshold. Such hits have low amplitudes and durations. They may not appear very often but they will lock out the channel for the duration of the HLT for every hit. Unfortunately, some electrical equipment can generate short, intense RF spikes. A little oxide on a coaxial connector or a minor cut in a cable shield may enable the cable to act as antennas for the preamp inputs. If the interference reoccurs at harmonics of 60 Hz, it can completely lock out a channel. A front end filter eliminating all hits with one count can be very useful with almost no effect on the detection of real emission.

Because most acoustic signals contain considerably more than three oscillations, a front end filter rejecting signals with durations of less than three wave lengths of the dominant frequency seen in the test can remove other forms of electrical noise which are short transients. . Filtering out signals of less than 50 μsec in FRP tests or 10 μsec in the Halon bottle tester has worked very well. Filtering out signals with rise times of less than a few wavelengths during location tests can remove signals which have started before the channel trigger was reset. These signals, while they are real emissions, have arrival times which will confuse the location algorithms. While such filters are useful, they should be used with restraint.

One essential parameter for any load test is an electrical signal proportional to the load. In the case of a direct hydraulic load drive, the hydraulic controller requires a signal from a load cell. This may or may not be easily available to the acoustic emission system. Where no load signal is available, such as in a resonance fatigue test, a signal from a strain gauge can be used. This gauge must be located in a region where the strain is a linear function of the load. The gauge can be calibrated by applying a static load to the structure.

On a proof test or load-to-failure test, the background noise level is usually constant and independent of load. The only filtering need here is to set the trigger threshold a few dB above the noise level. However, in fatigue tests, large amounts of noise can be generated where the load is low but the rate of change of the load is high. Most structural damage produced by the load should occur within 10% of the maximum load. Other emissions may be generated by rubbing friction in the specimen and have nothing to with induced damage. These can be filtered out by operating the system in the voltage time gate mode using the load signal as the reference. Using the voltage time gate to stop the signal acquisition unless the load is above 90% of its maximum value will ignore most frictional noise. As proof of the premise, almost all of the emission occurs on the rising or the peak load. Almost nothing is seen as the load falls from 100% to 90% of its maximum. A word of caution: in a resonance fatigue test, the signal driving the voltage time gate should be provided from the area of the specimen where failure is expected. The displacement signal from an area far from the driving load can have a phase that is measurably different from that of the driving load. The other alternative is to filter out only signals occurring near the maximum change in the driving load

5.1.7. AE System Setup for Location

The operation of the hardware in most AE systems will be similar. However, location programs and accompanying hardware setup procedures may vary between manufacturers. This monograph will deal only with PAC systems. The functions of different parameters and procedures will be described in some detail in the hope that users of other systems will be able to recognize similar parameters in their systems.

The location setup table allows the designation of different location programs for different sensor groups. The programs include Zonal Location (all hits for each sensor); Linear location (sensors in a line only); Planer Location (2 dimensions with isotropic or anisotropic acoustic velocities); Volumetric Location (3dimensions) and Cylindrical and Spherical Location (surfaces). Other special geometries may be available from the manufacturer on a custom basis.

With any location software, the first problem is to define an acoustic emission event. The hits arrive at the computer with an arrival time value for each hit. The computer stores these hits, including all measured parameters, in the order of their sensor arrival times. A working definition of an **acoustic emission event** for a computerized system is a sequence of hits all triggered by the same acoustic wave. These will all occur within a certain time period determined by the geometry of the sensor array and the acoustic properties of the structure. The computer system or external program determines what hits are included by using an **Event Window,** a period of time which should include all valid hits and which must be set by the operator or analyst. While the exact value of the event window is not critical, it should be long enough to accept all sensors hit by the same wave and short enough to exclude second hits on the same sensor, whether a wave reflected from a boundary or a retriggering of the same sensor on background noise.

In AEwin three parameters are associated with the event window: the **Event Definition Value,** the **Event Lockout Value,** and the **Overcal Value.** These three values are used at times by the program, but in AEwin they will be entered either as a distance or a time, depending on whether the location routine has been set up with distance or time units. If the location is set up using distance units (mm, for example), the Event Definition Value is the distance between the two most separated sensors which are expected to register the same signal. The distance is converted to a time value in the computer by dividing by the acoustic velocity. The exact triggering point on a waveform is uncertain, and this uncertainty increases as the wave propagates away from its origin. Allowance can be made for such uncertainty by including an Overcal Value to be added to the Event Definition Value. The Event Lockout value, like the Event Definition Value, starts when the first hit of an event is triggered and defines how long before the next event can start. These values define an event for the location program. They do not affect the detection or storage of hit data. In the case of post-test analysis, it may be just as easy to look through a read-out of the hit data and choose an Event Window based on that data.

The time of flight of the signal is used to define the time window for the event group. The author prefersto think of the event window in terms of a time as that is the AE data value of interest. However, one can consider the Event Definition Value to be the difference between the farthest two sensors that one wants to be included in the data set. Because electronically detected data always has uncertainty in it, the Overcal Value is set up to include hit data with somewhat longer

transit times. Thus the actual time window entered into the computer is the sum of the Event Definition and Overcal values divided by the acoustic velocity. This does not consider anisotropic velocities, different propagation modes, or structural elements with different velocities (carbon reinforced spar caps). The event lockout value is also a time used by the computer and is also calculated by dividing the entered distance by the velocity. It is the time interval between the measurement of one emission and the arming of that channel for the next. The values of these parameters are usually not critical but inappropriate values can distort the data set by missing later hits or possibly triggering on reflected waves.

Another entry in the location table that can be useful is **Hits per Event**, particularly when there is a large amount of data available. The location calculation for more than two sensors is a numerical approximation that works best with an over determined data set; it will be described in more detail in Chapter 7. This parameter sets the number of hits to be included in the location calculation. For a plane, three hits are necessary for location as there are three unknowns, i.e. the two coordinates of the source and the starting time when the event occurred. For a plane, the best data sets will contain 4 to 6 hits. Three hits result in a so-called exact calculation which is highly dependent for accuracy on on precise triggering on all three waveforms--one bad datum and the answer becomes meaningless. More than six hits often include acoustic waves which have traveled far and whose waveforms have evolved beyond easy definition of a trigger point. Calculations with an over determined data set *give a best fit to that data set. This result can be thought of as* the most probable location of the source for that data set. Changing the number of sensors included in the calculations will usually result in small changes in the answer given by the calculation. The last entry in the AEwin location table is maximum number of iterations to be used in the calculation. This is of little importance as calculations with AE data will reach the point of minimum deviation from the experimental data within 5 to 10 iterations. They either converge by then or blow up.

5.1.8. Example of Setup

The best way to illustrate an AE test setup is to go through, on paper, the steps required for a possible setup. The specimen will be a 9 meter FRP wind turbine blade. Velocities along the length of the blade of 3.0 mm/μsec and of 2.4 mm/μsec along the chord will be assumed. For this example, the velocity variation with angle will be the default in the AEwin 2D Anisotropic program. Separate location calculations for the compression and tension side of the blade will be used. It will be assumed that the majority of the damage produced in the blade will occur between 500 and 3500 mm, as seen in most 9-meter blade tests. The sensor layout, shown in Fig. 5-2, consists of 6 rows of 4 sensors each surrounding the blade every 500 mm along the blade. The first row is on the chord at 500 mm from the root. For consistency, the sensor numbering sequence starts with #1 placed on top of the shear web at station 500 mm on the compression side of the blade. The sensors are then placed in rows and numbered, clockwise, looking from the tip of the blade. The 2^{nd}, 4^{th}, and 6^{th} rows are rotated 45 degrees from the top of the shear web. The chord measurements for the sensors on the two sides refer to the positions of the top and bottom of the shear web. The convention used is that the measurement is positive toward the leading edge and negative toward the trailing edge on both sides of the blade. The sensors in front are placed as close to the center of the leading edge as possible and those on the rear are placed either on the top or bottom of the trailing edge surface. Measurements of the trailing edge positions of the sensors should be either to the center of the sensor's face or the point on the

other side of the blade directly below the sensor's center. All sensor positions should be measured to the nearest mm, if possible. Actual errors of a few mm are usually not important to the overall test.

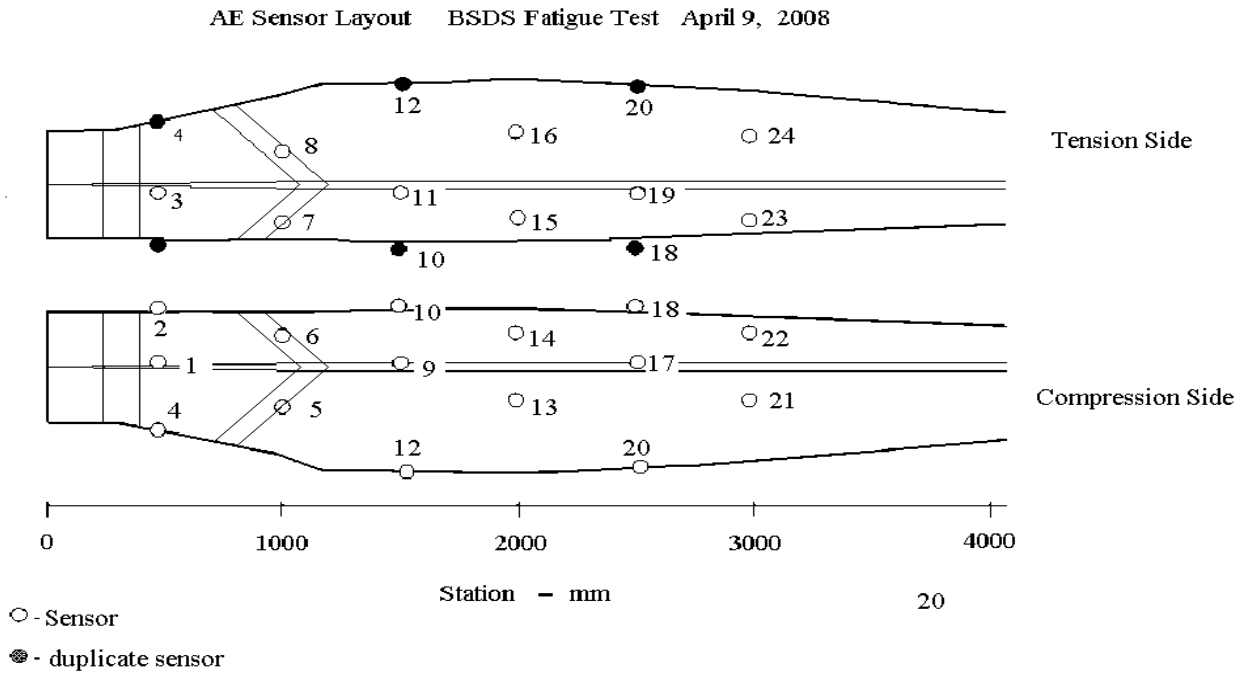

Figure 5-2. Layout diagram of 24 sensors on the BSDS wind turbine blade

Now the location programs can be set up. The compression side will use sensors 1, 2, 4, 5, 8, 9, 10, 12, 13, 16, 17, 18, 20, 21, and 24. The tension side will use sensors 2, 3, 4, 6, 7, 10, 11, 12, 14, 15, 18, 19, 20, 22 and 23. Unless the shear web is perpendicular to both surfaces, the leading and trailing edge sensors may have slightly different location values on the two surfaces. Using the AEwin program, set up two channel groups-- compression and tension--and enter the sensor numbers of the groups into the computer. Set the location type for each group to 2D anisotropic and then click the box marked *set all points* for each group. This allows the edge sensors to be used in the calculations of both sides. Then set the HLT parameter to 0.0 for both groups. This allows hits to occur at the same time for both location groups. Go to the location setup view and enter the sensor locations. Notice that in the AEwin software, the two velocities V_x and V_y are entered in different tables: the V_x in the general location set up table, and the V_y in the sensor view table.

The next step is to set up the real time graphs on the computer. For a single load test, a graph of the summation of the AE count as a function of load is probably the most useful. (Most of the more useful graphs are discussed in some depth in Chapter 7.) Then come location graphs for both sides, summation of absolute energy for located events graphs for both sides, a hits vs. sensor graph and distribution graphs for both hits and events vs. peak amplitude. In a fatigue test, a scatter point graph of the parametric voltage for each hit vs. time along with a similar graph for counts per hit can be useful both to see how well a load filter is working and to monitor the overall emission rate. A note of caution: an AE system can generate a huge number of graphs but each of these graphs needs memory and computational power. It is quite possible to greatly slow

down the system by setting up too many graphs. Modern computers are quite fast, but too many simultaneous graphs can leave the system far behind the test in real time. Conservatively, a dozen real time graphs should be about the maximum used. Many more graphs can be used during post-test analysis, but at a cost of a rapidly increasing replay time per file.

Finally, there is the problem of multiple files. AEwin allows the specification of maximum file size and whether the files are separate or a continuation. A 5-10 megabyte file size is convenient for analysis and transporting while files larger than a few hundred megabytes can become quite awkward. The author has found that separate files are easier to handle than continued files, and separate files are easily grouped together with an AEwin utility to make one large file when needed. If the files are recorded in continued mode, the continuing time base can make the individual files more cumbersome to analyze.

6.0 CHAPTER 6

6.1. Source Location

The main function of an acoustic emission test is to identify flaw growth in a structure as it undergoes an increasing or continuing stress. Ideally, the test should both locate the flaws and describe their growth rate as the stress level increases or the stress state continues in time. On simple structures a single AE sensor can report how the structure itself is behaving. However, complex structures will have many possible flaw sites. Such a structure, when large or constructed of multiple materials, will best be monitored with multiple sensors. Thus most of the growth in the field of AE in the last 40 years has been in the design of multi-sensor systems and their analysis techniques. The focus of these techniques has been the location of acoustic emission sources on large structures. Starting with the early work of Green et al. [2] at AeroJet Corporation, a primary structure of interest has been pressure vessels. Now, almost any structure that experiences changes of stress in normal operation is a candidate for acoustic testing and most of these tests involve source location.

The basic idea in source location is to cover a surface with a network of sensors. If one can determine the arrival times of an emission signal at several sensors, then, knowing the acoustic velocity, it is possible to triangulate back to the location of the source of that emission. The idea is simple, but already several assumptions have been made. First, an isotropic material is assumed so that there is one acoustic velocity. Second, the shortest path between a flaw and a sensor can be determined throughout the structure. Third, the acoustic signal is simple and its exact time of arrival can be measured. And fourth, the resulting set of nonlinear equations can be solved easily.

Assuming materials are isotropic may seem safe for a metal pressure vessel. However, assuming unique acoustic paths with known velocities may not be valid. The shortest distance between a flaw and a sensor may go through or around vessel penetrations or welds. Variations in the acoustic path may be small but they are real. The acoustic velocity in a plate is not a constant but is a function of frequency and plate thickness. The geometry and speed of the fracture of the flaw are unknown. There may be several frequencies and unknown polarizations in the excited acoustic wave. As it travels toward the sensor, the frequency and polarization components of an acoustic wave can change with distance. The result is that the waveforms detected at the separate sensors may be quite different from each other. The amplitude of the wave that first crosses the trigger level of the electronics will not always occur at the same portion of the waveform at different sensors. There will be variations in the triggering time of each sensor from what would be predicted by whatever model used in the analysis.

The equations for the distance between two points on a surface are nonlinear even for a flat plane. To locate a point on a plane one has two unknowns, the coordinates of the point. In an acoustic emission experiment, one records arrival times of the acoustic wave at the sensors, but in order to know distances, the starting time of the wave must be known. Therefore, to triangulate the location of an acoustic emission source, one has three unknowns, the two coordinates of the source on the plane and the time that the emission generated by that source occurred. A problem with sets of nonlinear equations is that there are at least several solutions to the set of equations (if there is any solution). Real experimental data is full of small uncertainties.

Triggering on slightly different parts of the wave form at different sensors as well as minor path differences from those predicted by the model can generate data sets which have strange to no solutions. Finally, analytic solutions even to an exact set of nonlinear equations do not come easily, if at all.

Another major problem with AE source location is that many structures have complex geometries and may have multiple acoustic paths between regions. One can get analytic solutions for the shortest path between two points for planes and spherical surfaces. One can also combine these two types of surfaces into cylinders with hemispherical end caps. Beyond these shapes, one has to approximate. Large surfaces which have gradual curves can be approximated by planes. An aircraft wing or wind turbine blade can be approximated by either two independent surfaces or one surface folded down the middle. Large curved surfaces can be approximated by a group of joined plates. In spite of these problems, AE source location as a major advantage in that exact modeling of a surface is often not necessary. Even if the model is far from a one-to-one approximation of the actual surface, all emission from one spot on the surface should located at one place on the model. While the location on the model may be some distance from the corresponding point on the structure, all the emissions that were located at that point actually originated from the same location on the structure. Thus, a grouping or cluster of points on the model corresponds to an actual location on the structure. While the theoretical and calculated locations may differ, the fact that there is an active flaw at a point on the structure is real. If the exact location of the flaw is needed, one can inject signals into the structure at various points until the same arrival sequence at the different sensors is found.

A way around the problem of analytical solutions is to use a numerical approximation, such as a nonlinear least squares fitting routine. For a single data set, such a calculation starts from a trial solution. In an AE calculation, this is usually a point inside the triangle formed by the first three sensors hit. The routine starts with this trial solution and calculates the travel times of the wave from that point to the excited sensors. It then takes the sum of the squares of the differences between the calculated travel times and measured arrival times for each sensor. If the sum is not zero, the program will make small shifts in the trial solution and from the changes in the sum, estimate what a better trial solution would be. This iteration is repeated until the sum ether reaches zero (a real solution) or a minimum (the best estimated solution). Because the first trial solution was a reasonable estimate from the physics of the test, the solution arrived at is usually the most probable location of the source. Often, a nonlinear least squares routine will calculate a goodness of fit parameter which is an estimate of how good the answer may be. Because of errors in the data, it is always possible to get solutions which are located well off the surface of interest. If the goodness of fit parameter is reasonable and the solution lies within the bounds of the sensor network, one can assume that the solution is the most probable location of the source. An over-determined data set, using hits from additional sensors outside the triangle of the first three hits, will generally improve the accuracy of the calculation. However, using more than six to eight sensors starts to degrade the calculation because the traveling waveforms have often lost most of their relationship to the original waveform and the triggering point may have little correlation to that of the initial waveform. Thus the measured arrival time may have little to do with the actual acoustic velocity.

Another approximation used in source location is that the acoustic velocity is isotropic and constant. This is usually not the case for composites and may not be the case for metallic

structures if they are made of plates with different thicknesses. A non-linear least squares program can use anisotropic velocities. A routine which uses the velocity distribution shown in Fig. 8-6 is included in the appendix. Because of the large amount of variation in AE data from composites, small anisotropies in the velocity are not that important. However, if the anisotropy in the velocity is greater than 10%, using the measured velocities in the location calculation may improve the fit. An anisotropic velocity routine available in AEwin software has a fixed angular dependence of the velocities. In many, but not all, composites, this should give adequate results.

An acoustic emission **cluster** is a group of emission sources that occur near the same location on the structure. Current commercial AE programs include various methods for detecting and defining a cluster. The importance of a cluster cannot be over emphasized. A growing flaw will generate a series of emissions. The actual source of these emissions may be a localized source such as the tip of a growing crack, or a more diffuse source such as a patch of corrosion. Because of minor errors in the measured arrival times, both types of sources can appear as a cluster of sources over a small but definite area. The test designer must define a cluster. The usual definition is at least some number of located sources occurring in a defined area on the surface of the specimen. It is often easier to define the clusters during or after the test. The most important characteristic of a cluster is its existence. The presence of a cluster indicates a specific region on the specimen that is generating acoustic emission. The second characteristic is the size of the cluster. This can either be the number of events or the amount of an acoustic emission parameter contained by the cluster. Most commercial programs allow the system to grade the clusters based on either the number of events contained or the amount of the parameter measured. The third characteristic is the behavior of the cluster with increasing stress. The sum of the number of events in the cluster plotted against stress or time can strongly indicate whether that cluster is produced by a flaw undergoing steady state, i.e. controlled growth, or uncontrolled growth leading to failure of the specimen. If the emission is fairly uniform such that the variation of the acoustic emission count or peak amplitude is not much over an order of magnitude, the number of located events in the cluster is an adequate measure of its growth. However, if the variation is large, as occurs in composites, a plot of the sum of the absolute energy of cluster members is a better measure of its behavior (see Fig.7-12). Unfortunately, at least with current AEwin software, plots of the absolute energy of a cluster as a function of load or time are not straightforward.

The author has been using a nonlinear least squares fitting routine in data analysis since the mid-1970s. At that time, this routine was used by several Sandia physicists and was applied to acoustic emission analysis. The name of the routine is NRL, but over the last 35 years in the course of many moves, all references to its origins have been lost. The program is the foundation of the current analysis techniques and a FORTRAN listing of the location program which was used on the Sandia Sensor Blade test is in the appendix. This program can locate emission sources and plot the locations with the absolute energy of each, color coded as to order of magnitude. It can also plot the absolute energy of the sources located in a cluster as a function of load or time. These graphs have been very useful in analyzing the results of wind turbine blade structural tests. A discussion of non-linear least squares programs, with examples, can be found in “Numerical Recipes in FORTRAN” [19].

7.0 CHAPTER 7

7.1. Analysis

The primary purposes of an acoustic emission test on a structure are the detection and monitoring of flaws which affect the integrity of the structure. It should be emphasized that an acoustic emission test is by definition not a nondestructive test as the detected emissions are produced by irreversible changes in the material under test. However, the sensitivity of an acoustic emission test is usually high enough to detect flaw growth long before reaching a severity level which will affect the strength of the structure.

A flaw can be defined as any defect or error in a structure that can affect the strength or wellbeing of the structure during normal use. For the field of acoustic emission, the term flaw will refer only to flaws that are influenced by the working loads on the structure. For example, a flaw such as a cracked step in the ladder leading to a crane is serious, but it is not influenced by the load hoisted by the crane. The growth of a flaw, as influenced by the load, can roughly be divided into three categories: **controlled flaw growth**, **uncontrolled flaw growth**, and **catastrophic flaw growth**. As an example, consider a piece of metal composed of many random crystallites. Micro-flaw growth can involve either the fracture of a crystallite, the fracture of a boundary between two crystallites, the fracture of a boundary between a crystallite and an inclusion in the metal, or the fracture of the inclusion. All of these cases will have a stress level where an applied stress vector will cause a fracture. In fact, there will probably be several stress levels where different stress vectors will cause a fracture of the same crystallite. The fracture of a single crystallite will usually rearrange the stress vectors on the surrounding crystallites. This rearrangement may leave the surrounding micro-stress vectors essentially unchanged or change the micro-stress level on some crystallites to some degree. An increase in a micro-stress level may be enough to fracture other crystallites. In such a case, an avalanche to macro-fracture can be the end result. Whatever the result, it completely depends on the local stress environment and local material environment. There is no way of predicting the exact stress level or the exact location of the first or any other micro-fracture.

Controlled flaw growth will occur when the fracture or group of fractures does not produce a rearrangement of the local stress fields which causes further fractures. The emission rate will remain relatively constant or even drop as the stress level is increased. A decrease in the rate usually indicates a relatively small number of regions where built-in higher micro-stress levels were left from the manufacturing process. When these have all fractured, the emission rate will decrease until the fracture stress level of more serious flaws is reached. Such regions where the micro-stress levels are significantly higher than the mean are often found in new FRP structures, but seldom in metal structures. In the absence of such manufacturing artifacts, most acoustic emission tests start out with no emission (above background noise level) and then proceed into a controlled flaw growth regime with a relatively steady emission rate over some range of applied external stress. When the emission rate starts to increase with stress, uncontrolled flaw growth has started.

In **uncontrolled flaw growth**, the micro-fractures generally produce an increase in the local stress fields of the surrounding regions. As the external stress field is raised, the rate of emissions increases. Slow at first, the rate increase tends toward an exponential increase. If the exponential

increase is not stopped, the test will rapidly proceed to the failure at the flaw. If the load increase is slow, there usually will be enough time in this uncontrolled flaw growth region to stop the test and prevent a serious failure. This is one of the primary purposes of many acoustic emission tests. In **catastrophic failure**, the exponential increase in flaw growth may be quite rapid. The speed of the failure is a property of the material. In brittle fracture, there is little or no acoustic emission preceding the failure. A typical example is the fracture of glass. An acoustic emission test may tell when a small glass part in a structure breaks, but it will seldom give advanced warning of brittle fracture.

Analysis of an acoustic emission test consists primarily of looking for the occurrence of acoustic emission and then measuring the rate of that emission with respect to the change of the test stress level. In structures where multi-channel tests are used, the location of the emission and the measurement of the emission rates for each located area are the goals. An analysis can be done either in real time (if the prevention of structural failure is the test objective) or in post-test analysis. Real-time analysis depends primarily on an operators experience and knowledge. It can become interesting, especially where the loading involves large energy levels, and can probably only be learned by experience.

Acoustic emission tests can be divided into two categories, depending on the type of test loading. The first category has a single loading to either a maximum applied load or to failure. The load may be applied continuously or in steps. In FRP tests, the steps may be separated by returns to a zero load between each step. This allows a determination of the Felicity ratio at the beginning of each step. In a continuous load with steps, the load hold between steps allows the determination of how fast the emission decreases as the loading stops. As a specimen nears failure, the emission will often continue for a period of time after the hold starts. When the emission continues through the hold period, that is a good time to declare the test over and reduce the load, unless the object of the test is actually to fail the specimen. The second type of loading is the fatigue test. The load is periodically cycled over a fixed load range. This range may be constant over the test but often it is increased after predetermined cycle intervals. The test may be monitored continuously or the AE system can be activated only at near peak loads with a voltage time gate. The practice of detecting emissions only at peak loads restricts the observed emission sources to those produced by actual flaw growth and eliminates frictional sources which are at a maximum during the periods of rapid load change. In fatigue tests there is usually an interval where the emission rate from flaw growth increases slowly with time. However, there can be exceptions to this rule. The author has analyzed one fatigue test where the failure occurred quite suddenly and only extensive post-test analysis revealed some pre-failure emission.

7.1.1. Test Graphics

Analysis of a test in real time is up to the operator of the AE system. The operator is totally dependent on the graphs that have been set up on the system. In the early days of AE testing, two of the most important instruments of the test setup were the oscilloscope and the audio channel. The scope would show the output of one AE channel. One could get a good idea from the scope of how rapidly the emission was occurring, its amplitude, and the general shape of the emission bursts. Non-emission noise signals showed up immediately. Impending failure of the specimen was quite evident as the whole scope would light up. The audio channel would use a beat frequency to bring the main AE frequencies into the audio range. An experienced operator could

obtain additional information about the status of the test from changes in the audio amplitude and frequency. From these instruments and an x-y recorder that plotted summed counts against load or time, an experienced operator could give a good picture of what was happening in the test.

With current digital AE systems, the oscilloscope and audio instrumentation are missing. They are replaced by real-time graphs on the computer screen. The following displays are useful in in both real time and post-test analysis.

7.1.1.1.

A graph of the hits, events, counts or absolute energy versus the load or time is essential. The author prefers the graph of the cumulative hits, etc. over the graph of the rate of hits, etc. because it is visually easier to differentiate a cumulative graph than to integrate a rate graph. The classic parameter vs. time graph has been used almost from the start of AE testing. The choice of AE parameter will depend on what is expected from the test. Hits or counts will show all detected AE, with counts being more sensitive to the intensity of the emission. A located events count is sensitive to emission from actual flaws but may miss regions where only one or two sensors are activated. Counts or absolute energy per event will give the most information about the state of flaw growth but can become confusing when there are multiple flaws. A rate of absolute energy per load interval graph is probably the most useful, but its use must be confined to post-test analysis since it requires a knowledge of the total behavior of all clusters.

Changes in the slope of the cumulative graph indicate changes in the acoustic emission rate. A steady rate in the absence of external noise indicates controlled flaw growth while an increasing rate indicates uncontrolled flaw growth. When the slope of the curve appears to increase toward an exponential, or shows a distinct knee, structural failure is usually approaching. Figure 7-1 shows a steady emission rate in 7-1*a* and an increasing emission rate in 7-1*b*. These graphs show the number of located events as a function of temperature (load) in two Halon bottle tests (chapter 10). Both bottles failed the test but for different reasons. In 7-1*a*, the number of events in a cluster exceeded a preset maximum, and in 7-1*b*, both the slope of the event vs. temperature curve for a cluster and the number of events in the cluster exceeded preset maxima. The test in 7-1*b* was terminated early by the computer program to prevent catastrophic failure.

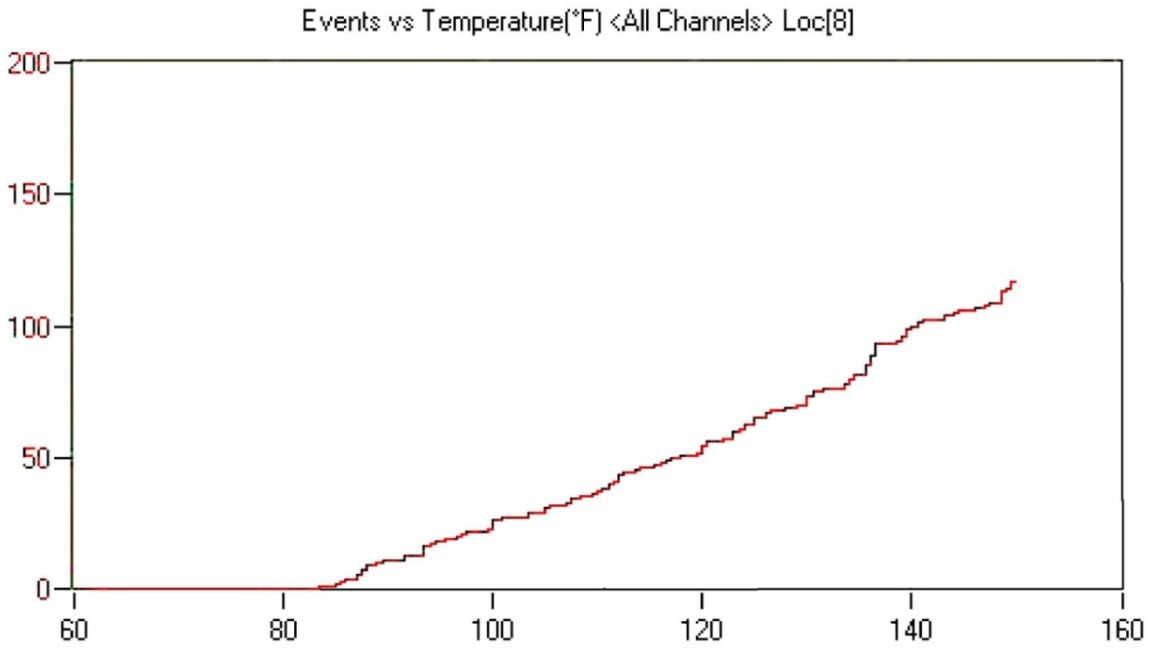

Stable flaw growth in Halon bottle (*a*)

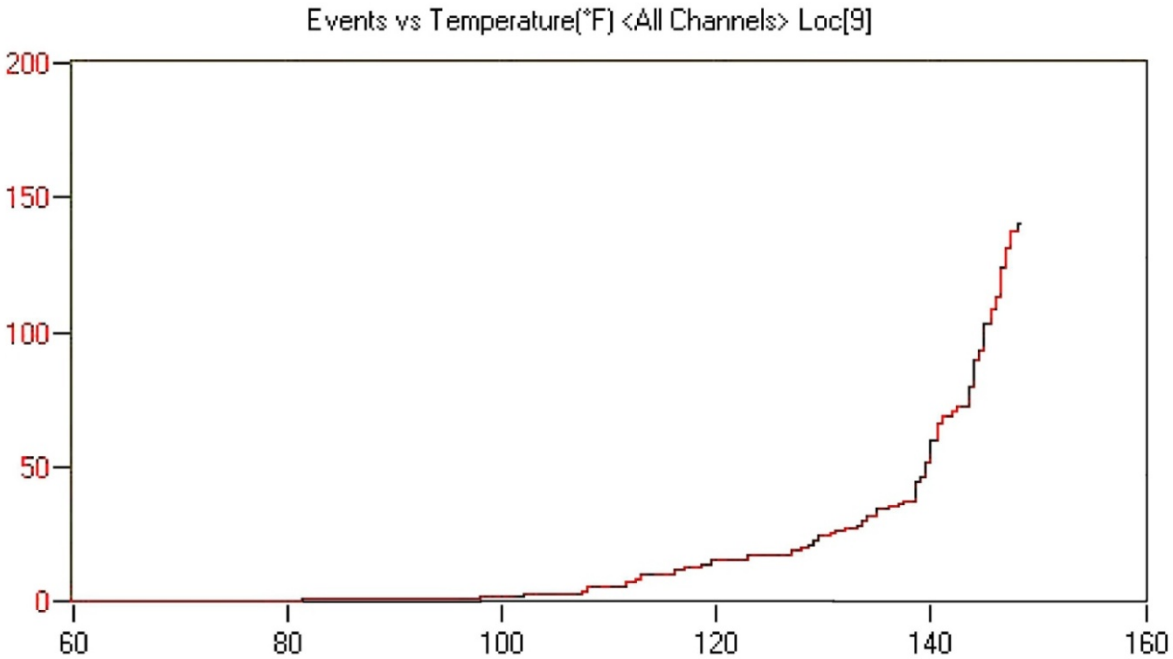

Transition from stable flaw growth to unstable flaw growth in a Halon bottle (*b*)

Figure 7-1. Stable to unstable flaw growth in a Halon bottle

7.1.1.2. Location graphs in real time.

These graphs plot the calculated location of each event as it occurs. The location calculation can be set up as a single graph or as multiple graphs. The graphs set up for the system monitor

probably will not have a one-to-one correspondence to the structure. Relatively small discrepancies between the graphical location and the actual

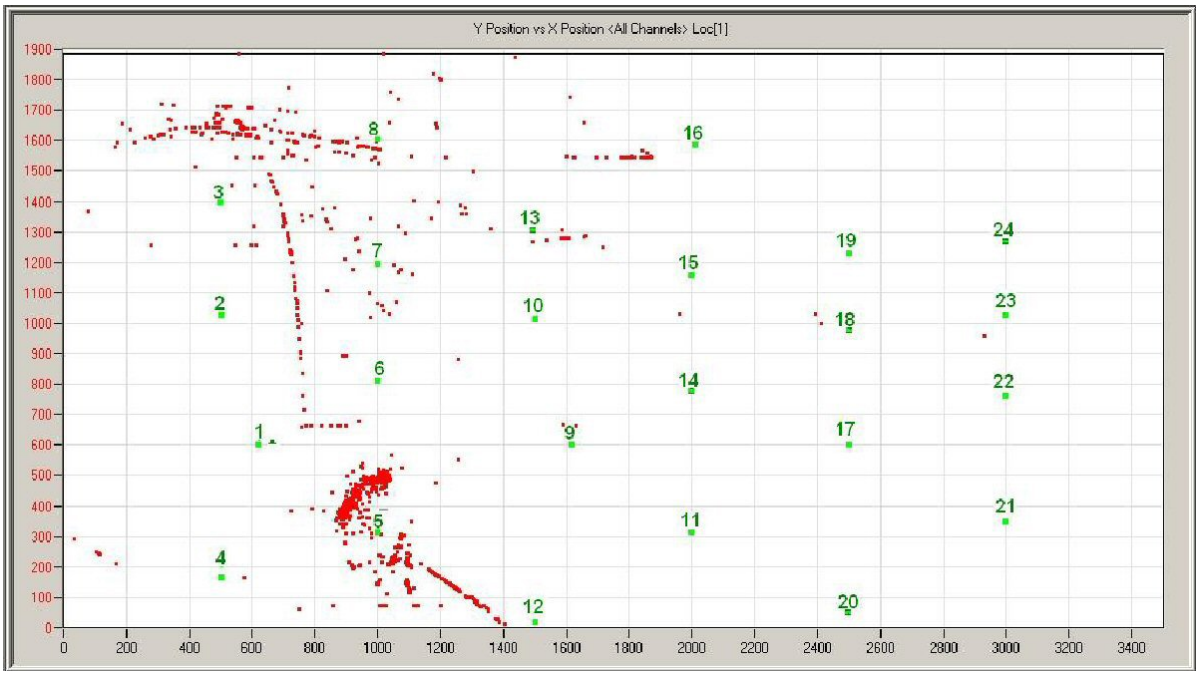

Figure 7-2. Location graph of data from BSDS wind turbine blade fatigue test

location of the cluster on the structure are not very important for real time monitoring. Usually, most emissions originating in one region on a structure will have their calculated locations in a similar region on a graph even though the two regions may have somewhat different locations on the structure. The appearance of a cluster of events on a real-time graph indicates a growing flaw and the behavior of the events with load will define how serious the flaw is, even if the calculated location appears to be vague.

Figure 7-2 is a location graph from the BSDS wind turbine blade fatigue test (Chapter 9). The graph covers 15,000 cycles early in the next-to-last loading level for the test. This representation approximates the blade as a cylinder to allow the entire blade surface to be monitored on one graph. The approximation is relatively good for the first meter of the blade and relatively poor from 3 meters to the end of the blade. Sensors 2, 10 and 18 are located on the leading edge with sensors 1, 9 and 17 on the spar cap on the low pressure side, and sensors 3, 13 and 19 located on the spar cap of the high pressure side of the blade. Sensors 4, 12 and 20 are located at the trailing edge. The distinct lines in 7-4 are artifacts often seen in tests involving source location. Straight lines are often artifacts of the calculation while curved lines often arise from RF interference. Both may be caused by beat frequency interference signals which are locked to the load frequency. They may appear to be acoustic in origin but the regular patterns often seen in the data indicate that they are not signals from a growing flaw. They are usually seen as events which only contain three hits. As a rule, AE from a flaw is random in occurrence. Any regular patterns seen in the raw data either imply signals with non-flaw origins or events along a structural feature.

Another point that should be mentioned in setting up location graphs like Figure 7-2, is that software based on a nonlinear least squares routine can use information from any number of sensors up from the minimum necessary for the geometry of the calculation. For a surface, the minimum number of sensors is three. There will usually be more 3 sensor events than 4, 5 or 6 sensor events, just because of the normal variation in amplitudes of the events. A 3 sensor event on a surface usually implies an exact calculation. The location graph 7-2 was calculated using all events containing 3 to 6 sensors. If the calculation had been restricted to 4 to 6 sensors, the straight lines and most of the distinct curved lines in Fig. 7-2 disappear, but the cluster around sensor 5 and the scattered points above sensor 3 remain. The use of 4 to 6 sensors for planar location is always desirable if there is enough data to produce a reasonable graph.

7.1.1.3. Graphs of the peak amplitude distributions of hits and events.

Figures 7-3, *a* and *b*, show peak amplitude distributions from the data graphed in Figure 7-2. The hit distribution shows most of the hits were below 65dB peak amplitude while the events fell into two groups, one near 54 dB and one near 71 dB. There were a large number of hits compared with the number of located events for each peak, however there were many more events per hit near 71 dB than near 54 dB. This implies the growth of two different flaws which should be apparent on a location graph. The location graph in Figure 7-2 shows two small clusters, a rather diffuse one near sensor 3 and a more compact one near sensor 5. From the graphs in Figs.7-2 and 7-3 it is difficult to tell which cluster goes with which amplitude distribution. However, in post-test analysis either the simple graphs seen in Figure 7-4*a* and 7-4*b* or source location program which includes color differentiation by source energy (Chapter 8) can help identify the clusters.

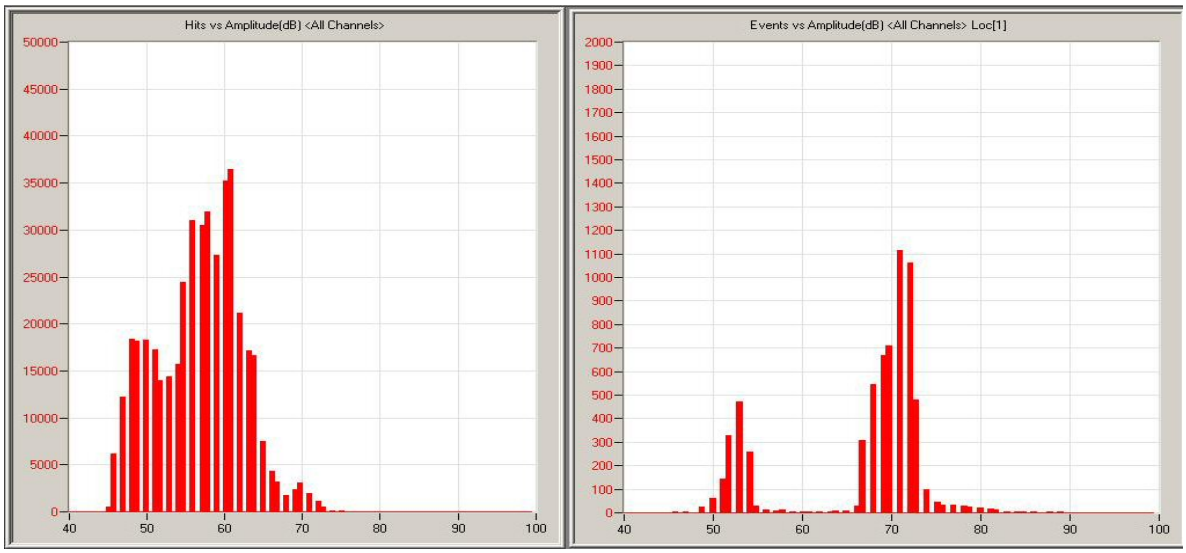

Figure 7-3. Amplitude distributions of hits and events from the same BSDS data (*left, a*, and *right, b*).

7.1.1.4.

In the location graph 7-2, two clusters appear: a diffuse one between sensors 3 and 4, and a more compact one near sensor 5. The summed absolute energies from sensors surrounding each cluster are plotted against time in Figures 7-4*a* and 7-4*b*. The cluster near sensor 5 shows about six times more energy release than the cluster between sensors 3 and 4. Thus the cluster near sensor

5 is the more active. This would also be obvious if the location plot included color differentiation of the sources by energy.

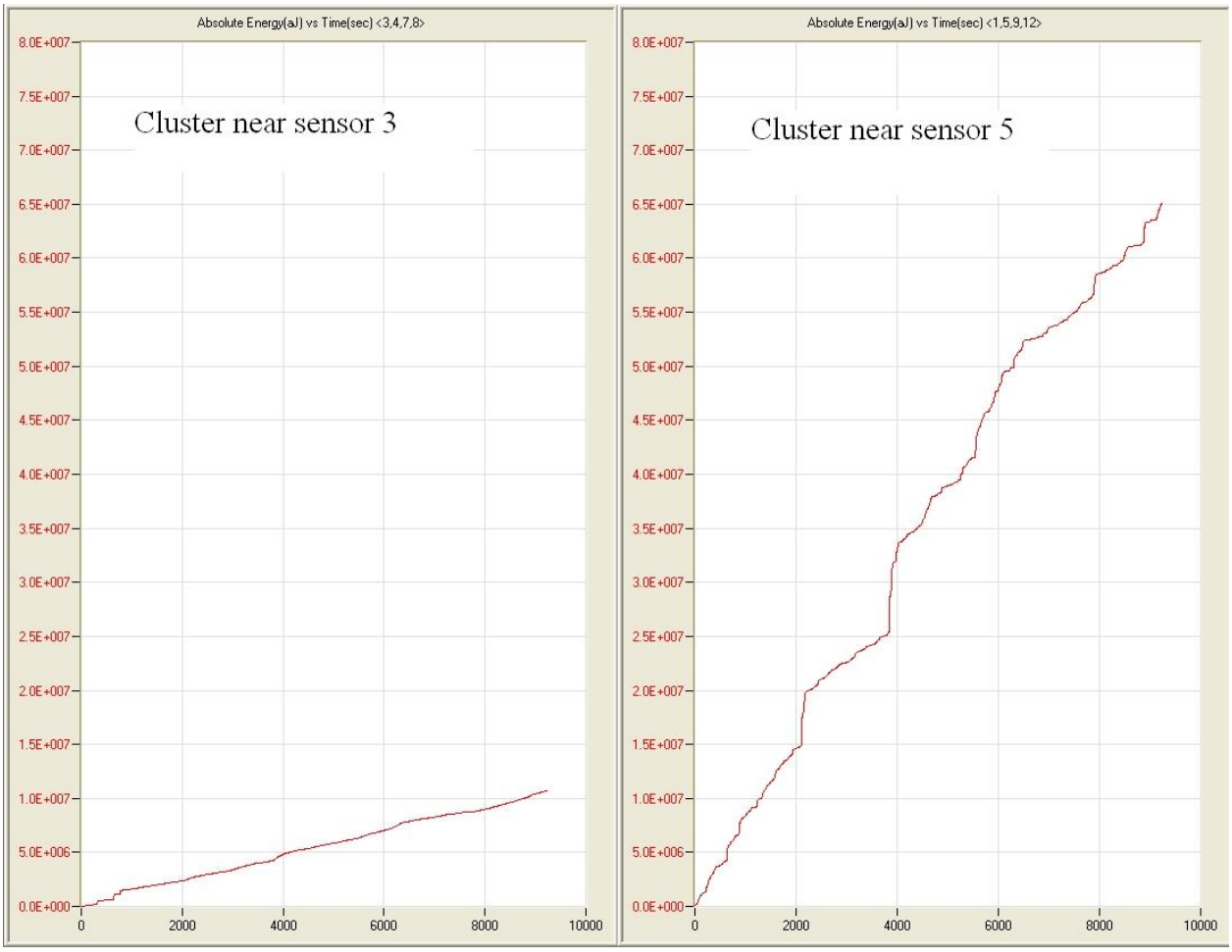

Figure 7-4. Total Absolute Energy as a function of time for clusters near sensor 3 (*left, a*) and sensor 5 (*right, b*) for data seen in Figure 7-2.

7.1.1.5. A bar graph of the number of hits per channel.

Figures 7-5*a* and *b* show a linear and a log plot of the hits per channel from the same data as shown in Figures 7-2, 7-3 and 7-4. The linear plot *a* shows that channel 13 is receiving most of the hits. It is so dominant that most of the other sensors appear inactive. Using a log plot of the same data, *b*, we see that is not the case and that only sensors 11, 15, 21 and 23 appear totally inactive while sensors 6, 17 and 22 have only a few hits. It also appears that the part of the structure covered by sensors 14 through 24 is showing very little emission. This data was from a fatigue test, so a temporary stoppage of the loading did not affect the test. The low amplitude channels were tested with lead breaks shortly before this data set was recorded. All channels tested good except channel 11. It was determined that the electronics on channel 11 were not working but the sensor was. So the sensor at position 11 was connected to channel 13, which had a very low activity, and the switch was inputted to the layout file. Whether the excess signals seen on channel 13 in Fig. 7-3 were caused by this switch is not known. However, the data in

Figure 7-3 and resulting lead break tests did show that the lack of emission from sensors 14 to 24 was real and not an electronic problem.

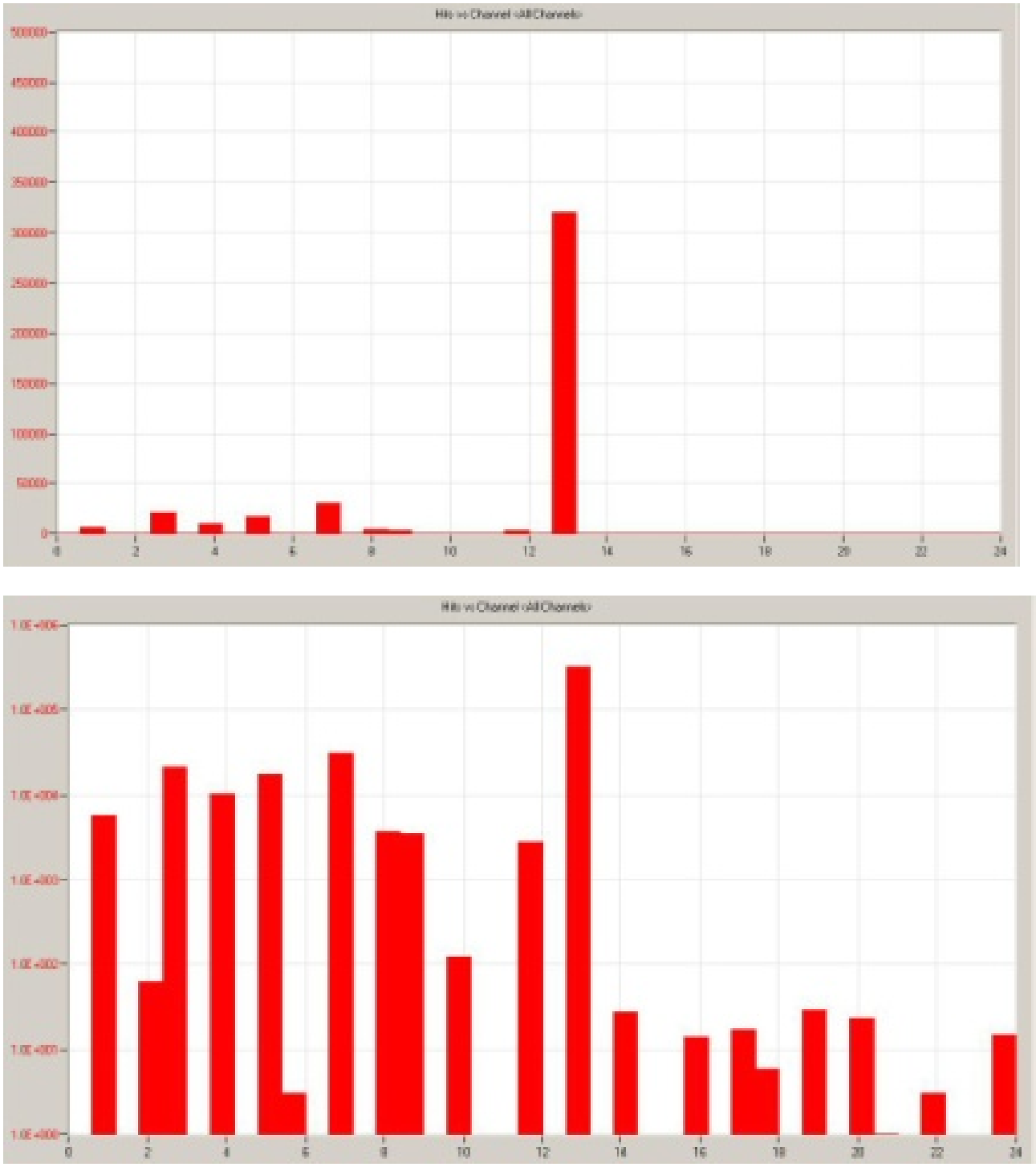

Figure 7-5. Hits vs. Channel, *a.* Linear Plot (*top*) and *b*. Logarithmic plot (*bottom*).

7.1.1.6. A scatter point graph as a function of time of the load value for each hit and an accompanying scatter point graph of the acoustic count for each hit.

These graphs are useful for fatigue tests. In a fatigue test, flaw growth is only going to occur at or near the peak load. However, in a complex structure, such as a wind turbine blade, there are often areas inside the blade where apparent frictional emission is generated. This emission is usually most intense at the mid-load region, where the rate of change in the load is a maximum. If the load is offset so that one peak of the cycle is at the normal zero load of the specimen, then the maximum load is at the opposite peak of the cycle. By using a voltage controlled gate to accept data only at the top ten percent of the load, one can greatly reduce the amount of data being collected. If the load is not offset, one may want to accept data from both the positive and negative load peaks. (One caution: in a resonant fatigue test, the load signal from one position on the blade may be out of phase with the displacement at the location of a flaw. The gate must be set so that it includes the displacement peaks at the flaw positions, even if it means accepting larger data files.)

Figure 7-6 shows the count and load curves for a small portion of a test which had a large amount of emission occurring throughout the entire load cycle. The recorded data included all

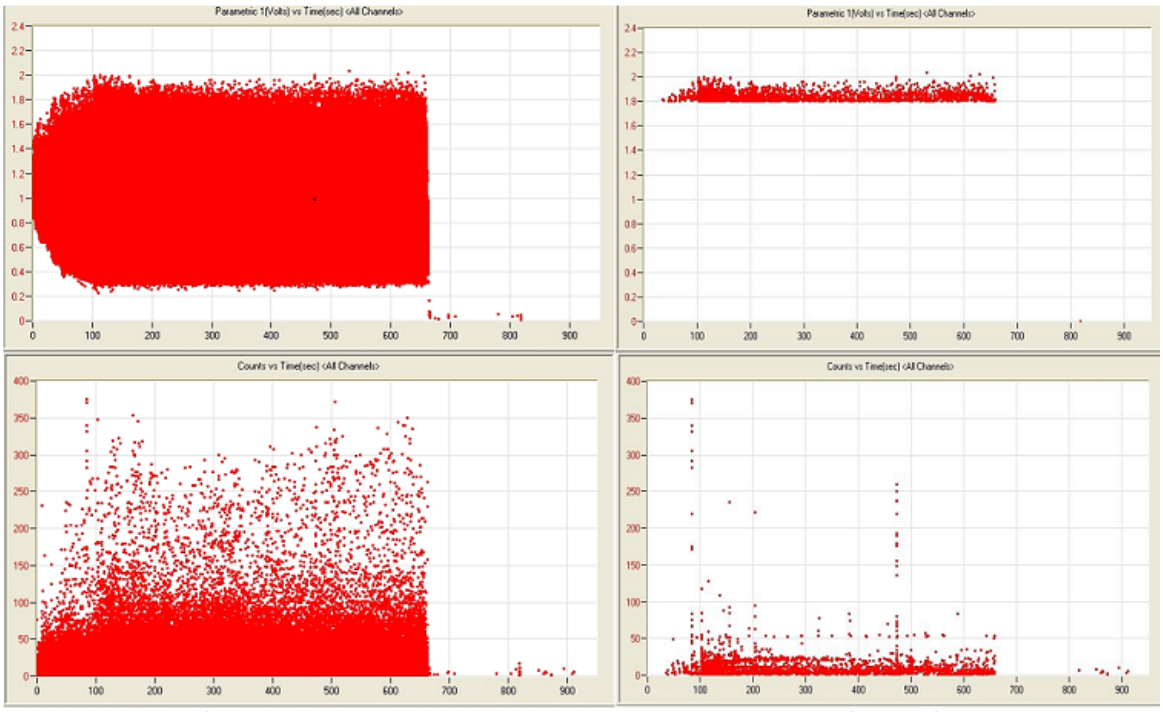

Fig. 7-6*a* Fig. 7-6*b*

Figure 7-6. Graphs of scatter point plots of counts and load parameter (*top*) and the AE count (*bottom*) for hits from a short period of time during a resonate blade test. Fig. 7-6*a* (*left*) contains curves for the complete data set, while Fig. 7-6*b* (*right*) contains only hits which occurred during the top 10% of the load cycle.

hits. The upper graphs are plots of the load parameter as a function of time for each hit. Figure 7-6*a* includes all the data recorded. Figure 7-6*b* is the same data which was filtered to remove all data which at loads lower than 90% of the maximum load. In the lower curves, the AE count for each hit seen in the upper curve is plotted. Figure 7-6*b* shows exactly what the data set would have looked like if a voltage time gate was used to pass only hits which occurred at loads 90% of the maximum load or higher. This reduced the number of hits in the data set from 566,077 to 2,851 and the number of located events went from 5,585 to 7. Notice, the several vertical line of hits in 7-5*b* count curve. These are high energy sources that have excited more than six sensors. Thus the filtering greatly reduced the data file size but still detected emissions from several large sources. The few large sources was consistent with this particular period of this test These graphs show the value of accepting data only at load peaks. Data filtering is necessary when one obtains many gigabytes of data per test but one must try to insure that what is being filtered out is not useful data. It is impossible to say that all of the hits seen in Figure 7-5*a* were useless noise. However, there is so much data collected in an average AE test that much of it is redundant. If the value of the filtered data is unknown, it may be better to record the data and then filter the files in the post processing process.

There is one more procedure which can be useful in determining what signals are produced by actual flaw growth and which result from some other mechanism during a fatigue test. A wind turbine blade fatigue test applies a large amount of force and motion to a blade and it is certain that not all of the acoustic signals are produced by material failures. Since acoustic emission is a result of random processes, it is of value to look at the output of such a process. An easy experimental example is the melting of an ice cube in a glass of water. As each crystallite of ice melts, it changes the local stress fields in the ice cube. This results in a continuing micro cracking in the ice cube and a steady generation of acoustic emission. Plotting the distribution of the absolute energies from the emissions produced by a melting ice cube gives the curve shown in Figure 7-6. While there are many more emissions at the low energy end of the curve, all energy values appear represented. With 7500 emissions, almost every energy value between 0 and 200 units has at least one burst. There are no peaks in this energy distribution nor are there any gaps. We expect acoustic emission from flaw growth to have this general distribution of energies.

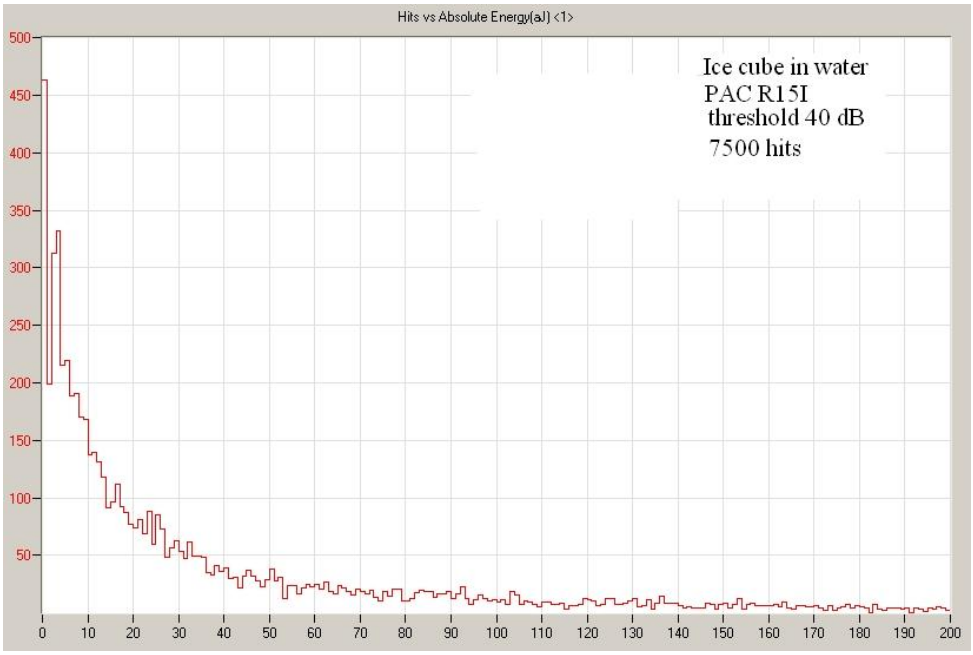

Figure 7-7. Distribution of hits versus absolute energy for emissions generated by melting ice cubes.

Now look at Figure 7-8. This shows the distribution of energies from five sensors spanning two built-in flaws in a wind turbine blade undergoing fatigue testing. Channels 17 and 21 follow the distribution seen in the ice cube emission. Channels 18 and 20 have more structure but still show a broad distribution of emission energies. Even channel 23, which had very little emission, does show a broad distribution of energies. These curves indicate that this data is real emission produced by structural failures in the blade. However, at the root end of this blade where the strength of the blade is much higher, data from the same set seen in Figure 7-8 showed a large amount of emission located in one area on the blade surface. This is seen in Figure 7-9 displayed as a strange pattern of curved lines which have nothing to do with the blade structure. Sensors 1 and 5 are located on the opposite side of the blade from sensors 2 and 6. The energy distribution from the six sensors in the root region is shown in Figure 7-10. While sensor 6, which was adjacent to the drive fixture, shows an energy distribution similar to that from the ice cube, sensors 1 through 4 show that all the energies detected by each sensor lie within narrow energy bands. Those acoustic signals appear to be produced by some other mechanism than flaw degradation. We can conclude that while the signals from sensor 6 were probably produced by small relative movements between the blade surface and the drive fixture, located emissions using data from sensors 1 through 4 were complete artifacts produced by signals excited by the motion of the fatigue driving mechanism. When the located emissions do not appear to make sense, either from a strange location or strange distributions on the blade, this type of analysis can be very useful.

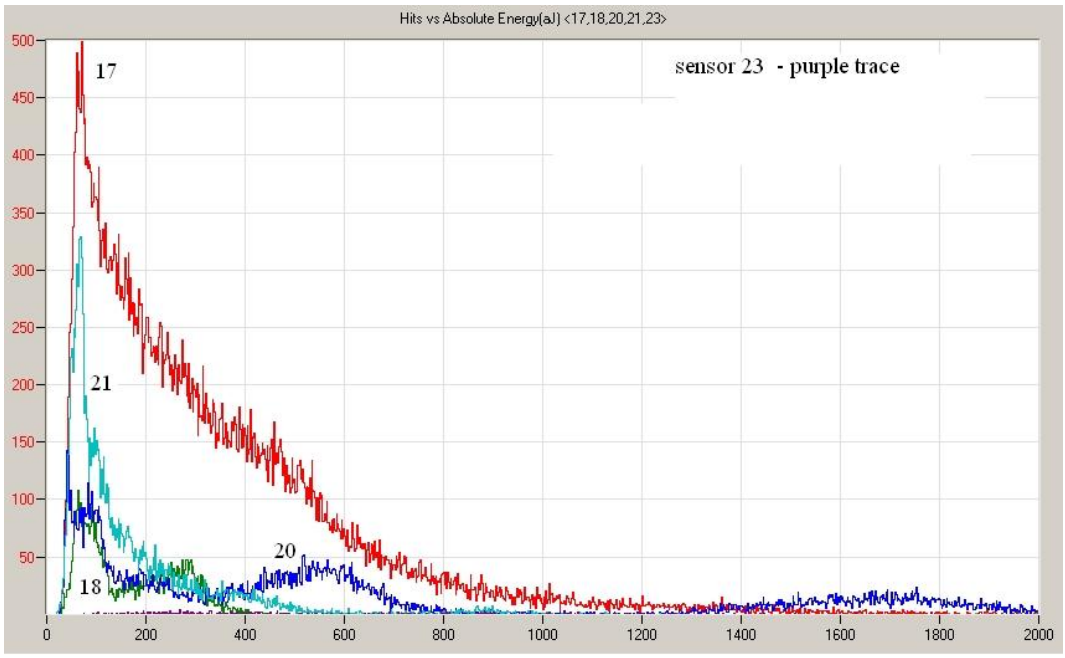

Figure 7-8. Hits vs. Energy distributions from five sensors near built in flaws in blade

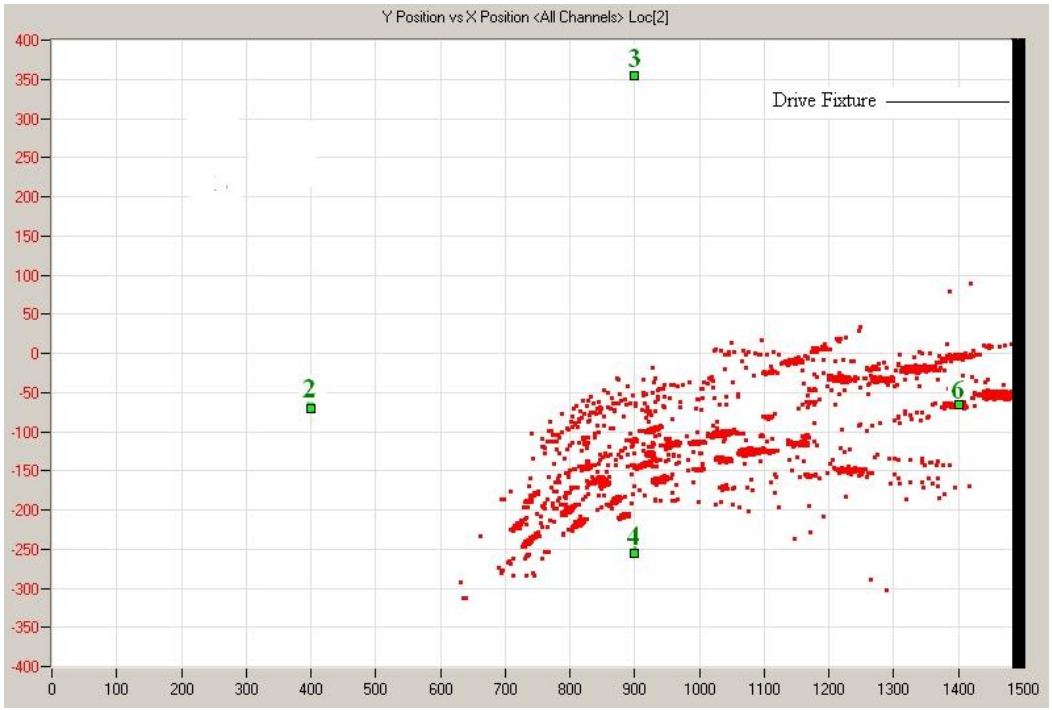

Figure 7-9. Apparent flaw locations on high pressure surface of blade root near drive fixture

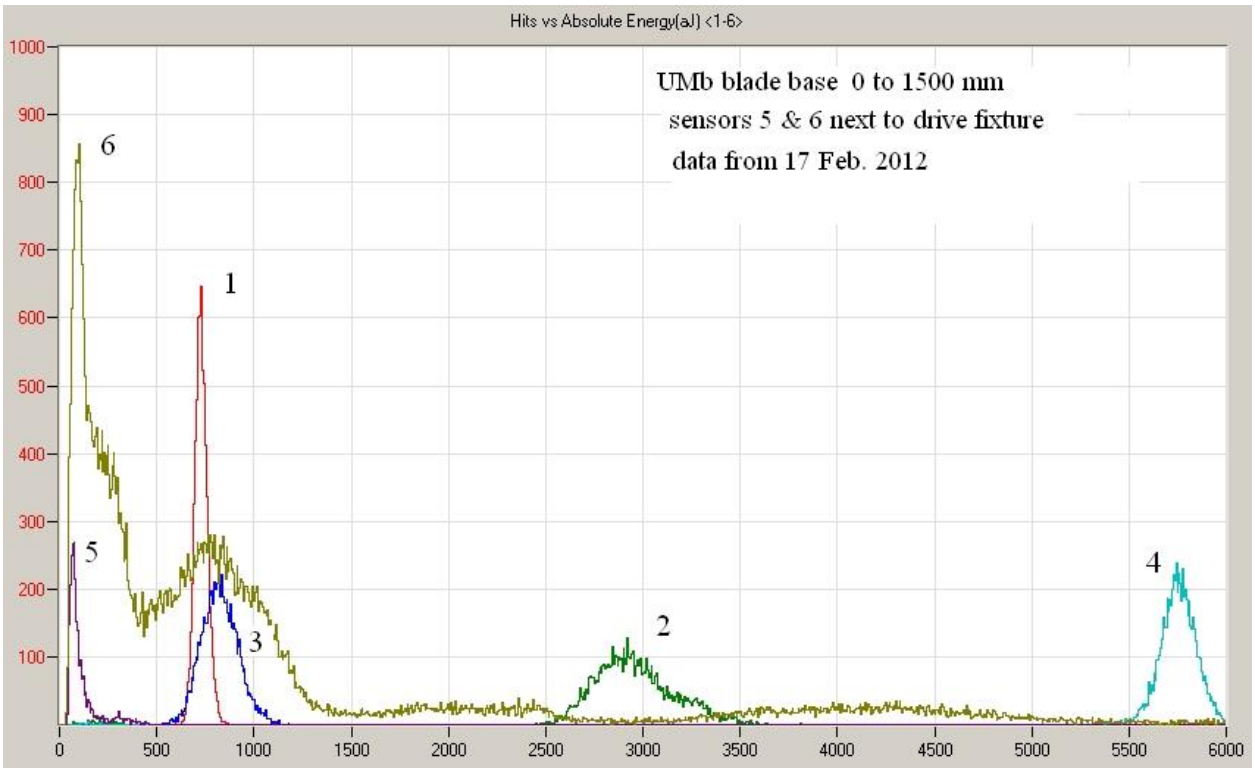

Figure 7-10. Hits vs. Energy distributions for six sensors on root of blade. Same data as seen in Figure 7-9

The figures in this chapter, with the exception of Figures 7-7, are the graphs the author considers most useful to the operator running the test. On a fatigue test, the operator has often set up graphs of absolute energy rate vs. time for both sides of the blade. Unfortunately, there has seldom been a significant difference in the two graphs, so there is no recommendation for such graphs unless there is a real expectation that different regions of the structure will be affected differently by the increasing load or cycle count.

7.1.2. Post-Test Analysis

The first step in post-test analysis should be a critical review of all the data collected during the test. It is usually valuable to create a time line of the loading sequence and to identify when all events occurred during that sequence. At the time when the emission starts, replay that data and look at the listing display. If there are a large number of 3-hit locations, look at the delta times. If these times are almost identical for many of the hits and/or the hit durations, or hit energies are very similar for the different located events, the events are probably not generated by flaws. In a fatigue test, any hits or events which occur regularly in phase with the load signal will seldom be produced by flaw growth, even if they occur at the load peaks. Microscopic flaw growth depends on the local material environment. Regular crack advancement during a recurring load will be seen only near failure, if at all.

It is often useful to combine several sequential data files into one larger data file that covers a single time sequence. AEwin has a “link separate data files” utility which works well. One word of caution: AEwin slows down the replay drastically when the file is too large. If the test was a

single loading of a structure and there were pauses during the loading, look for when the emission did not stop instantly during a loading pause. This early indication of flaw growth specifies where one should start looking for locatable events.

Most of post-test analysis consists of trying to determine flaw locations and their behavior under stress. During the time of the test, one is limited to the graphs which were implemented for the test and for the current time period. The number of real-time graphs is limited by the speed and capacity of the computer. However, there is no such limitation in post- test analysis and the number of possible graphs available in current AE software is very large. The start of the post-test analysis should use the original real time graphs to replay the test. After that, other graphic analysis should be used as desired.

Unfortunately, there are some analyses which are not available, at least in the AEwin software. A group of source location programs evolved over the author's career in the practice of acoustic emission testing, for example, the FORTRAN program discussed in Chapter 6 (and listed in the Appendix). One useful technique used in this program is to color code the located emissions on a graph with respect to their absolute energy. Another is to define specific locations on a location graph as clusters and then to plot a graph of AE parameter versus time or load for each cluster. AEwin does show clusters but does not allow one to choose an arbitrary size or location for each cluster, nor does it allow the plotting of an arbitrary AE parameter such as the absolute energy of the event for members of the cluster. Finally, AEwin does allow for anisotropic acoustic velocities but specifies a single shape of the anisotropy. In at least the TX blades, the acoustic surface velocity anisotropy was unique to the blades. In many AE tests the results are not ambiguous and the commercial programs can produce acceptable results. However, most of the AE testing at Sandia has been analyzed with variations of the listed FORTRAN program and they are used in the following example.

Figure 7-11 is very similar to Figure 7-2. It uses the same data, but covers many more cycles of the next-to-last load block. The figure shows four areas that appear to have clusters starting. This data is shown here so that the incipient clusters can be identified. Figure 7-12 shows the located events on the tension side of the blade during the last loading of the test. This was produced with the author's FORTRAN programs. As can be seen, there is so much located emission that the original clusters are hidden.

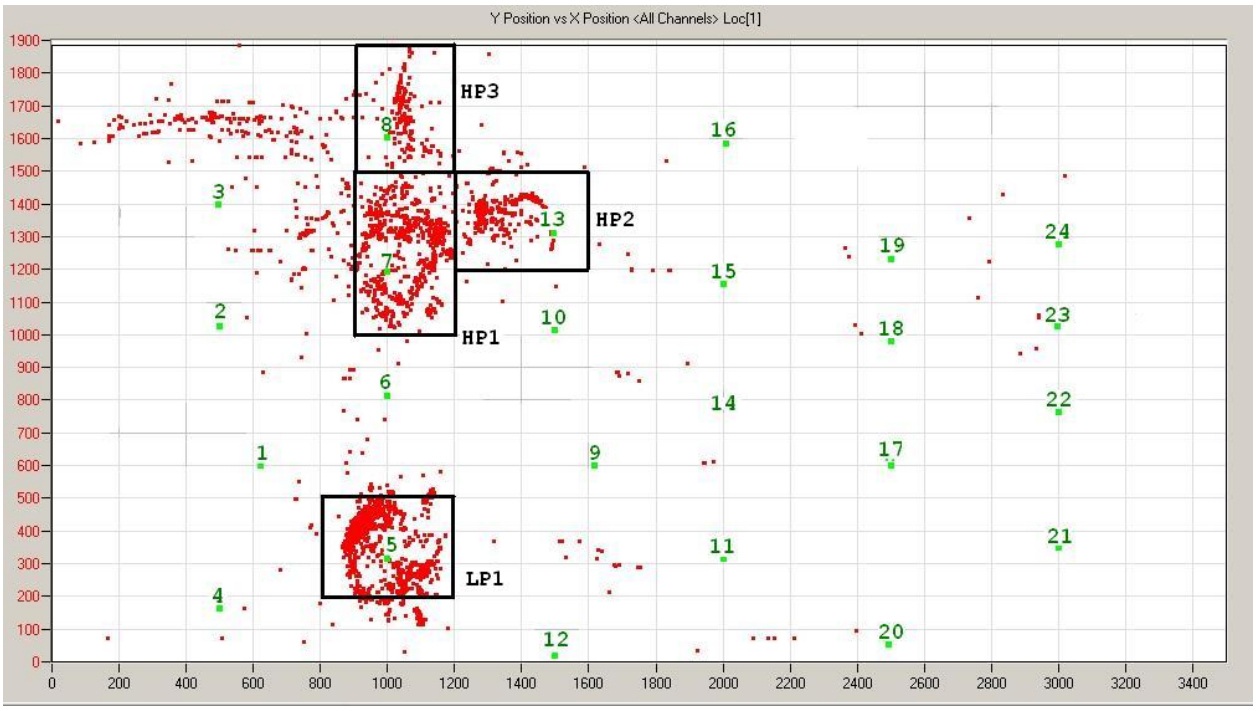

Figure 7-11. Location graph from extended data set of Figure 6-4 showing locations of incipient clusters

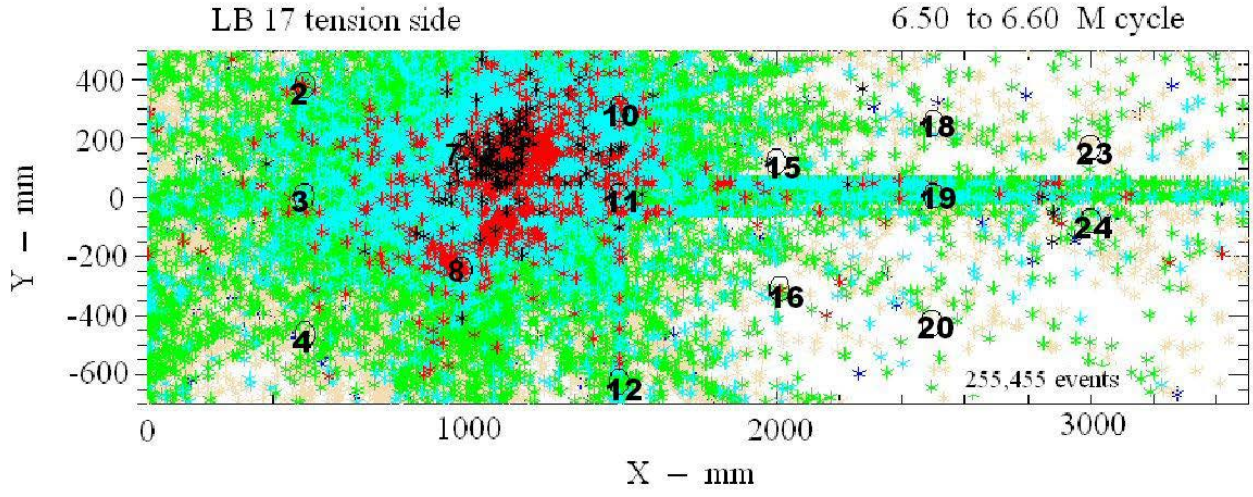

Figure 7-12. Location graph of tension side of blade during last loading. The view is an inverted image of the top half of 6-6. Absolute energies of events are in MeV. The code is 1<blue<10<tan<10^2 <green<10^3<cyan<10^4<red<10^5<black. The conventions of the graph are that the shear web position is zero chord on both sides of the blade. Positive values are toward the leading edge and negative values are toward the trailing edge.

Figure 7-13 shows the total energy vs. cycle graphs for the four clusters seen in Figure 6-6. The cluster on the low pressure (compression) side of the blade shows a decreasing slope as the test moves toward failure. A decreasing slope suggests that unstable flaw growth has ceased. This was the major cluster on the low pressure side of the blade and shows that the failure was

confined to the high pressure (tension) side of the blade. Most of the energy release was in cluster HP1. The major failure appears to have started at about 73,000 cycles. The emission rapidly increased until around 90,000 cycles where it becomes almost constant until failure. Interestingly, this rapid increase in the energy release rate is seen in all three clusters on the high pressure side. Furthermore, there are indications in all three clusters that the energy release rate slowed down just before failure. When the 12,000 cycles were examined in detail, it was found that the release rate where the failure occurred was little different from the release rate of the front high pressure surface of the blade from 500 to 1500 mm. Therefore, the whole front surface of the blade between 500 mm and 1500 mm was failing and the actual fracture could have occurred anywhere on that surface. This blade appeared to be without any serious flaws, most of the surface being of uniform strength. The actual failure position occurred almost randomly on the blade. Further details of this test are given in Chapter 9.

In summary, the post-test analyses are the most important part of an AE test. In most cases, the customer is not too interested in the test details and analysis as long as the methods are believable. What is important is the information which the AE gives about the test. If a test is not taken to actual failure, what is the location of the worst flaw and what is an estimation of how close the specimen was to failure? On a proof test, were there any signs of flaw growth at all during the test and was the test sensitive enough to see minor flaw growth? Fine details of the analysis are often not needed in a final test report, but the estimate of the health of the specimen is all important.

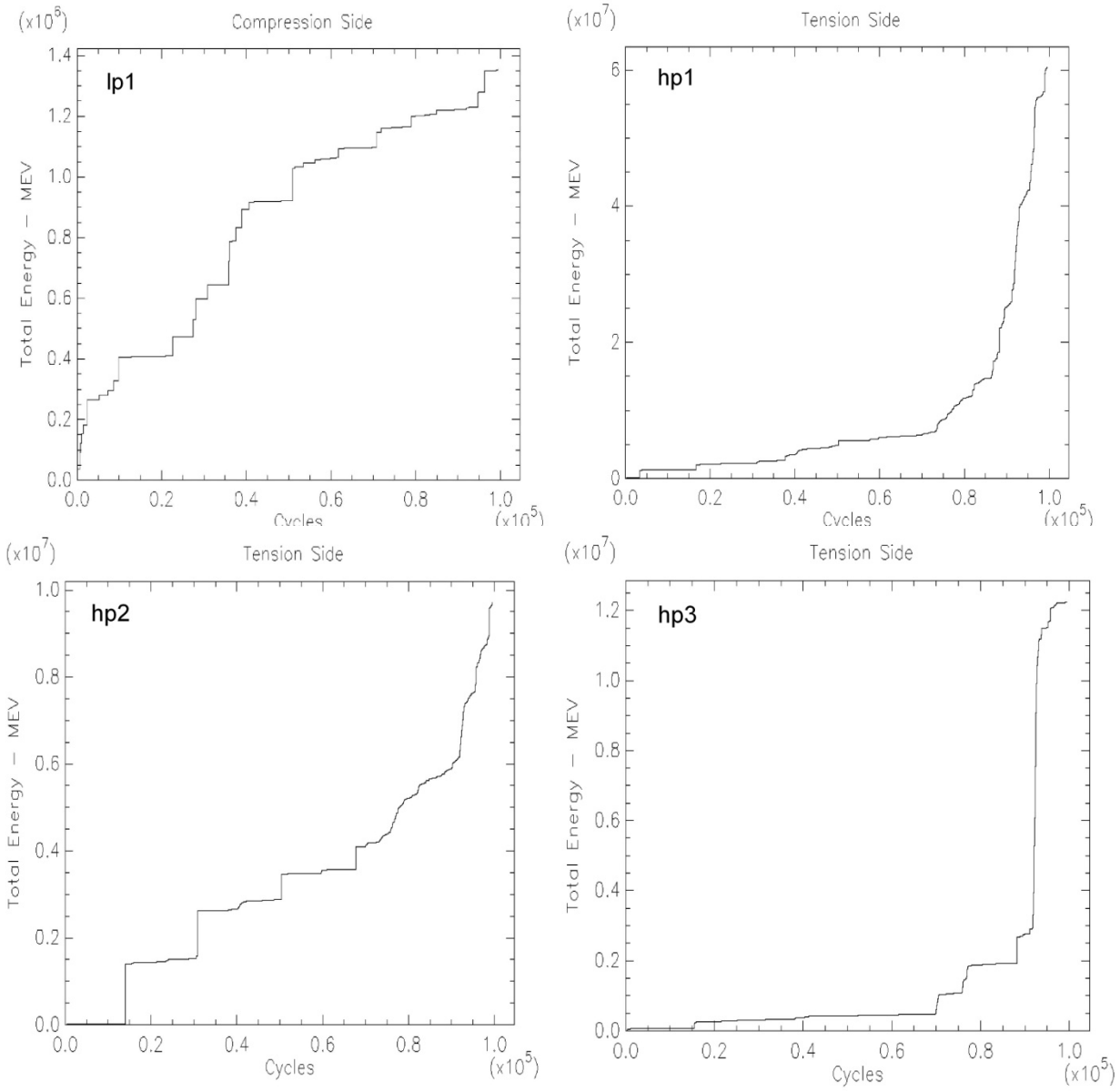

Figure 7-13. Total energy vs. cycle graphs for four clusters for the last load value of the BSDS blade fatigue test

8.0 CHAPTER 8

8.1. TX-100 Blade Fatigue Test

The first example of an acoustic emission test setup and analysis is the fatigue test of the Sandia TX-100 blade [14, 15] performed at the National Wind Technology Center (NWTC). This was a 9-meter wind turbine blade with a special skin designed to rotate the tip angle of incidence as the load on the blade increased. The modification consisted of a single layer of carbon fibers on the skin surfaces which were oriented at 20 degrees from the axis of the blade. The first TX blade was subjected to a static load test to obtain structural characteristics of the blade. That blade failed near the 1.0 meter station on the low-pressure surface. There was also significant acoustic activity on the high-pressure side near the root and on both surfaces near the 4.6 meter station where the internal shear web with its accompanying spar caps ended. These results suggested local stress concentrations at these locations. Previous fatigue tests on this type and size of wind turbine blade had been carried out with a hydraulic actuator driving the free end of the blade up and down. For this fatigue test, the blade was cantilevered to the test stand at the base, a static load was placed near the tip and a hydraulic fixture driving two moderate weights up and down was mounted on a saddle about 1.6 meters from the base of the blade to produce inertial loading. The resonant frequency of the first flap mode of the blade was measured and the two weights were driven up and down at this frequency. At resonance, the tip of the blade had a large amplitude swing. To agree with previous tests, the blade was tested with the low-pressure side down and a weight mounted towards the end of the blade. This weight was adjusted so that that the actual load on the low-pressure side was always positive. With this geometry, the failure was expected to be similar to that of the static test, occurring around 1 to 2 meters from the base on the low-pressure side of the blade.

A 24-channel PAC DISP system using AEwin software was used for data acquisition. The sensors, PAC R6I, contain a built-in preamplifier. Their response covers the band width of 30 to 150 KHz, peaking around 60 KHz. The load signal was taken from a dedicated strain gauge mounted on the surface of the blade near the driving actuators. It was calibrated with a dead weight test load and the output amplified and fed to the DISP system. The decision about which areas of the blade to monitor was based on the results of the TX blade static test. Locations of the sensors, the driving fixture position and construction details of the blade's upper and lower surfaces are shown in Figure 8-1. The low-pressure surface from 500 mm to 3500mm was instrumented with 13 sensors. This array covers the region where failure had occurred in many of the previous 9-meter blade tests. Finite element analyses of the blade had indicated the possibility of problems around the abrupt end of the shear web at 4600mm. One array of four sensors was placed on the low pressure-side of the blade and a second array of three sensors was placed the high-pressure surface, with both centered around station 4600 mm. Finally, an array of four sensors was located on the high pressure side of the blade just inboard of the driving fixture. These placements were based on our assumption that the failure would be on the low-pressure side of the blade, but because we had not previously

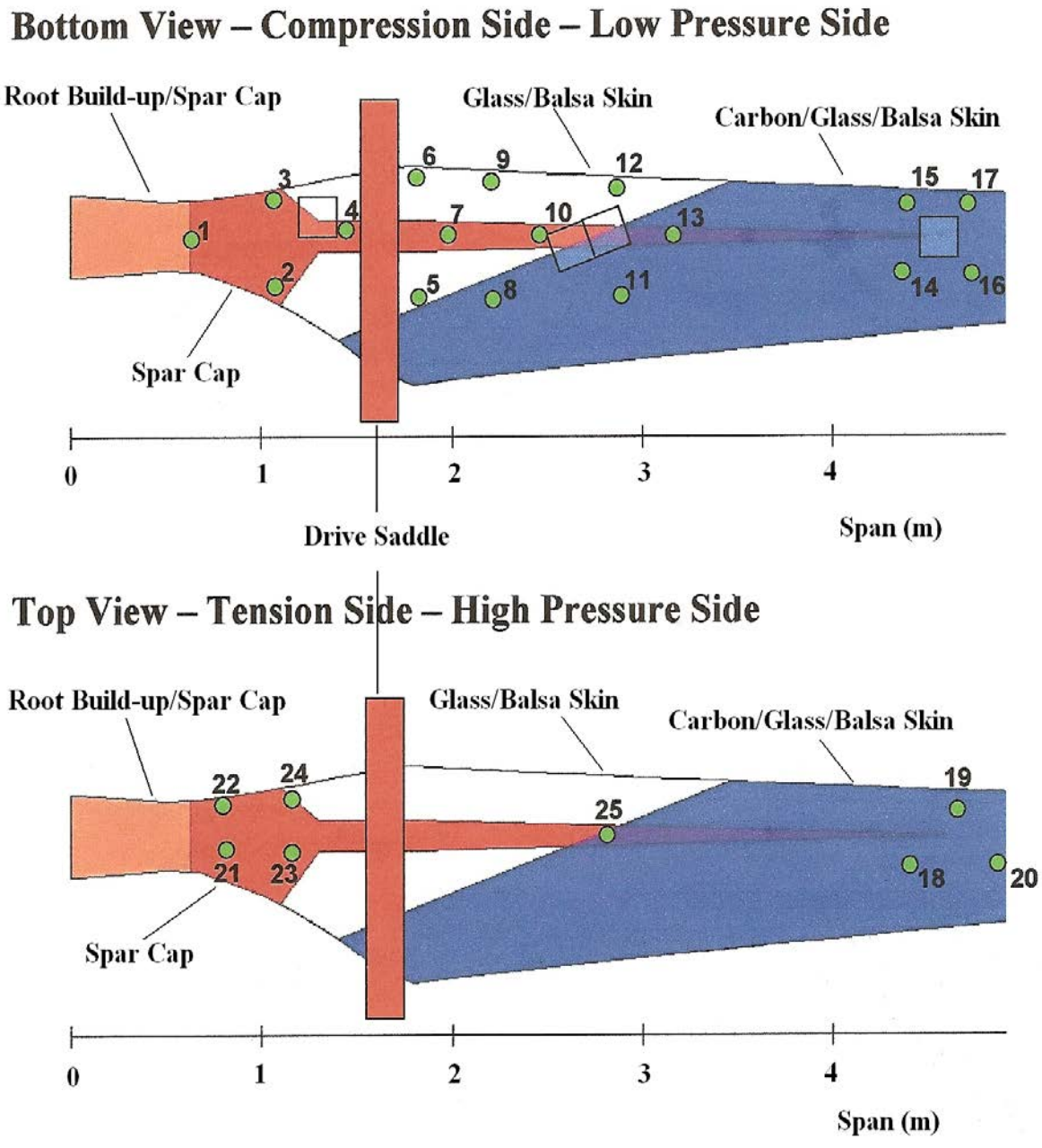

Figure 8-1. Construction diagram and sensor layout for TX Blade Fatigue test

monitored a blade driven into resonance, we should cover all bases. The sensors were bonded, as usual, with GE Silicone II adhesive. The sensor placement coordinates were referenced to the inboard end of the blade and the approximate center line of the blade as defined by the center of the spar cap above and below the internal shear web. Acoustic velocities were measured on the skin behind the shear web both perpendicular and parallel to the shear web. These velocities were quite close to each other at 3.1 mm/μsec parallel to the blade axis and 2.9 mm/μsec

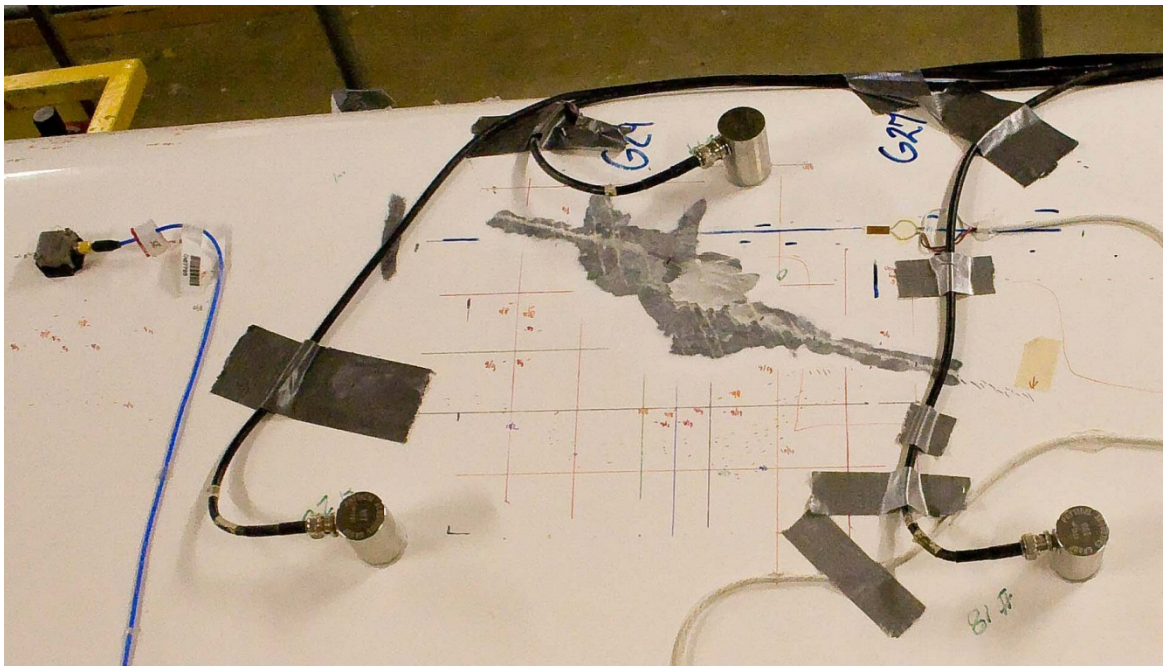

Figure 8-2. Picture of surface crack on tension side of blade around 2000 Kcycles

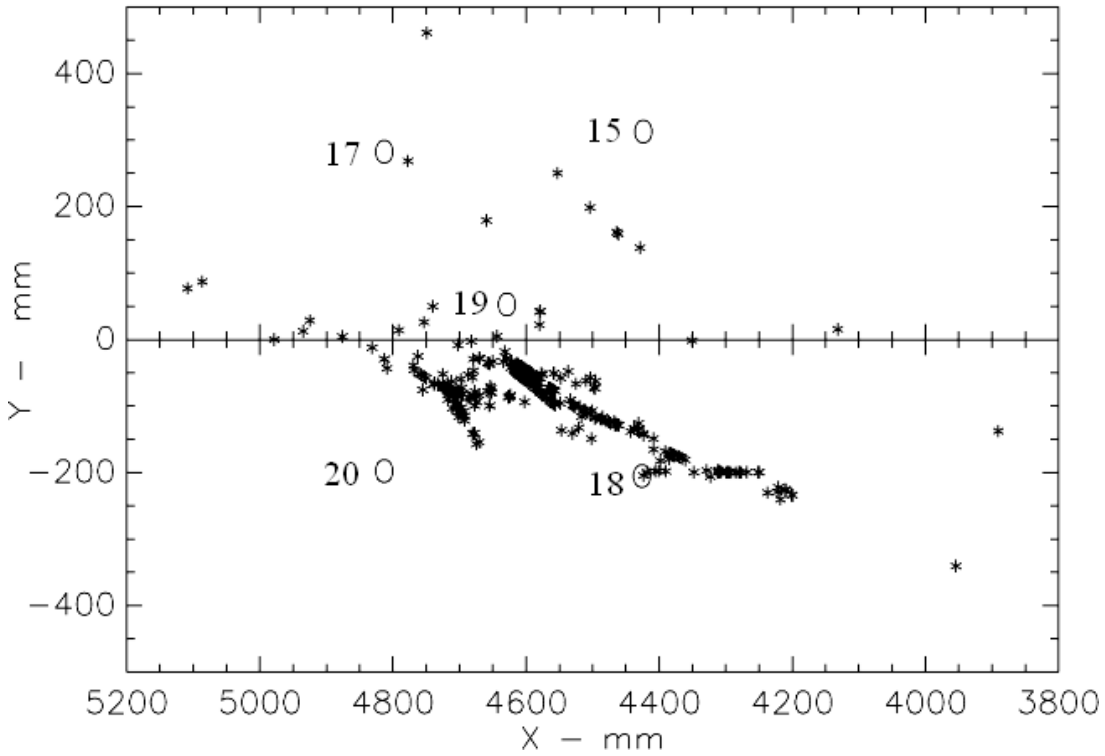

Figure 8-3. Final source location calculation of same area of blade around 2000 Kcycles

perpendicular to it. With such close proximity, we did not hesitate to use 3.0 mm/μsec in the AEwin location software which assumed an isotropic acoustic velocity. The collected data set included hit arrival time, sensor number, rise time, count, signal duration, signal peak amplitude

and signal absolute energy. During most of the test, waveform data was collected. The digitization rate was 2.0 MHz and the first two milliseconds of each wave were digitized and recorded. Almost all of the acoustic emission signals were shorter than two milliseconds because of the high attenuation of the blade skin.

The test was monitored by several NDT methods in addition to acoustic emission. At least two of the other systems generated acoustic signals in the blade. This required the AE system to stop taking data when the other methods were in use. Because of these resultant gaps in the data record, the cycle counting feature of the software could not be employed. All cycle data had to be obtained from the NWTC operators' log and the time data from the AE system (start, stop and running times). The inclusion of the waveform data created huge data files (e.g. one hit contained 28 Bytes of data without waveforms and about 8100 Bytes including waveforms). They were sent by TCP over the internet in batches of one hundred 5 MB files at a time. Toward the end of the test, the waveform acquisition was stopped and each 5 MB file then contained about 16,135 hits instead of the earlier 600-hit files with waveforms.

The test results were far from what had been expected. After minor emission on the few initial cycles, almost all the emission was seen coming from the region around the end of the shear web at 4600 mm, with the majority from the high pressure surface. Sensor 19, which was located approximately at the end of the shear web, showed almost continuous low-level emission from the first cycle. It was thought at first to be rubbing noise, but the waveform and its location near the peak load of each cycle indicated that it was probably real emission. By the time the test reached 2000 kilocycles, a surface crack was developing near sensor 19. This became quite noticeable as can be seen in Figure 8-2. In the post-test analysis, it was found that data from just the three sensors on the high-pressure side did not give satisfactory results. The two sensors, 15 and 17 on the low-pressure side of the blade were just past the leading edge and were often hit in the sensor 19 hit sequence data. Their inclusion in the calculation much improved the location graphs. Figure 8-3 shows the final calculated source locations from the same time period as the picture in Figure 8-2. The absolute energy per cycle for the emissions within the triangle formed by sensors 18, 19 and 20 was calculated from 3000 to 4000 kilocycles and is shown in Figure 8-4. The peak between 3780 and 3810 kilocycles indicates where a major fracture of the blade occurred. The damaged blade continued to disintegrate until the test was stopped at 4000 kilocycles to prevent complete failure of the blade which might harm the testing apparatus.

The initial velocity measurement had shown that the parallel and perpendicular velocities were fairly close to each other. However, off the major axes there appeared to be

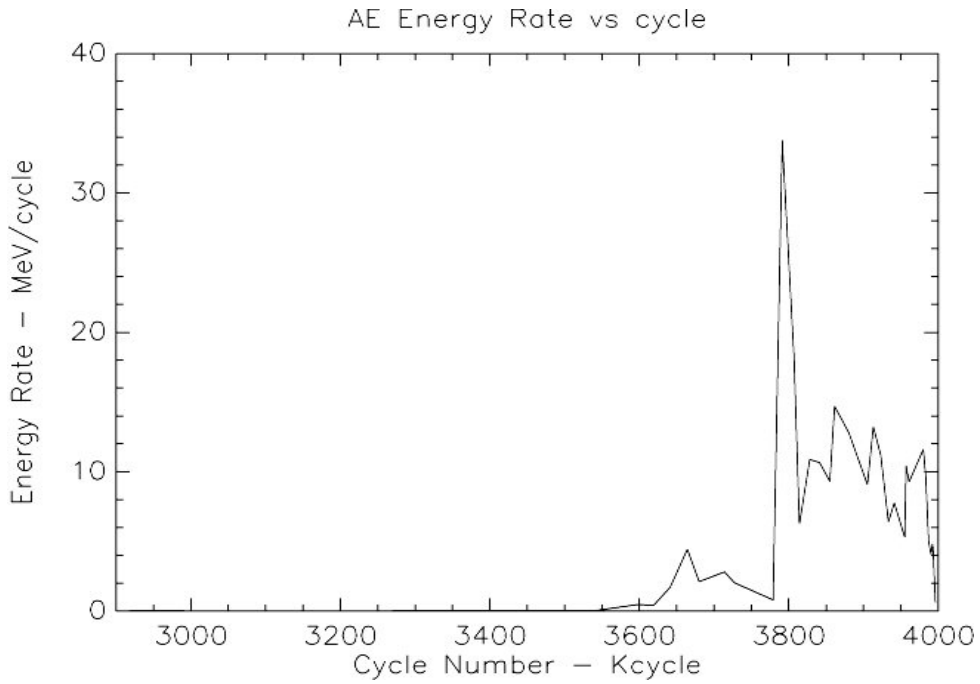

Figure 8-4. Energy rate from tension side of blade near end of shear web showing peak when major damage started

a much larger variation in the acoustic velocities. A one meter section of the TX-100 Blade broken previously in the static test was obtained. It was decided to make an accurate measurement of the velocities. Lead break measurements were made of the velocity in the section skin behind the shear web. An average value for the velocity was calculated every ten degrees. The result for the velocity, shown in Figure 8-5 is quite dramatic considering that the diameter of the carbon fibers in the surface layer of the blade is almost microscopic. It appears that most of the energy in the Rayleigh wave created by the lead break must be contained in the surface interface with the air. The effect of the 20-degree orientation of the fibers dominates. In order to include this information in a FORTRAN location program, an analytic function that fits this velocity data was devised. It is included on the accompanying disk as a subroutine. The graph in Figure 8-3 was generated by this program.

This test showed that accurate acoustic emission source location is possible on an FRP structure if enough sensors and an accurate measurement of the velocity are available. Adding some filtering and color coding the energies of the events improved the location graph shown in Figure 8-6 to that shown in Figure 8-3. Restricting the calculation to events with hits from four to five sensors in the data set resulted in a decrease in the number of data points in Figure 8-6. This graph (8-6) pins down the location of the major flaw although the first graph (8-3) agrees better with the visual damage. One possible explanation is that the three-hit events were not included in Figure 8-6 and that they usually had lower signal amplitudes. These signals were more likely Rayleigh waves that have their highest amplitudes at the surface where the carbon fibers were. They are most affected by the surface with the 20 degree off-axis carbon fibers. Thus Figure 8-3 shows the effect of the anisotropic velocity seen in Figure 8-5 while the result from a more isotropic velocity is seen in Figure 8-6. The major conclusion of the AE test was that the only problems seen in the blade structure were in the stressed regions where the shear web abruptly

ended. There was strong evidence that load level at the start of the test was already producing minor damage in these regions.

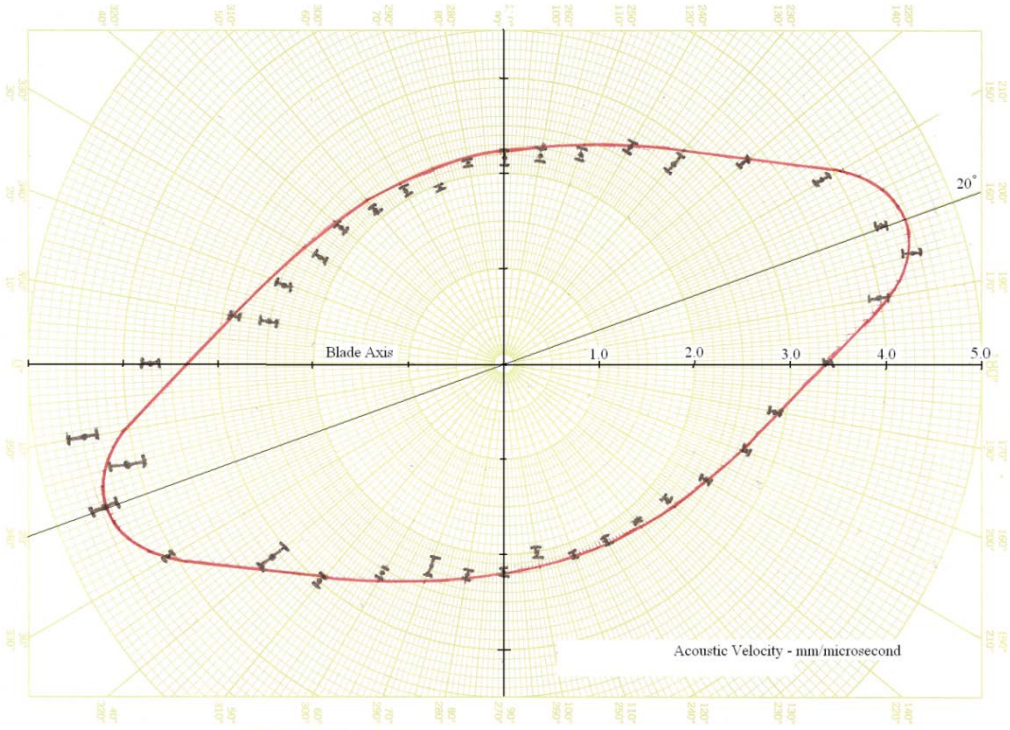

Figure 8-5. Measured acoustic velocity of TX blade as function of angle from blade axis

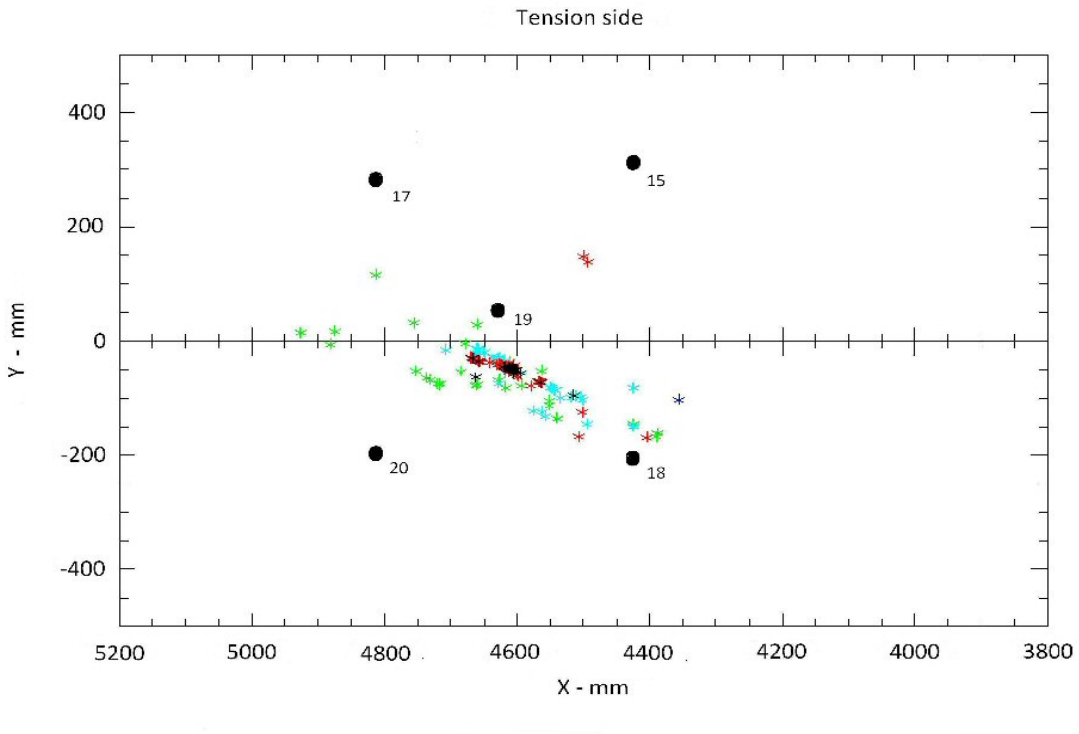

Figure 8-6. Same data as Fig. 8-3, with filtering and color code: black > 10^5 MeV, red > 10^4 MeV

9.0 CHAPTER 9

9.1. BSDS blade

Our second example of a test setup and analysis is the fatigue test [19] of the BSDS blade, also performed at the NWTC. The BSDS design is a 9 meter blade which incorporates flatback airfoils in the inboard section of the blade. These airfoils give the blade a thick, structurally efficient geometry. Cross sections of the blade at 0.5 and 1.0 meters are shown in Figure 9-1. Not shown in the figure is the shear web down the center of the blade with carbon fiber reinforced spar caps on the top and bottom of the web. The fatigue test was performed using a hydraulic cylinder to apply single point cyclic loading to the blade in both the flap and edge orientations. The loads were applied to a saddle located at a station 5.0 meters from the base of the blade. Loading frequencies started at 1.5 Hz and had to be slowly decreased as the load was increased due to limitations of the hydraulic cylinder. The final load frequency was 0.65 Hz.

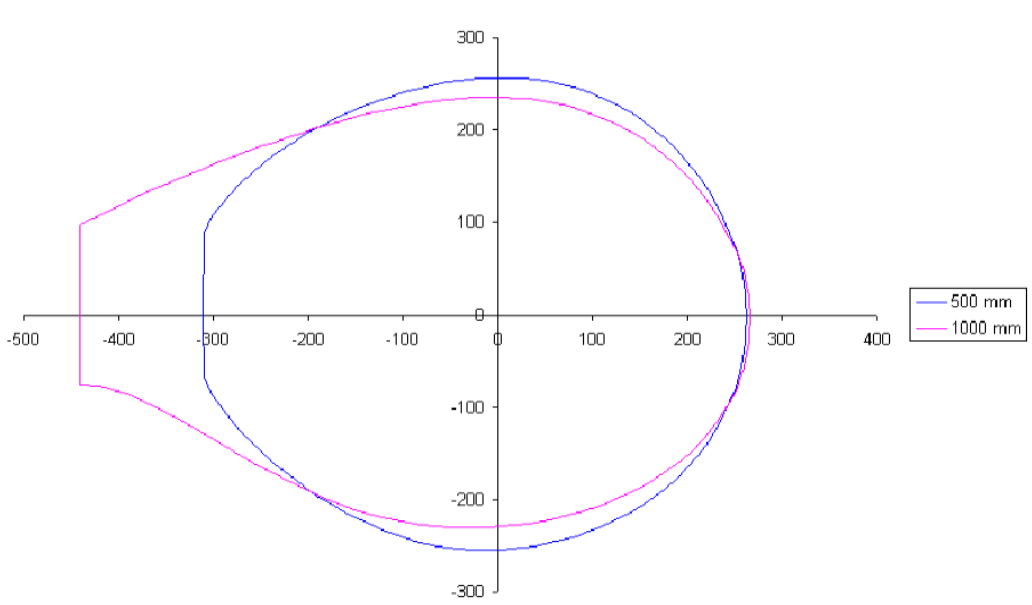

BSDS Blade cross sections at stations 500 mm and 1000 mm

Figure 9-1. Flat-back airfoils of BSDS blade for stations 500 and 1000 mm

A static test of a BSDS blade was conducted and acoustically monitored. That blade proved to be considerably stronger than previously tested 9-meter blades. The static load was distributed through two whiffle trees to three fixtures on the blade. The inboard fixture was located at approximately station 3000 mm. Acoustic emission from the first test indicated the start of failure around a 9500 lb. load on the low-pressure side between stations 2000 and 2600 mm. The failure occurred at a load of about 10,800 lb. at a location between the inboard and second fixtures. This was unexpected so there were no sensors located beyond station 2600. The stub of the blade was reloaded and soon failed near station 2000 mm during the first reload step. There

were no sensors beyond station 2600 mm on the first static test, so there was no data from the region of the first failure. The second loading was done without any acoustic emission instrumentation due to severe budget restrictions. On the first loading, one sensor was mounted on the high-pressure side of the blade over the shear web at station 970 mm. It recorded about an order of magnitude more detected acoustic energy during the test than the sensor mounted approximately above it on the low-pressure side.

These static tests indicated that there was appreciable emission from both the low pressure and high-pressure sides of the blade and that failure could occur out beyond station 3000 mm although a longer term hold at a load of 9500 lb, could have led to failure on the low-pressure side between stations 2500 and 3000 mm. The decision was made to monitor the whole surface of the blade between station 500 mm and station 3000 mm. It was thought that the blade failure outside of station 3000 mm may have been due to the distributed load applied to the outer end of the blade during the first static test and that single point fatigue loading would probably cause failure inboard of station 3000 mm. A pattern of 24 sensors, six rows of four sensors each, was used. The first row was located at station 500 mm with sensors above and below the shear web and two more placed on the leading and trailing edges. The next row also contained four sensors and was located at station 1000 mm, but it was rotated 45^{o} from the first row, around the center of the blade. This pattern continued every 500 mm out to station 3000 mm. This is the pattern described in Chapter 5 and shown in Figure 5-2.

The BSDS blade with its flat back airfoil appears as a distorted cylinder. In order to display the entire surface of the blade and use the leading and trailing edge sensors for calculations on both sides of the blade, the AE system was setup in cylindrical mode, but with the actual sensor locations inserted. It was hoped that this would warp the cylinder surface into a form equivalent to the blade. This appeared possible since the different airfoils and construction made the blade much more similar to a tube than the other 9-meter blades that have been tested. It also allowed the author to set up his own programs for separate graphs of the high-pressure and low-pressure sides of the blade. This approach appeared to work fairly well, although the author recommends that separate location programs be used for the two sides of a blade in future tests.

The data collected by the AE system consisted of the sensor number, the arrival time of the wave at that sensor, the amplitude of the load at the instant of arrival at each sensor, the log of the peak amplitude of the wave, the rise time and duration of the transient wave, the acoustic emission count and the absolute energy of the waveform generated by the sensor. The digitized waveform was recorded for some of the early data, but as found in the TX-100 test, the information obtained did not appear worth the huge increase in the amount of data it would have produced. Other system settings were the same as in the TX-100 test. The load signal was again taken from a strain gauge mounted on the blade and calibrated with static loads. This signal drove a voltage time gate which allowed the system to acquire data only when the load signal was over 90% of the peak load. Front end filtering in place during the data acquisition removed all hits with a single count, or a duration less than 50 μsec. This filter duration is equal to three wavelengths of sound at 60 kHz. A close look at the data shows that very few events would have been affected if this filter time had been lowered to 30 μsec or two wavelengths at 60 kHz.

The acoustic velocity was measured to check for anisotropy. Surprisingly the velocity was measured to be isotropic at 2.5 mm/μsec in the skin beyond 1.5 m from the base of the blade.

Near the base of the blade, the velocity varied from 4.40 mm/µsec along the blade axis to 2.85 mm/µsec perpendicular to the blade axis. The spar caps had a velocity of 4.6 mm/µsec along the blade axis but were too narrow to cause worry about the velocity perpendicular to the axis. These velocities were used in the FORTRAN location programs. In the AEwin software for data acquisition with the cylinder setup, a velocity of 2.6 mm/µsec was used.

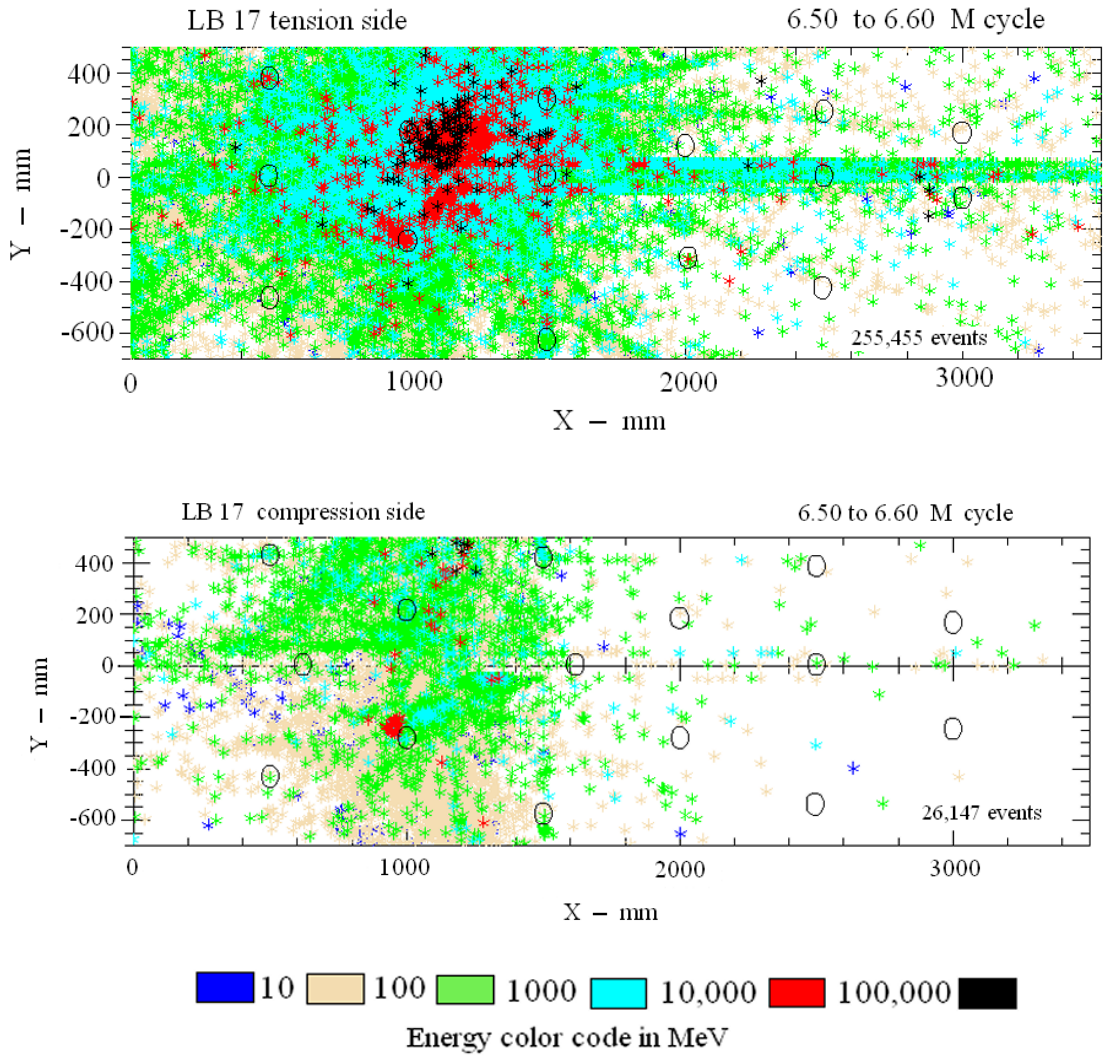

Figure 9-2. Location graphs for the tension and compression sides of the blade on the last 200 kilocycles of the test.

The test was run first for one million cycles in the normal flap mode. The blade was then rotated and the test run for another one million cycles in an edge mode where the motion was parallel to the chord of the blade. No significant emission was seen for either of these loading sequences. The blade was then returned to the flap mode for the rest of the test. After restarting the test, ten-percent increases in the load were made, first at half million cycle increments and then at one quarter million cycle increments. This was continued until the blade finally failed at a level of 418% of the initial load at 6,600,000 cycles. During most of the test, random hits were seen but

no located events appeared until 4,945,000 cycles when, events were seen on the tension side of the blade. These stopped after several thousand cycles but resumed at 5,165,000 cycles and located events on the tension side were then continuously seen until failure. On the compression side, located events did not appear until 5,850,000 cycles and then continued until failure.

Test results were complex. There was far more emission from the tension side of the blade. Figure 9-2 shows the location graphs for both tension and compression sides of the blade for the last 100,000 cycles of the test. Essentially the whole tension side of the blade from the base to around station 2000 mm was emitting. A very broad area from the shear web to the leading edge of the blade and from station 1000 to 1300 mm appeared to be failing. The compression side showed much less emission with the very large emissions up near the leading edge. (The three sensors at the top of the two graphs are the same.) There is one tight cluster on the compression side located very close to sensor 5. This cluster was seen for the last 300,000 cycles but did not seem to grow.

The energy emission rates showed a relatively constant rate of about 20 Mev per cycle for the clusters on the compression side over the last 300,000 cycles. On the other hand, the energy release rate on the tension side of the blade started at roughly 10 Mev per cycle and ended at around 10,000 Mev per cycle. The conclusion from these results is that a minor flaw appeared on the compression side of the blade and emitted steadily throughout the rest of the test. However, it showed no sign of growth and appeared to have no effect on the blade failure. The data from the tension side of the blade showed a steady growth over the entire side between the base and station 2000 mm. Figure 7-13 shows the total energy released over the last 100,000 cycles from the main cluster regions on both compression and tension sides of the blade. Most of the energy on the tension side was released in the last 12,000 cycles. From the broad distribution of high energy emissions seen in Figure 9-2, the question arises: Was this failure a growing tear, or was it a broad failure over the tension surface? Figure 9-3 is a plot of the energy released, over the last 12,000 cycles, from the whole tension surface in this region and the energy released from the smaller area containing most of the high energy events. They both have a steady slope indicating that the whole surface area was failing and that a crack seen after the test was just part of that general failure.

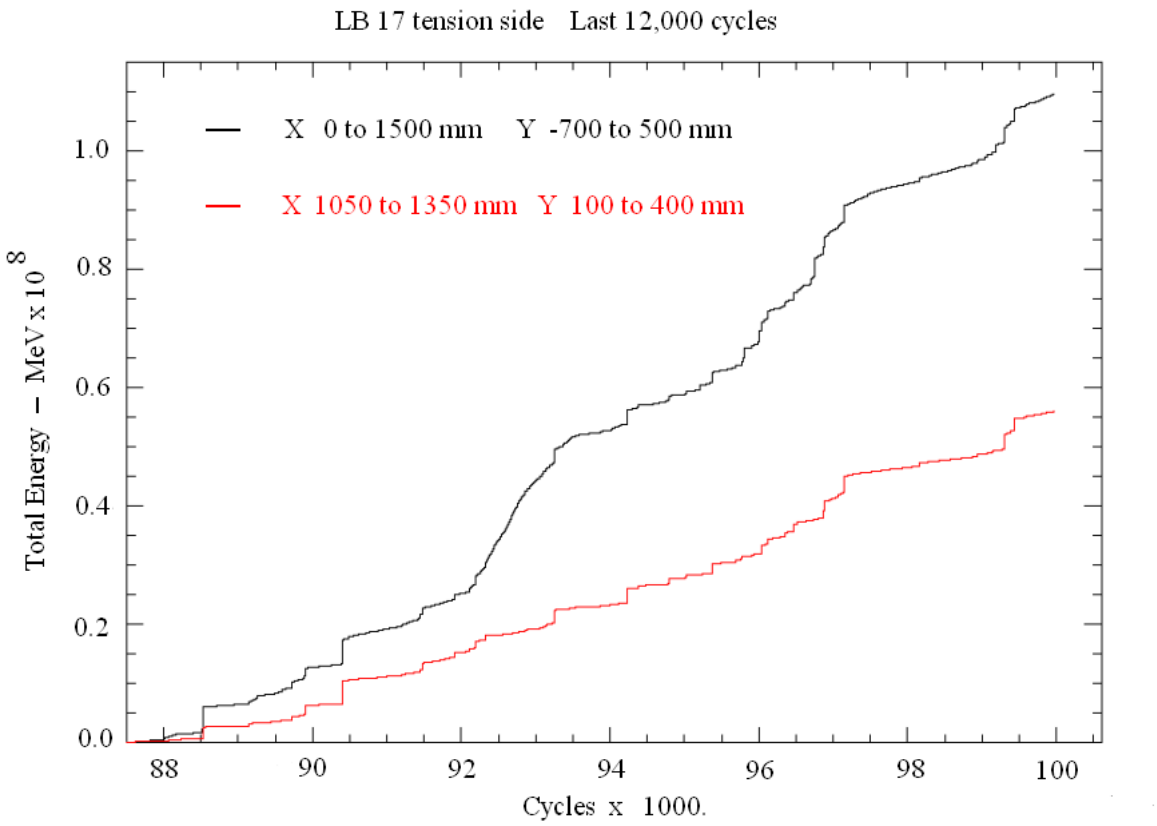

Figure 9-3. Total energy released on tension side during the last 1200 cycles from the entire end of the blade and just from the failure region

The conclusion drawn from the acoustic data was that the BSDS blade had no major flaws and that the failure occurred when material in the entire inboard region of the blade reached the end of its fatigue life. This was consistent with a blade failure at a longer life and higher load than had been predicted.

10.0 CHAPTER 10

10.1. Halon Bottle Tester

The final example of acoustic emission setup to be reviewed is the Acoustic Emission Halon Bottle Tester [19]. This is a commercially available system that was developed at Sandia National Laboratories. These bottles are spherical metal containers with diameters ranging from four to fifteen inches. They are filled with Halon-1301 and over-pressured with nitrogen gas to around 600 psi. After the bottle is filled, the fill port is welded shut. When the extinguisher is needed, a squib charge is fired, breaking a rupture disk and releasing the Halon gas into the cargo hold or engine compartment. The only previously accepted method of testing these hermetically sealed bottles was to cut them open, empty them, and then hydrostatically overpressure them in a water bath in order to measure their elastic and inelastic expansion. Those bottles that passed the test were refilled with Halon and resealed. This procedure is expensive, time consuming, and can potentially leave the bottle in worse shape than before the test. It is also insensitive. Of the few recent test failures, most occurred when the bottle exploded in the water bath.

Sandia answered an industry request to develop a better non-destructive test method for Halon-1301 fire extinguisher spheres. Initial experiments showed that over pressurizing these bottles by heating them in an industrial oven was possible and that some of them produced detectable low level acoustic emission when heated to around 150°F. These results showed the feasibility of developing an acoustic emission test for such bottles. The author developed and designed a commercial acoustic emission Halon bottle tester with the cooperation of the ATA (Air Transport Association), the bottle manufactures, Federal Express, and Physical Acoustics Corp. A commercial version of that tester built by Physical Acoustics Corp. has been in use at American Airlines for the last ten years.

The acoustic emission test method used was the location of the sources on the sphere and the determination of whether they were grouped in clusters. The location algorithm was based on spherical geometry which meant that the important variable between the bottles was the radius of the sphere. The fixture shown in Figure 10-1 was designed to hold the bottle and let six sensors be moved in and out along radii of a sphere while being suitable for heating in an industrial oven. The sensors are pressed against the bottle wall by springs mounted on rods which are located 90 degrees apart at the six poles of the sphere. With this arrangement, the same fixture and analysis program could be used for all of the different sized bottles. The source location program was similar to that described in chapter 7.

The sensors used were the PAC nano-30. These are small, 0.31 inch diameter and 0.29 inch high and have maximum sensitivity between 200 and 400 kHz. A 250 to 600 kHz band width filter was used in an external preamplifier. The high frequency was chosen for two reasons: first, good location accuracy was desired, and second, research showed that acoustic signals in the bottle wall could excite acoustic waves in the liquid Halon. These waves would bounce around inside the bottle for relatively long times compared with an emission signal in the bottle wall. These acoustic waves in the liquid usually had frequencies below 100 kHz. By using AE frequencies between 300 and 400 kHz, these waves are completely ignored by the test system. As the sensors are a permanent part of the fixture, an attempt was made to dry couple them to the bottles. A thin circle of hard rubber is glued to their wear plate to help the sensor to conform to the slight

curvature of the bottle and make good contact. When things work right, this is an adequate acoustic coupling, but in a production environment, a thin film of

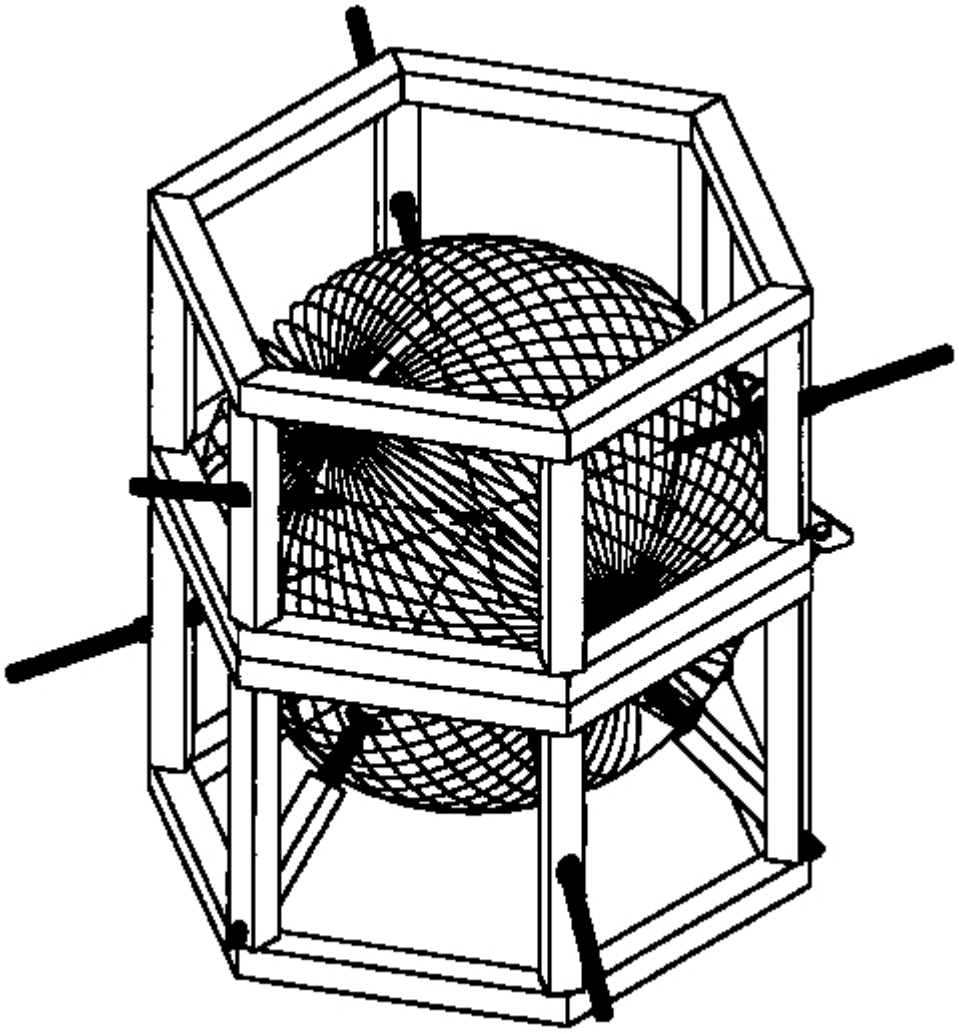

Figure 10-1. Acoustic Emission Halon Bottle Tester, fixture for spheres 4” to 16” diameter

grease improved the coupling. The AE signals in the bottles are relatively weak so the trigger threshold was set as low as possible. With a preamplifier gain of 40 dB, a trigger threshold of 25 was used. With these gain and band pass settings, the noise level of the system starts to trigger when the threshold is decreased to 22 dB. A full set of acoustic parameters were taken, including waveforms, but by the end of the development stage, only the arrival times at the sensors and the temperature of the bottle wall were used in the analysis; the waveforms were dropped from the data sets.

The first step in the test is to load the bottle in the fixture. There is no preferred orientation of the sphere. The actual orientation in the fixture will vary between individual bottles as the operator searches for a position where none of the sensors touch welds, ports, mounting lugs or stick-on

labels. Once the bottle is in the fixture and the system is turned on, the testing program takes over. An AST test (automatic sensor test) is performed; unless all sensors are adequately

coupled, the program stops and requests that coupling be checked. The problem may be that the sensor spring tensions are too uneven or the bottle is not centered in the fixture. After adjustment, another attempt is made. The program will not continue until the coupling meets the programs specifications. Here is where a little grease on the sensor pad can help. Once the program determines satisfactory sensor coupling, the oven heaters are turned on and acoustic emission monitoring is started. An emission event is defined as at least four sensors detecting an acoustic signal within a specified time. This time is defined as 20% longer than it takes for a flexural wave to go half way around the sphere and is calculated from the dimensions of the sphere under test. The program attempts to locate the source using an acoustic velocity of 2.05 mm/μsec. If that does not work, a lower velocity of 1.18 mm/μsec is tried. No attempt is made to use different velocities for different sensors. If the source is located, it is then checked for proximity to another source. If it is within 15° of arc of a great circle of the sphere, it is declared a member of a cluster. The center of the cluster is defined as the average position of all of the members of a cluster. After a cluster is defined, the program first checks each new event for membership in all previously defined clusters. If the event is not a cluster member, then the program looks through the previous non-cluster events for another cluster to be defined. Figure

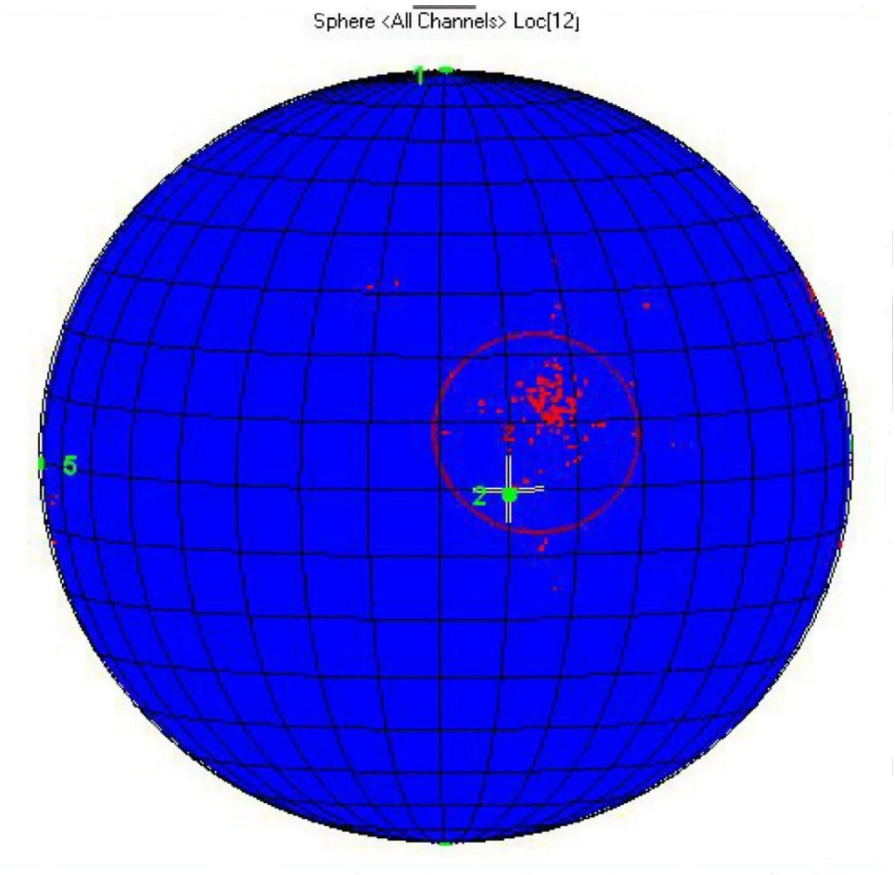

Figure 10-2. Diagram of halon bottle showing located events and cluster outline. This bottle failed the test badly with 156 events in the cluster, but no sign of uncontrolled flaw growth.

10-2 shows a display of such a cluster on a sphere.

How to grade the clusters was the primary problem in analyzing the data. In the development of the system, 206 bottles of all sizes had been tested. Some showed no hits, but most had a few hits and maybe one small cluster. Extensive analysis suggested that an important measure was the number of events in a cluster. The significant signature of the cluster was the distribution of those events as a function of temperature (which is linearly related to internal pressure). A strictly empirical observation was that a suspect cluster had 18 or more events occurring above 110°F. If the events showed a pseudo-exponential behavior, then the bottle was on its way to failure. Later we added two other criteria. If the cluster contained 36 or more events above 110°F, the bottle was declared failed, no matter what the temperature dependence of the cluster events was, and if the cluster had over 70 events and showed exponential behavior, the system would be stopped and the bottle allowed to cool before being removed and scrapped. The detection of pseudo-exponential behavior is a simple procedure; the number of cluster events which occurred between 130°F and 150°F is divided by the number of cluster events which occurred between 110°F and 130°F. If this ratio is 3.0 or greater, the cluster is in exponential growth and the bottle shows signs failure. After the American Airlines system had been running for a few years, data from another 400 bottles was added to the original 206 and the whole set was reanalyzed [19]. No reason was found to change the failure criteria. The bottle failure rate was about 5% for the initial run of American Airline bottles, some of which were up to 30 years old. After almost all of the bottles had been tested once, the failure rate dropped to around 1%.

The rationale behind the acoustic emission test was to find incipient cracks in the bottles. The very first flaw found was a small piece of tungsten in a tack weld on a bottle exterior. This was the only weld inclusion found in the first 600 bottles tested. At American Airlines, several of the failed bottles were cut open. Almost all were found to have a round area on the inside where there was surface etching. Wall thickness measurements of these areas showed a decrease in thickness up to 25% in the worst case. This can be explained as follows: Most bottles are stored or installed in the same position; the exhaust ports usually point up in storage. A small amount of corroding agent, if more dense than the liquid Halon, will settle to the bottom where over a long period of time, corrosion will occur in a circular area whose diameter depends on the depth of the corroding pool. The corroding agent is thought to arise from the slow reaction between the Halon and traces of water. The most likely products of such a reaction are hydrofluoric and hydrobromic acids. Most bottles are stainless steel, so corrosion is a slow process (this is not the case for the few titanium bottles tested).Microscopic examination shows etching of the inner surface with exposure of subsurface grains. The acoustic emission emitted by the bottles, when pressurized by heating, is produced either by flaking of corrosion products or micro cracking between grains which have been partially exposed. This mechanism explains the very low amplitude of the emission.

A final note: The AE Halon Bottle Tester system has been a success. American Airlines has estimated that its bottle shop has saved over a million dollars a year since it replaced the Hydrostatic test with the Acoustic Emission Halon Bottle Tester.

References

[1] Kaiser, J. “Untersuchungen uber das Auftreten Gerauschen beim Zugversuch. (A Study of Acoustic Phenomena in Tensile Tests).” Ph.D. Thesis. Technische Hochschule of Munchen. Munich Germany, 1950.Translated UCRL-Trans-1082(L).

[2] Green, A. T. “Stress Wave Detection: Saturn S-II.” NASA-CR-61161, Final Report. Aerojet-General Corporation, Sacramento, Calif., Dec 1966 [NTIS: X67-18378].

[3] Beattie, A.G. “Acoustic Emission, Principles and Instrumentation.” JAE 2: 96, 1983.

[4] Barrett, C.S. “A Low Temperature Transformation in Lithium.” Physical Review 72(3): 245, Aug. 1, 1947.

[5] Cady, W.G. Piezoelectricty, Vol. 1 & 2. Dover Publications, NY and W.P. Mason. “Piezoelectric Crystals and Their Application to Ultrasonics.” D. van Nostrand Co. Princeton. 1950.

[6] Beattie, A.G. “Acoustic Emission Couplants I: the ASTM Survey.” JAE 2: 67, 1983.

[7] Beattie, A.G., J.A. Barron, R.S. Algers and C.C. Feng. “Acoustic Emission Couplants II: Coupling Efficiencies of Assorted Materials.” JAE 2: 69, 1983.

[8] “Ferroelectricity,” Wikipedia, <wikipedia.org> July 2013.

[9] Bell, D. A. “Noise,” in Handbook of Electronic Engineering, L.E.C. Hughes and F.W. Holland, Chemical Rubber Co. Cleveland OH, 1967.

[10] Breckenridge, F.R. “Acoustic Emission Transducer Calibration by Means of the Seismic Pulse,” JAE 1: 87, 1982.

[11] Ono, K., H. Cho, and T. Matsuo. “Bar and Plate-wave Characterization of AE Sensors,” JAE 26: 72, 2008.

[12] Ono, K., H. Cho, and T. Matsuo. “New Characterization Methods of AE Sensors,” JAE 28: 256, 2010.

[13] “AEwin SOFTWARE, Installation, Operation and User’s Reference Manual,” Mistras Group, Princeton Junction, NJ, 1996.

[14] Press, W.H., S.A. Teukolsky, W.T. Vetterling, and B.P. Flannery. Numerical Recipes in Fortran, 2nd edition. Cambridge University Press, 1992.

[15] Rumsey, M.A., J.R. White, R.J. Werlink, A.G, Beattie, C.W. Pitchford, J. vanDam “Experimental Results of Structural Health Monitoring of Wind Turbine Blades” <http://windpower.sandia.gov/asme/AIAA-2008-1348.pdf>, 2008.

[16] Berry, D., T. Ashwill. “Design of 9-Meter Carbon-Fiberglass Prototype Blades: CX-100 and TX-100,” SAND2007-0201 September 2007.

[17] Beattie, A.G. “Fatigue Test of an Experimental Wind Turbine Blade, Acoustic Emission Results from the BSDS Blade,” unpublished, 2009.

[18] Beattie, A.G. ‘An Acoustic Emission Tester for Aircraft Halon-1301 Fire Extinguisher Bottles,” JAE 15: 63 1997.

[19] Beattie, A.G., D.D. Thornton. “The Acoustic Emission Halon 1301 Fire Extinguisher Bottle Tester: Results of Tests on 649 Bottles” JAE 23: 331 2005.

Appendix: Program SSENCMP

A FORTRAN program listing which reads an AEwin data file from the fatigue test of the Sandia Sensor Blade fatigue test is given in this appendix. The program was compiled in Fortran 77 by an Absoft compiler and includes the use of PLplot graphics routines. It analyses data for locations on the compression side of the blade. Brief notes on this program follow.

The program starts with the measured positions of all the sensors the blade. It then has an exclusion list of sensors on the tension of the blade which are not used in this calculation, since this program is for the compression side of the blade. The data are then read in from a binary .DTA file. The file is searched for the byte sequence which defines the start of the AE data. When this is found, the file is rewound and then positioned at the start of the data. The program then looks for hit data with the hit parameters that are recorded in this test. A different set of parameters on a test would require changes in this sequence. The parameters in this sequence are the test time, sensor number, (if the sensor is in the exclusion list, the program goes to the next hit) rise time, count, duration, amplitude, absolute energy and load. There is also some filtering using rise time and duration in this section (which can be omitted). The next step is to search for hits that fall in the same time window. The program accepts event hit sequences with from 3 or 4 hits to a maximum of 14 hits. The sensor number is matched to the sensor position coordinates and a trial location solution (the averaged coordinates of the first three sensors hit) is determined. This starts the non-linear least squares program in the center of the triangle of the first hit sensors. The delta times for the event set are calculated and the least squares program called. If the goodness-of-fit parameter, RSQ, is between 0.7 and 1.0 the solution is kept. This location is then matched to the energy of the event (the sum of the absolute energies of the first three sensors hit) and checked to see if it lies within the specified boundaries on the blade. (On the first run of the program, the boundaries are set for the entire instrumented compression side surface of the blade. On later runs the coordinates of clusters found on the first run can be used). The located events are then sorted as to their energy values and a color code assigned to different energy orders of magnitude. The color coded locations are then plotted on a graph of the surface of the blade. On succeeding runs, locations can be restricted to a defined cluster and an energy vs. number of cycles graph plotted for the cluster. The program is changed to the tension side of the blade by changing the exclusion list of sensors.

The only part of the non-linear least squares program (NLR) which pertains to the blade is the subroutine, FCDEMT. This routine calculates the sensor delta times for each trial solution. It uses the sensor coordinates in the chosen geometry (planar, spherical, cylindrical with end caps) and a model for the acoustic velocities. The model in this version of the program goes from a higher velocity at station 0 mm to a lower constant velocity at station 1000 mm and beyond. It also includes a higher velocity in the spar cap. At the end of this program listing, another version of FCDEMT is included that incorporates the measured TX-100 blade acoustic velocity distribution shown in Figure 8-5.

```
      Program ssencmp
c     This program searches a SAMOS data file for the sandsen blade   c
      fatigue test and reads the hit data.
c     It calculates the AE source locations for the compression
c    surface using the measured velocity, and graphs the locations


      real*8 rtim,dtim,tim,const,ttim(24)
     BYTE indaset(200000),tster(9),id,itm
      BYTE buf2(50000),rlen(2),benr(4),dup(10000)
      CHARACTER*1 buf(10000)
      Integer*4 isen(15),iris(15),icnt(15)
      Integer*4 idur(15),iamp(15),idu
      real*4 load(15),tenr,parm(2),w(6),td(6)
            Dimension gy(15),dy(30000),gx(30000)
      CHARACTER*4 tst
      CHARACTER*2048 test
      EQUIVALENCE (indaset,test),(tenr,benr)
      EQUIVALENCE (tst,tster),(len,rlen),(id,idd)
      EQUIVALENCE (buf,dup)
      Character*40 name
      Common /zot/xsen(6),ysen(6),pi
      common /zat/senx(24),seny(24),nsn(9)
      common /zut/x1(20000),y1(20000),x2(250000),y2(250000),
     +  x3(150000),y3(150000),x4(150000),y4(150000),x5(13000),y5(13000),
     +  x6(5000),y6(5000),nn1,nn2,nn3,nn4,nn5,nn6

!     coordinates of all sensors  -- nsn -sensors not used on this
!     side of the blade
      Data senx/46.,83.,0.,81.,500.,0.,0.,500.,995.,
     +  993.,0.,1020.,1460.,0.,0.,1475.,2080.,2055.,0.,
     +  2060.,2473.,0.,0.,2488./
      Data seny/0.0,255.,0.,-341.,140.,0.,0.,-140.,-35.,
     +  280.,0.,-280.,140.,0.,0.,-285.,-36.,385.,0.,-610.,
     +  195.,0.,0.,-278./
      Data nsn/3,6,7,11,14,15,19,22,23/
      const=2.5d-7

      tster(1)=#07     ! byte sequence just before data starts
      tster(2)=#00
      tster(3)=#80
      tster(4)=#00
      tster(5)=#00
      tster(6)=#00
      tster(7)=#00
      tster(8)=#00
      tster(9)=#00

      print *,'Enter the name of the input File'
```

```
      Read(*,1000)name

1000  Format( A40)

      dtim=0.001200    ! event determination time gate
      Open(1,file=name,form='binary',status='old')

      Read(1)(indaset(I),I=1,50000) ! start reading binary data file
      num=index(test,tst)
      print *,num
      rewind(1)
      read(1)(buf2(i),i=1,num)
      do 10 i=1,50
      read(1)itm
      if(itm.ne.0) then
       rlen(1)=itm
       go to 19
      end if
10    continue

      nrej=0
      noffbld=0
      n=0
      in=0
      nev=0
      nn1=0
      nn2=0
      nn3=0
      nn4=0
      nn5=0
      nn6=0
      pi=3.1415927

20   continue

      read(1,err=512)rlen(1)
19    read(1,err=512)rlen(2)
      read(1,err=512)id
      if(idd.ne.1)then
       read(1,err=512)(buf2(i),i=1,len-1)
       go to 20
      else
       read(1,err=512)(buf(i),i=1,len-1)
      end if


      iflg=0
      rtim=0.     !read hit parameters must agree with layout set up

      do 25 i=1,6
25   rtim=rtim+(256.**(i-1))*ICHAR(buf(i))
      tim=rtim*const
      msen=ICHAR(buf(7))
      do 40 i=1,9
```

```
      if(msen.eq.nsn(i))  goto 20
40    continue
      nflg=0
      mris=ICHAR(buf(8))+256*ICHAR(buf(9))
      if(mris.le.5) go to 20
      mcnt=ICHAR(buf(10))+256*ICHAR(buf(11))
      idu=0
      do 27 i=1,4
27    idu=idu+(256**(i-1))*ICHAR(buf(i+11))
      mdur=idu
      if(mris.ge.mdur/2) go to 20
      mamp=ICHAR(buf(16))
      do 28 i=1,4
28    benr(i)=dup(i+16)
      enr=tenr*6.7041e-6
      mpr=ICHAR(buf(22))+256*ICHAR(buf(23))
      if(mpr.le.32767)then
       par=mpr/32767.
      else
       par=(mpr-65536)/32767.
      end if
      aload=10.*par
      n=n+1
      in=in+1
      if(in.eq.1)then        ! determine event members
       ttim(in)=tim
       isen(in)=msen
       iris(in)=mris
       icnt(in)=mcnt
       gy(in)=enr
       idur(in)=mdur
       iamp(in)=mamp
       load(in)=aload
       go to 20
      else
       if(tim.le.ttim(1)+dtim)then
        ttim(in)=tim
        isen(in)=msen
        iris(in)=mris
        icnt(in)=mcnt
        idur(in)=mdur
        iamp(in)=mamp
        gy(in)=enr
        load(in)=aload
        nflg=1
        if(in.eq.14) go to 50 !accept no more than 14 his in event
        go to 20
       else
         if(in.lt.4)then  ! 3 hits min lt, 4 hits min le
          go to 35
         else
          in=in-1
          iflg=1
          go to 50
```

```
         end if
        end if
       end if
35      ttim(1)=tim
        isen(1)=msen
        iris(1)=mris
        icnt(1)=mcnt
        idur(1)=mdur
        iamp(1)=mamp
        gy(1)=enr
        load(1)=aload
        do 31 i=2,14
         ttim(i)=0.
         isen(i)=0
         iris(i)=0
         icnt(i)=0
         idur(i)=0
         iamp(i)=0
         gy(i)=0.
31       load(i)=0.
         in=1
         go to 20
50    continue
      if(isen(2).eq.20)then ! sensor 20 was not working in this test
       in=0
       go to 20
      end if
      if(in.gt.3) in=3
      do 55 i=1,in
      xsen(i)=senx(isen(i))
55    ysen(i)=seny(isen(i))
      nparm=2
      ndata=in-1
      parm(1)=(xsen(1)+xsen(2)+xsen(3))/3.0 !starting loc estimate
      parm(2)=(ysen(1)+ysen(2)+ysen(3))/3.0
      do 67 i=1,6
67    w(i)=1.0    ! weighting factors for calc not used here
      do 69 i=2,in
69    td(i-1)=(ttim(i)-ttim(1))*1.e6 !delta times

      CALL NLR(ndata,nparm,td,parm,w,rsq)

      if(rsq.ge.0.7) then  !accept results with fit parm down to 0.7
       go to 80
      end if
      nrej=nrej+1
      if(iflg.eq.1) go to 35
       in=0
       go to 20
80    continue
      x=parm(1) ! answers
      y=parm(2)        ! accept window on blade
      if(x.lt.650..or.x.gt.950..or.y.gt.250..or.y.lt.-50.) go to 90
      energy=gy(1)+gy(2)+gy(3)
```

```
      If(energy.lt.10.)then  ! ignore events with very low energy
       in=0
       go to 20
      end if

      nev=nev+1
       write(*,600)nev,ttim(1),x,y,rsq,energy,in,load(1),
     +  (isen(i),i=1,3)
600    format(i6,2x,f11.4,' x =',f5.0,' y =',f5.0,' r =',f4.2,
     +  2x,f11.2,x,i2,x,f4.2,x,3i2)
                        ! sort as to energy for graph
      if(energy.lt.10.) then
       nn1=nn1+1
       x1(nn1)=x
       y1(nn1)=y
       go to 85
      else if(energy.lt.100.)then
       nn2=nn2+1
       x2(nn2)=x
       y2(nn2)=y
      else if(energy.lt.1000.)then
       nn3=nn3+1
       x3(nn3)=x
       y3(nn3)=y
       go to 85
      else if(energy.lt.10000.)then
       nn4=nn4+1
       x4(nn4)=x
       y4(nn4)=y
       go to 85
      else if(energy .lt.100000.)then
       nn5=nn5+1
       x5(nn5)=x
       y5(nn5)=y
       go to 85
      else
       nn6=nn6+1
       x6(nn6)=x
       y6(nn6)=y
      end if
85    continue


      gx(nev)=ttim(1)        ! * 1.86 to convert to cycles
      dy(nev)=energy

      go to 91
90    noffbld=noffbld+1
91    if(iflg.eq.1) go to 35
      in=0
      go to 20

512   continue
      write( *,1010)n,nev,nrej,noffbld
```

```
1010  format(i8,' hits, events =',i6,' rej =',i6,'off blade =',i6)

!     CALL grafel(gx,dy,nev) !energy graph
      print *,nn1,nn2,nn3,nn4,nn5,nn6
      CALL cgraf       !location graph
      END



      SUBROUTINE FCDEMT(T,XY)   !arrival time calculation, used in NLR
      COMMON /zot/xs(6),ys(6),pi
      COMMON /WNLGPH/PAD(2754),k
      DIMENSION XY(2)
      x=XY(1)
      y=XY(2)
      xo=x-xs(1)
      yo=y-ys(1)
      xk=x-xs(k+1)
      yk=y-ys(k+1)
      cso=abs(xo/((xo**2+yo**2)**0.5))
      csk=abs(xk/((xk**2+yk**2)**0.5))
      d0=(xo**2+yo**2)**0.5
      dk=(xk**2+yk**2)**0.5

      if(x.le.500.) v=4.0
      if(x.gt.500.and.x.le.1000.)then
       v=2.55+((1000.-x)/500.)*1.45

      else
       v=2.55
      end if
            v0=v
            vk=v
                  ! velocity varies with distance from base
      if(abs(y).le.75..and.abs(ys(1)).lt.75.) then
       if(abs(y).le.25..and.abs(ys(1)).lt.25.) then
        v0=7.0
       else
        va=7.0-v
        v0=v+va*(cos(((abs(y)-25.)/50.)*pi)/2.+0.5)
       end if
      end if

      if(abs(y).le.75.and.abs(ys(k+1)).lt.75.) then
       if(abs(y).le.25..and.abs(ys(k+1)).lt.25.) then
        vk=7.0
       else
        vb=7.0-v
        vk=v+vb*(cos(((abs(y)-25.)/50.)*pi)/2.+0.5)
       end if
      end if
      T=dk/vk-d0/v0 !calculated arrival times
    RETURN
    END
```

```
      ! SUBROUTINE NLR non-linear least squares routine

       SUBROUTINE NLR(ND,NPARM,DAT,PARM,WEIGHT,RSQ)
      DIMENSION BS(25),BA(25),YMF(550),P(25),AX(25,25),B(25)
      DIMENSION DAT(1),PARM(1),WEIGHT(1)
      COMMON /WNLGPH/ Y(550),YP(550),X(550,2),WT(550),UWP,N,K,M,I
      COMMON/WNLGDB/ A(25,25),AY(25,25),DB(25),SA(25),G(25),XLL,
      1XKDB,GMA,ZTA,JCL,IFDPO,IFWT
C     ........ INITIALIZATION AND DATA INPUT ........
      NTM = 0
      N=ND
      DO 1000 I=1,N
      Y(I)=DAT(I)
      WT(I)=WEIGHT(I)
 1000 CONTINUE
      K=NPARM
      DO 1020 I=1,K
      B(I)=PARM(I)
 1020 CONTINUE
 903 FORMAT(F1.0,F10.0,F10.0)
      M=1
      NITR=26
      IY=0
      IFWT=1
      IFDPO=1
      XNK = N-K
      KEND=2
      ITR = 0
      JCL = 0
      XKDB = 1.0
      IF (IFWT.EQ.1) GO TO 24
      DO 20 I=1,N
   20 IF(WT(I).EQ.0.0) WT(I)=1.0
   24 CONTINUE
C     ..... DUB IN CRITICAL-VALUE CONSTANTS (CHANGEABLE IN SUBZMT).
      DEL = 1.0E-5
      EPS = 1.0E-5
      FF = 4.0
      GMC = 45.0
      TAU = 0.001
      XL = 0.01
      ZTA = 1.0E-31
      CALL GETPHI (B,PHI)
      GO TO 62
C     ........ PTP MATRIX, ITERATIONS, AND TESTS FOR FIT ........
   60 ITR = ITR+1
      IF (NITR.GT.1) NITR=NITR-1
      XKDB = 1.0
   62 DO 64 I=1,K
      G(I) = 0.0
      BS(I) = B(I)
      DO 64 J=1,K
   64 A(I,J) = 0.0
```

```
C   ..... FIND PARTIALS, EITHER ESTIMATED OR ANALYTIC
   DO 82 I=1,N
   CALL FCDEMT (F,B)
   YP(I) = F
   YMF(I) = Y(I)-F
   DO 68 J=1,K
   DBW = B(J)*DEL
   IF(DBW .EQ. 0.)   DBW=DEL
   TWS = B(J)
   B(J) = B(J)+DBW
   CALL FCDEMT (FWS,B)
   B(J) = TWS
  68 P(J) = (FWS-F)/DBW
C   ..... MAKE PARTIALS MATRIX
  80 DO 82 J=1,K
   G(J) = G(J)+YMF(I)*P(J)
   1*WT(I)
   DO 82 L=J,K
   A(L,J) = A(L,J)+P(L)*P(J)
   1*WT(I)
  82 A(J,L) = A(L,J)
   PHIZ = PHI
   IF(XNK .EQ. 0.)   XNK=1.0
   SE = SQRT(PHIZ/XNK)
   DO 86 I=1,K
   DO 86 J=1,K
  86 AX(I,J) = A(I,J)
C   ..... SAVE SQUARE ROOTS OF DIAGONAL ELEMENTS
   DO 98 I=1,K
      if(A(i,i).lt.0.) A(i,i)=0.0
   SA(I) = SQRT(A(I,I))
   IF (SA(I).EQ.0.0) GO TO 94
   G(I) = G(I)/SA(I)
   DO 92 J=1,K
  92 A(I,J) = A(I,J)/SA(I)
   GO TO 98
  94 G(I) = 0.0
   DO 96 J=1,K
   A(I,J) = 0.0
  96 A(J,I) = 0.0
  98 CONTINUE
   DO 104 J=1,K
   IF (SA(J).EQ.0.0) GO TO 102
   DO 100 I=1,K
 100 A(I,J) = A(I,J)/SA(J)
 102 A(J,J) = 1.0
   DO 104 I=1,K
 104 AY(I,J) = A(I,J)
C   ..... WRITE TEST PARAMETERS AND FIND INITIAL INCREMENTS
   CALL GETDBS (BS,B,XL,PHI,JUMP)
   IF(JUMP.EQ.1) GO TO 700
C   ..... EPSILON TEST
   DO 170 J=1,K
   IF (ABS(DB(J)/(ABS(B(J))+TAU)).GE.EPS) GO TO 172
```

```
 170 CONTINUE
   GO TO 700
C   ..... MAXIMUM NO. OF ITERATIONS (FORCE OFF) TEST
 172 IF (NITR.NE.1) GO TO 171
   GO TO 700
C   ..... DETERMINE PARAMETERS FOR NEXT ITERATION
 171 IF (XL.LE.1.0E-08.AND.PHI.LE.PHIZ) GO TO 60
   XLS = XL/10.0
   CALL GETDBS (BS,BA,XLS,PHI1,JUMP)
   IF(JUMP.EQ.1) GO TO 700
   IF (PHI1.GT.PHIZ) GO TO 176
   XL = XLS
   PHI = PHI1
   DO 174 J=1,K
 174 B(J) = BA(J)
   GO TO 60
 176 IF (PHI.LE.PHIZ) GO TO 60
 178 XL = 10.0*XL
 180 CALL GETDBS (BS,B,XL,PHI,JUMP)
   IF(JUMP.EQ.1) GO TO 700
   IF (PHI.LE.PHIZ) GO TO 60
   IF (GMA.GE.GMC) GO TO 178
   XKDB = XKDB/5.0
C   ..... GAMMA EPSILON TEST
   DO 182 J=1,K
   IF (ABS(DB(J)/(ABS(B(J))+TAU)).GE.EPS) GO TO 180
 182 CONTINUE
C   C
C   ........ CONFIDENCE LIMITS AND DATA OUTPUT ........
 700 IF (JCL-1) 702,10,701
 701 CONTINUE
 702 CONTINUE
C   ..... CALCULATE R SQUARED
   SSY = 0.0
   SW = 0.0
   CHISQ = 0.0
   DO 707 I=1,N
   SSY = SSY+Y(I)*WT(I)
 707 SW = SW+WT(I)
   SW = SSY/SW
   SYG = SSY
   SSY = 0.0
   DO 708 I=1,N
 708 SSY = SSY+(Y(I)-SW)**2
     RSQ = 1.0-PHIZ/SSY
   BL=B(K)
C   ..... FIND AND WRITE PTP INVERSE.
   CALL GJRMIX (AX,25,K,ZTA,MSNG)
   IF (MSNG.EQ.2) GO TO 10
   KST = 1
 711 KEND = KST+4
   IF (KEND.GT.K) KEND=K
   IF (KEND.EQ.K) GO TO 713
   KST = KST+5
```

```
   GO TO 711
 713 DO 715 J=1,K
   IF (AX(J,J).GE.0.0) GO TO 715
   GO TO 10
 715 SA(J) = SQRT(AX(J,J))
C   ..... FIND AND WRITE PARAMETER CORRELATION MATRIX.
   DO 720 I=1,K
   DO 718 J=I,K
   WS = SA(I)*SA(J)
   IF (WS.GT.0.0) GO TO 716
   AX(I,J) = 0.0
   GO TO 718
 716 AX(I,J) = AX(I,J)/WS
 718 AX(J,I) = AX(I,J)
   AX(I,I) = 1.0
 720 SA(I) = SA(I)*SE
   KST = -9
 721 KST = KST+10
   KEND = KST+9
   IF (KEND.GT.K) KEND=K
   IF (KEND.LT.K) GO TO 721
C   ..... FIND AND WRITE PARAMETER ERRORS AND SUPPORT PLANES.
   WS = K
   DO 750 J=1,K
   B(J) = BS(J)
 750 CONTINUE
C   ..... NONLINEAR CONFIDENCE LIMITS
   PC = PHIZ*(1.0+FF*WS/XNK)
   XNK = 2.0*(PHIZ-PC)
   DO 780 J=1,K
   ITR = 1
   DO 764 L=1,2
   SPL = 1.
   B(J) = BS(J)+SPL*SA(J)
   CALL GETPHI (B,PHI)
   IF (PHI.LT.PC) GO TO 756
   DO 754 IY=1,9
   SPL = SPL/2.0
   B(J) = BS(J)+SPL*SA(J)
   CALL GETPHI (B,PHI1)
   IF (PHI1.LT.PC) GO TO 762
 754 CONTINUE
   GO TO 760
 756 DO 758 IY=1,3
   SPL = SPL+1.
   B(J) = BS(J)+SPL*SA(J)
   CALL GETPHI (B,PHI1)
   IF (PHI1.GE.PC) GO TO 762
 758 CONTINUE
 760 ITR = ITR+L
   GO TO 764
 762 WS = SPL-1.0
     OPL = 2.0*((PHIZ+PHI1/WS)/SPL-PHI/WS)
   OPU = (PHI*SPL-PHI1/SPL)/WS-PHIZ/SPL*(SPL+1.0)
```

```
   B(J) = BS(J)+(SQRT(OPU**2-OPL*XNK)-OPU)*SA(J)/OPL
   CALL GETPHI (B,PHI)
   BA(L) = B(J)
   G(L) = PHI
 764 CONTINUE
 780 B(J) = BS(J)
 790 CONTINUE
 800 CONTINUE
C   C
  10 CONTINUE
   DO 3000 I=1,K
   PARM(I)=B(I)
3000 CONTINUE
   RETURN
 924 FORMAT(5X,19H... FORCE OFF AFTER,I5,10H ITERATION,A1)
   END


   SUBROUTINE GETPHI (B,PHI)
C   THE SUBROUTINE CALLED BY THIS SUBPROGRAM IS
C   FCDEMT
   DIMENSION B(25)
   COMMON /WNLGPH/ Y(550),YP(550),X(550,2),WT(550),UWP,N,K,M,I
   PHI = 0.0
   UWP = 0.0
   DO 302 I=1,N
   CALL FCDEMT (F,B)
   FMYQ = (Y(I)-F)**2
   PHI = PHI+FMYQ*WT(I)
 302 UWP = UWP+FMYQ
   RETURN
   END


   SUBROUTINE GETDBS (BS,B,XL,PHI,JUMP)
C   THE SUBROUTINES CALLED BY THIS SUBPROGRAM ARE
C   GJRMIX, GETPHI
   DIMENSION B(25),BS(25)
   COMMON /WNLGPH/ Y(550),YP(550),X(550,2),WT(550),UWP,N,K,M,I
   COMMON /WNLGDB/ A(25,25),AY(25,25),DB(25),SA(25),G(25),XLL,
   1XKDB,GMA,ZTA,JCL,IFDPO,IFWT
   JUMP = 0
   XLL = 0.0
   DTG = 0.0
   GTG = 0.0
   DO 202 I=1,K
   DO 201 J=1,K
 201 A(I,J) = AY(I,J)
 202 A(I,I) = A(I,I)+XL
   CALL GJRMIX (A,25,K,ZTA,MSNG)
   IF (MSNG.EQ.1) GO TO 204
   JCL = 1
   GO TO 602
 204 DO 210 I=1,K
```

```
      DB(I) = 0.0
      DO 208 J=1,K
  208 DB(I) = DB(I)+A(I,J)*G(J)
      IF(DB(I) .EQ. 0.) GO TO 210
         if(SA(i).eq.0.) SA(i)=0.0001
      DB(I) = DB(I)/SA(I)*XKDB
      DTG = DTG+DB(I)*G(I)
      GTG = GTG+G(I)**2
      XLL = XLL+DB(I)**2
  210 B(I) = BS(I)+DB(I)
      XLL = SQRT(XLL)
      IF (K.EQ.1) GO TO 214
      IF(GTG .EQ. 0) GO TO 602
      CGM = DTG/(XLL*SQRT(GTG))
      JGM = 1
      IF (CGM.GT.0.0) GO TO 212
      JGM = 2
      CGM = ABS(CGM)
  212  GMA = 57.2957795*(1.5707288+CGM*(-0.2121144+CGM*(0.074261-CGM*
      10.0187293)))*SQRT(1.0-CGM)
      IF (JGM.EQ.1) GO TO 216
      GMA = 180.0-GMA
      IF (XL.LT.1.0) GO TO 216
      JCL = 2
      GO TO 602
  214 GMA = 0.0
  216 CALL GETPHI (B,PHI)
      IFDPO=1
      IF (IFDPO.NE.1) GO TO 600
      RETURN
  602 JUMP = 1
  600 RETURN
      END


      SUBROUTINE GJRMIX (A,N,IM,EPS,MSING)
      DIMENSION A(N,N),B(25),C(25)
      INTEGER P(25),Q(25)
C     .. DETERMINATION OF THE PIVOT ELEMENT.

      MSING = 1
      DO 10 K=1,IM
      PIVOT = 0.0
      DO 20 I=K,IM
      DO 20 J=K,IM
      IF (ABS(A(I,J)).LE.ABS(PIVOT)) GO TO 20
      PIVOT = A(I,J)
      P(K) = I
      Q(K) = J
   20 CONTINUE
      IF (ABS(PIVOT).LE.EPS) GO TO 40
C     .. EXCHANGE OF THE PIVOTAL ROW WITH THE KTH ROW.
      IF (P(K).EQ.K) GO TO 80
      DO 70 J=1,IM
```

```
   L = P(K)
   Z = A(L,J)
   A(L,J) = A(K,J)
  70 A(K,J) = Z
C   .. EXCHANGE OF THE PIVOTAL COLUMN WITH THE KTH COLUMN.
  80 IF (Q(K).EQ.K) GO TO 90
   DO 100 I=1,IM
   L = Q(K)
   Z = A(I,L)
   A(I,L) = A(I,K)
 100 A(I,K) = Z
C   .. JORDAN STEP.
  90 DO 110 J=1,IM
   IF (J.NE.K) GO TO 130
   B(J) = 1.0/PIVOT
   C(J) = 1.0
   GO TO 140
 130 B(J) = -A(K,J)/PIVOT
   C(J) = A(J,K)
 140 A(K,J) = 0.0
 110 A(J,K) = 0.0
   DO 10 I=1,IM
   DO 10 J=1,IM
  10 A(I,J) = A(I,J)+C(I)*B(J)
C   .. REORDERING THE MATRIX.
   DO 155 M=1,IM
   K = IM-M+1
   IF (P(K).EQ.K) GO TO 170
   DO 180 I=1,IM
   L = P(K)
   Z = A(I,L)
   A(I,L) = A(I,K)
 180 A(I,K) = Z
 170 IF (Q(K).EQ.K) GO TO 155
   DO 150 J=1,IM
   L = Q(K)
   Z = A(L,J)
   A(L,J) = A(K,J)
 150 A(K,J) = Z
 155 CONTINUE
   GO TO 151
C   .. WRITE MESSAGE IF MATRIX IS SINGULAR.
  40 CONTINUE
   MSING = 2
 151 RETURN
   END


      ! GRAPHICAL ROUTINES USE PLplot graphics library


      SUBROUTINE grafel(eld,enr,nev)
```

```
      dimension xx(100000),x(200000),y(200000),eld(1),enr(1)
      do 10 i=1,nev
10    xx(i)=eld(i)
      do 20 i=1,nev

       x(2*i-1)=xx(i)
       x(2*i)=xx(i)
       y(2*i+1)=enr(i)+y(2*(i-1))
       y(2*i)=enr(i)+y(2*(i-1))
20    continue
      y(1)=0.
      x(2*nev+1)=xx(nev)
      ymax=1.05*y(2*nev)
      xmin=0.                      !     xmax=1.05*eld(nev)
      xmax=xx(nev)*1.05                  !     xmin=0
      call plinit()
      call plcol0(15)
      call plenv(xmin,xmax,0.0,ymax,0,0)
      call pllab('Time - Sec','Total Energy - MEV',
     + ' Compression Side')
      nn=2*nev
      Call plline(nn,x,y)
      Call plend
      return
      end

   SUBROUTINE cgraf
      dimension mclr(6),snx(15),sny(15)
      common /zat/senx(24),seny(24),nsn(9)
      common /zut/x1(20000),y1(20000),x2(250000),y2(250000),
     +  x3(150000),y3(150000),x4(150000),y4(150000),x5(13000),y5(13000),
     +  x6(5000),y6(5000),nn1,nn2,nn3,nn4,nn5,nn6

      data mclr/14,9,3,11,1,15/ ! colors - salmon,blue,green,cyan,red,
                          ! black

      n=0
      do 10 i=1,24
      do 9 j=1,9
      if(i.eq.nsn(j))go to 10
9     continue
      n=n+1
      snx(n)=senx(i)
      sny(n)=seny(i)
10    continue
      call plinit()

      call plcol0(15)
      call plschr(0.,1.0)
      call plenv(650.,950.,-50.,250.,1,1)
      call pllab('X - mm','Y - mm','compression side')

      call plcol0(mclr(1))
      call plpoin(nn1,x1,y1,42)
```

```
call plcol0(mclr(2))
call plpoin(nn2,x2,y2,42)

call plcol0(mclr(3))
call plpoin(nn3,x3,y3,42)

call plcol0(mclr(4))
call plpoin(nn4,x4,y4,42)

call plcol0(mclr(5))
call plpoin(nn5,x5,y5,42)

call plcol0(mclr(6))
call plpoin(nn6,x6,y6,42)

call plcol0(15)
call plschr(0.,3.)
call plpoin(15,snx,sny,79)

call plend
return
end
```

SUBROUTINE FCDEMT for TX blade:
Contains acoustic velocity calculated for Figure 8-6

```
SUBROUTINE FCDEMT(T,XY)
COMMON /zot/xs(5),ys(5)
COMMON /WNLGPH/PAD(2754),k
DIMENSION XY(2)
pi=3.14159265
of20=0.3490659
x=XY(1)
y=XY(2)
xo=x-xs(1)
yo=y-ys(1)
xk=x-xs(k+1)
yk=y-ys(k+1)
cso=acos(xo/((xo**2+yo**2)**0.5))
csk=acos(xk/((xk**2+yk**2)**0.5))
if(yo.gt.0.0) then
 ango=cso-of20
else
 ango=cso+of20
end if
if(yk.gt.0.0) then
 angk=csk-of20
else
 angk=csk+of20
end if
if(xo.lt.0.0) ango=pi-ango
```

```
  if(xk.lt.0.0) angk=pi-angk
  if(ango.le.of20)then
   v0=2.10+2.40*exp(-(2.3851*ango)**2.0)
  else
   v0=2.10+2.40*exp(-(2.4062*abs(ango))**1.15)
  end if
  if(angk.le.of20)then
   vk=2.10+2.40*exp(-(2.3851*angk)**2.0)
  else
   vk=2.10+2.40*exp(-(2.4062*(angk))**1.15)
  end if
  d0=(xo**2+yo**2)**0.5
  dk=(xk**2+yk**2)**0.5
  T=dk/vk-d0/v0
RETURN
END
```

Index of Terms

Distribution

EXTERNAL DISTRIBUTION

James Ahlgrimm
Wind and Water Power Program, EE-2B
Office of Energy Efficiency and Renewable Energy
U.S. Department of Energy
1000 Independence Ave., SW
Washington, DC 20585
Jim.Ahlgrimm@ee.doe.gov

Shreyas Ananthan
Wind and Water Power Program, EE-2B
Office of Energy Efficiency and Renewable Energy
U.S. Department of Energy
1000 Independence Ave., SW
Washington, DC 20585
Shreyas.Ananthan@EE.Doe.Gov

Athanasios Anastasopoulos
El. Venizelou 7 & Delfon
14452 Metamorphosis, Athens, GREECE
nassos@enviroacoustics.gr

Alan Beattie
2022 Greeley St.
Ames, IA 50014
agbeattie@centurylink.net

Dale E. Berg
12421 Chelwood Trail NE
Albuquerque, NM 87112-4627
dale.berg@att.net

Derek Berry
National Renewable Energy Laboratory
Mail Stop 3911
1617 Cole Blvd.
Golden, CO 80401-3305
Derek.Berry@nrel.gov

Chris Bley
InspecTools
POB 1645
Fair Oaks, CA 95628
Chris.Bley@InspecTools.com

Douglas Cairns
Montana State University - Bozeman
PO Box 173800
315 Roberts Hall
Bozeman, MT 59717-3800
DCairns@me.montana.edu

Daniele Costantini
Micron Optics, Inc.
1852 Century Place NE
Atlanta, GA 30345
DCostantini@micronoptics.com

Michael Derby
Wind and Water Power Program, EE-2B
Office of Energy Efficiency and Renewable Energy
U.S. Department of Energy
1000 Independence Ave., SW
Washington, DC 20585
Michael.Derby@ee.doe.gov

Michael Desmond
National Renewable Energy Laboratory
Mail Stop 3911
1617 Cole Blvd.
Golden, CO 80401
Michael.Desmond@nrel.gov

Thomas F. Drouillard
Acoustic Emission Working Group (AEWG)
11791 Spruce Canyon Circle
Golden, CO 80403, USA
tfdrouillard@yahoo.com

Charles R. Farrar
Los Alamos National Laboratories
BO Box 1663 - MSP946
Los Alamos, NM 87545
farrar@lanl.gov

Anindya Ghoshal
United Technologies
411 Silver Lane, MS 129-73
East Hartford, CT 06108
ghoshaa@utrc.utc.com

Valery Godinez-Azcuaga
Physical Acoustics Corporation
195 Clarksville Rd.
Princeton Jct., NJ 08550
valery.godinez@mistrasgroup.com

Tom W. Graver
Micron Optics, Inc.
1852 Century Place NE
Atlanta, GA 30345
twgraver@micronoptics.com

Todd C. Haber
Micron Optics, Inc.
1852 Century Place NE
Atlanta, GA 30345
tchaber@micronoptics.com

Mark Higgins
Wind and Water Power Program, EE-2B
Office of Energy Efficiency and Renewable Energy
U.S. Department of Energy
1000 Independence Ave., SW
Washington, DC 20585
Mark.Higgins@ee.doe.gov

Scott Hughes
National Renewable Energy Laboratory
Mail Stop 3911
1617 Cole Blvd.
Golden, CO 80401
Scott.Hughes@nrel.gov

Francesco Lanza di Scalea
University of California - San Diego
9500 Gilman Drive
La Jolla, CA 92093-0085
flanza@ucsd.edu

Lawrence Livermore National Laboratory
Attn: N. Dunipace (1)
P.O. Box 808, MS L-795
Livermore, CA 94551-0808

John T. Lindberg,
Electric Power Research Institute
1300 West WT Harris Blvd.
Charlotte, NC 28262
jlindberg@epri.com

David Miller
Montana State University - Bozeman
PO Box 173800
103 Roberts Hall
Bozeman, MT 59717-3800
dmiller@me.montana.edu

James R. Mitchell
Structural Diagnostic Services, Inc.
711 Cow Hill Road
Mystic, CT 06355-1111
860-536-3380
360-647-6681
MitchEng@aol.com

Mansour H. Mohamed
3TEX
109 MacKenan Drive
Cary, NC 27511
mansourm@3tex.com

John W. Newman
Digital Wind Systems, Inc.
One Tower Bridge, Suite 900
West Conshohocken, PA 19428
JNewman@LaserNDT.com

John W. Newman,
Laser Technology, Inc.
1055 West Germantown Pike
Norristown, PA 19403
JNewman@LaserNDT.com

Christopher Niezrecki
University of Massachusetts - Lowell
One University Avenue
Lowell, MA 01854-2881
Christopher_Niezrecki@uml.edu

Rogier P.L. Nijsse
Knowledge Centre WMC
Kluisgat 5
1771 MV Wieringerwerf
THE NETHERLANDS
R.P.L.Nijssen@kc-wmc.nl

Maya Nissim
EDP Renewables North America, LLC
808 Travis, Suite 700
Houston, TX 77002
Maya.Nissim@edpr.com

Stephen C. Nolet
TPI Composites, Inc.
373 Market Street
Warren, RI 02885-0328
snolet@tpicomposites.com

Chief Technical Officer
Acellent Technologies, Inc.
835 Stewart Drive
Sunnyvale, CA 94085

Kanji Ono
Department of Materials Science and Engineering
UCLA Engineering
410 Westwood Plaza
Los Angeles, CA 90095-1595
(310) 825-5233
kanjiono@gmail.com

Didem Ozevin
University of Illinois at Chicago
842 W. Taylor St, 3073 ERF
Chicago, IL 60607
dozevin@uic.edu

Frank E. Peters
Center for Nondestructive Evaluation
Iowa State University
1915 Scholl Road
Ames, IO 50011-3042
fpeters@iastate.edu

Adrian Pollock
Physical Acoustics Corporation
195 Clarksville Road
Princeton Jct., NJ 08550 USA
apollock@pacndt.com

Nathan Post
Wind Technology Testing Center
80 Terminal St.
Charlestown MA 02129
Nathan.Post@nrel.gov

Charles Shepard
American Airlines Maintenance & Engineering Center
3900 N. Mingo Rd.
Tulsa OK 74116
charles.shepard@aa.com

Herbert J. Sutherland
1700 Camino Gusto NW
Albuquerque, NM 87107-2615
HJS.Consulting@att.net

Mahmoud Reda Taha
124 Tapy Hall
Department of Civil Engineering
MSC01 1070
1 University of New Mexico
Albuquerque, NM 87131-0001
mrtaha@unm.edu

Andrei N. Zagrai
New Mexico Tech
801 Leroy Place, Weir 124
Socorro, NM 87801-4750
azagrai@nmt.edu

Jose R. Zayas
Wind and Water Power Program, EE-3A
Office of Energy Efficiency and Renewable Energy
U.S. Department of Energy
1000 Independence Ave., SW
Washington, DC 20585
Jose.Zayas@EE.Doe.Gov

INTERNAL DISTRIBUTION

MS 0555, Kyle R. Thompson, 1522
MS 0557, David G. Moore, 1522
MS 0615, Dennis P. Roach, 6620
MS 0615, Thomas M. Rice, 6621
MS 0615, Stephen Neidigk, 6621
MS 0615, Randy L. Duvall, 6621
MS 0615, Michel D. Bode, 6621
MS 0751, Alex Rinehart, 6914
MS 0751, Scott T. Broome, 6914
MS 1124, D. Todd Griffith, 6122
MS 1124, Brian T. Naughton, 6121
MS 1124, Joshua A. Paquette, 6121
MS 1124, Mark A. Rumsey, 6121
MS 1124, Jonathan White, 6121
MS 1124, Wind Library, 6121 (5)
MS 1349, Bernadette A. Hernandez-Sanchez, 1815

MS 0899, Technical Library, 9536 (Electronic)


Sandia National Laboratories